INTERNATIONAL ATOMIC ENERGY AGENCY
UNITED NATIONS EDUCATIONAL, SCIENTIFIC AND CULTURAL ORGANIZATION

INTERNATIONAL CENTRE FOR THEORETICAL PHYSICS
34100 TRIESTE (ITALY) - P.O. B. 586 - MIRAMARE - STRADA COSTIERA 11 - TELEPHONES: 224281/2/3/4/5/6
CABLE: CENTRATOM - TELEX 460392-1

SMR/115 - 32

WINTER COLLEGE ON LASERS, ATOMIC AND MOLECULAR PHYSICS

(21 January - 22 March 1985)

- PHASE-CONJUGATION BY STIMULATED SCATTERING
- PHASE-CONJUGATION BY PHOTOREFRACTIVE EFFECT
- USE OF OPTICAL BEAM PHASE CONJUGATION IN PHYSICAL MEASUREMENT

R. HELLWARTH
Departments of Electrical Engineering & Physics
University of Southern California
Los Angeles, CA 90089-0484
U.S.A.

It is now widely employed for phase-conjugation. Because it is essentially an effect that is nonlinear in beam energies rather than beam powers, it can phase-conjugate low-power (even microwatt) beams, but taking longer to respond to the lower powers employed. Barium titanate, for example, responds typically in tenths of seconds at one Watt cm^{-2} levels, depending on beam angles, applied fields, and other factors. This crystal also yields large conjugate-wave gains.

A remarkable property of the photorefractive effect is that it can produce phase-conjugation in either the manner and geometry of stimulated backscattering, as depicted in Fig. 1.3., or in the manner and geometry of four-wave mixing, as depicted in Fig. 1.4. A more detailed description of the optical nonlinearities of photorefractive materials is given in Section 3.

2. Phase-conjugation By Stimulated Scattering

The remarkably simple device of Fig. 1.3 is perhaps the most difficult method of phase-conjugation to understand. We will first review the basic nature of stimulated scattering and then show how the theory of the phase conjugator proceeds without going through the details, many of which are best handled by numerical computation.

In its simplest form, stimulated scattering is the exponential power gain e^G experienced by a weak monochromatic probe wave at ω when it traverses a strong monochromatic pump wave at a higher frequency ν in a transparent medium having an (Raman-active) excitation whose frequency is $\nu-\omega$.

When this excitation is acoustic the process is called "stimulated Brillouin scattering"; when vibrational it is called "stimulated Raman scattering," etc., for a number of different physical processes. The rate of growth of the gain factor G with distance ℓ along the probe beam is given by

$$dG/d\ell = gI \qquad (2.1)$$

where I is the intensity of the pump beam and g is a stimulated growth coefficient often listed in Tables (see Ref. 23). For example for sound in CS_2, g~0.2 cm/MW for backward scattered waves, and this varies little with wavelength.

In a device such as in Fig. 1.3., the input signal (which experiences the gain) is noise from the spontaneous (Brillouin, Raman, etc.) scattering. This noise is relatively weak and both theory and experience show that G~20-25 is necessary in steady state to make the stimulated scattering comparable to the input power.[1]

2.1. Origins of phase-conjugate character.

The basic gain concept above refers to plane waves. Zel'dovich, et al.,[24] discovered that for multi-mode pump beams, the stimulated backscattering can be phase-conjugate under at least some conditions with the arrangement of Fig. 1.3. When one must deal with multi-mode beams and expects phase-conjugation, the theory is altered in a surprising way. To see how, let us consider an image-bearing beam focused so as to couple 100% into a multi-mode optical waveguide. In the guide ($0<z<L$) the incident beam field amplitude can be written (assume uniform direction of the electric field throughout)

$$E=\sum_{n=1}^{N} A_n c_n(x,y,)e^{ik_n z}, 0<z<L \tag{2.2}$$

where the sum is over the N guided modes. The transverse mode patterns $c_n(x,y)$ are normalized and obey

$$\int dxdy c_n^* c_m = \delta_{mn}. \tag{2.3}$$

The mode propagation constants k_n are obtained from guide theory. The mode excitation amplitudes are obtained from the field pattern $E_o(x,y)$ at the entrance to the guide by

$$A_n = \int dxdy c_n^* E_o. \tag{2.4}$$

We will assume the backscattering alters (2.2) negligibly. One now tries solutions for the

backscattered waves amplitudes F(x,y,z) generated by the nonlinear polarization density of the form

$$\sum_{n=1}^{N} B_n c_n(x,y)e^{-ik_n z-\gamma z/2}, \tag{2.5}$$

which differ from the normal guided solutions to Maxwell's equations by an exponential growth factor. Clearly, if $B_n \propto A_n^*$ we have achieved a perfect phase conjugator at the entrance plane z=0. Unfortunately, this process never achieves this perfectly and this fact complicates the theory.

The nonlinear polarization density for stimulated backscattering of any type has the form, in the medium in the guide;

$$-iqE^*EF, \tag{2.6}$$

where q is a function of $\nu-\omega$ which is real and positive at resonance peaks where gain is highest.

Substituting (2.4)-(2.6) in Maxwell's equations, integrating over the guide interior after multiplying by $c_i^* \exp(ik_i z+\gamma z/2)$, and neglecting terms of order (γ/k) smaller, one obtains coupled linear equations for the backscattered wave coefficients of the form

$$\gamma B_i = U_{ijk\ell} A_j^* A_k B_\ell \tag{2.7}$$

which is an eigenvalue equation for the gain parameter γ. Since i,j,k,ℓ=1,2,...N, where N is the number of guided modes, there are N sets of $B_{i,\alpha}$ (α=1,2,...N) which are solutions, each set having its own eigenvalue γ_α. Numerical and analytical solutions of (2.7) for various assumptions about the input-beam amplitudes A_n have led to the following conclusions about the solutions. For details see Ref. 2 which is attached as Appendix XI.

1. One of the solutions may be close to phase-conjugate. We label this the α=1 solution and refer to it as the "phase-conjugate mode". It has a non-conjugate fraction f_1 that, for randomly distributed values of the input amplitudes and phases is approximately

$$f_1 \sim N^{-3/2} + (NL\Delta\lambda/S)^2/40 \qquad (2.8)$$

where $\Delta\lambda$ is the Stokes wavelength shift $2\pi c(\omega^{-1}-\nu^{-1})$ and S is the area of the guide. One can see from (2.8) the main conditions necessary for this part of the backscattered wave to be phase conjugate, i.e., that makes $f_1 << 1$.

II. The gain coefficient γ_1 for the phase conjugate wave is, when $f_1 << 1$, approximately

$$\gamma_1 \sim 2gP_o/S \qquad (2.9)$$

where g is the usual tabulated gain coefficient defined above and P_o is the power of the incident beam: $\Sigma_n |A_n|^2 k_n c^2/8\pi\nu$.

III. There are N-1 other solution sets $B_{i,\alpha}$ who non-conjugate fractions f_α for the "non-conjugate modes" are

$$\gamma_s \sim gP_o/S, \ \alpha=1 \qquad (2.10)$$

or about half that of the conjugate mode. The gains might be termed normal, since they are the same as for a plane input wave of same average pump beam intensity. The phase-conjugate mode gain may then be called "anomalous", being twice that for a plane-wave pump of the same intensity.

V. Any observed non-conjugate fraction f_o can be expected to be made up of f_1 above plus f_s the sum total of background emission from the N-1 solutions with lower gain. In Ref. 1 (Ch. 7) it is estimated that

$$F_s \sim \frac{1}{2} Ne^{-G} \qquad (2.11)$$

in the steady state. This limits the number of modes that can be usefully conjugated by stimulated backscattering.

It is not entirely clear for what classes of pump-wave amplitude distributions A_n in (2.7) that the above conclusions are valid. This question deserves more numerical study.

We summarize some of these results in the following schematic Fig. 2.1 of the power distributions in the guide of the incident beam and the scattered solutions.

Fig. 2.1. Schematic of the incident beam power P_o, the phase-conjugate mode power P_1, and the non-conjugate mode powers P_α as a function of distance z along the guide. Incident power flows to the right.

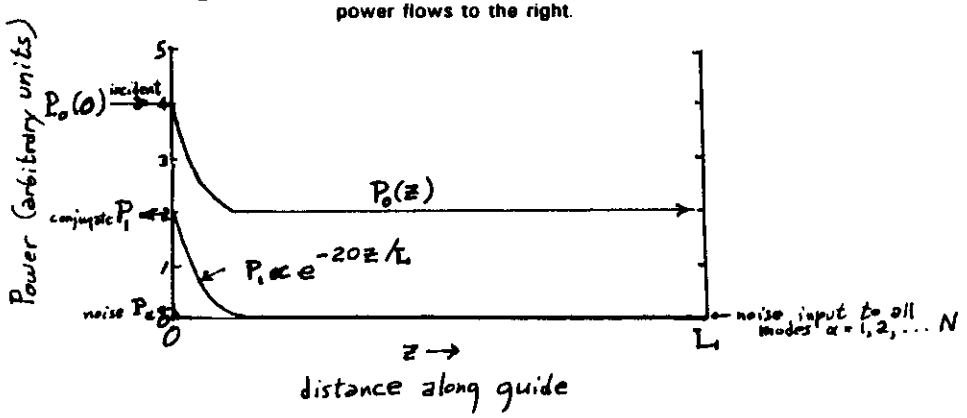

2.2. Unguided Waves.

Experimentally it has been found that, nder some conditions that are poorly understood, stimulated scattering from an unguided image-bearing beam can be its phase-conjugate, or, more precisely, have a small non-conjugate fraction f. The theory for this case is mathematically more involved and no reliable conditions have yet been derived for it, i.e., the non-conjugate fraction f has not been estimated. Of course more power is required when waves are unguided. However, the convenience of unguided interactions when power is available makes this case well worth further study.

2.3. Pulse Shortening.

Hon has demonstrated simultaneously the compression in time and phase-conjugation of a 20 nsc 1.06 micron pulse by stimulated Brillouin backscattering in glass.[25] The conjugate pulse emerged having about 2 nsc length. Pulse compression by

transient stimulated backscattering has been studied theoretically and experimentally. (See Refs. 1 and 23 for some results and other references.) The combination of conjugation and compression (or even transient scattering) has not yet been analyzed, and remains an interesting question.

The analysis of simple pulse compression of a plane wave shows two distinct useful regimes. In one, gcl_o is much less than the natural bandwidth of the excitation, in the other regime it is larger. Both regimes are now fairly well understood, the second case producting the less dramatic shortening. Pulses shorter than a period of the backscattering excitation are not expected.

3. Phase-conjugation By Photorefractive Effect

The photorefractive effect, as described in Section 1.3.2, has been observed in a number of acentric crystals, including lithium niobate, bismuth silicate ($Bi_{12}OSi_{20}$), barium titanate, potassium tantalate, gallium arsenide, and strontium barium niobate. Both the beam geometries of stimulated backscattering (Fig. 1.3) and four-wave mixing (Fig. 1.4) produce phase conjugation with the special form of the nonlinearity characteristic of the photorefractive effect. Entirely unique other geometries perform also. The geometry of Fig. 1.4 has produced cw intensity gains in excess of 100, and has been used to make new self-oscillating structures. This was done with single crystals of $BaTiO_3$ at room temperature and typically 10 mW argon laser beams, with which response times (e.g., buildup times for light in self-oscillating structures)are of the order of a second. (See Ref. 26, attached as Appendix IX, for details.) The pump beams can actually be created spontaneously by a kind of stimulated scattering from the input E-beam, as we explain below.[27] This makes beam patterns as shown schematically in Fig. 3.1.

Fig. 3.1. Schematic of self-pumped phase-conjugator using photorefractive effect.

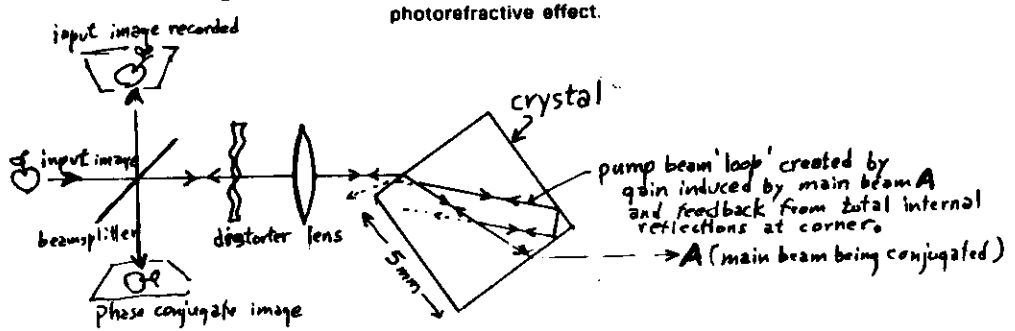

The generation of pump beams internally in the crystal is a result of two beam coupling which occurs similarly as for stimulated scattering but without any shift in frequency (as well as sometimes with a shift). This two-beam coupling also produces phase-conjugation by itself, with beam geometry as illustrated in Fig. 3.2.[28]

To understand these effects, one must understand how two intersecting beams at the same frequency produce a refractive index grating. A model based on the optically-induced exchange of an electron between divalent and trivalent impurities has worked well for some crystals. This is illustrated in Fig. 3.3. The sequential steps from light intensity variation, to charge density variation, to electric field variation, to refractive index variation (from the electro-optic effect) are illustrated in Fig. 3.4.

The mathematics for deriving the charge density variation from the intensity variation using the hopping model are outlined in Fig. 3.5 for no externally applied field. The extension to a constant externally applied field is straightforward and introduces no new parameters. This linearized theory is valid for small fractional intensity and charge variations.

The refractive index change, or more directly, the change $\Delta\varepsilon_{ij}$ in the optical dielectric tensor, is calculated for the electro-optic effect by the usual relation

Figure 3.2. Schematic of beam trajectories in phase-conjugation experiment employing two-beam coupling (forward-to-backward) in photorefractive crystal.

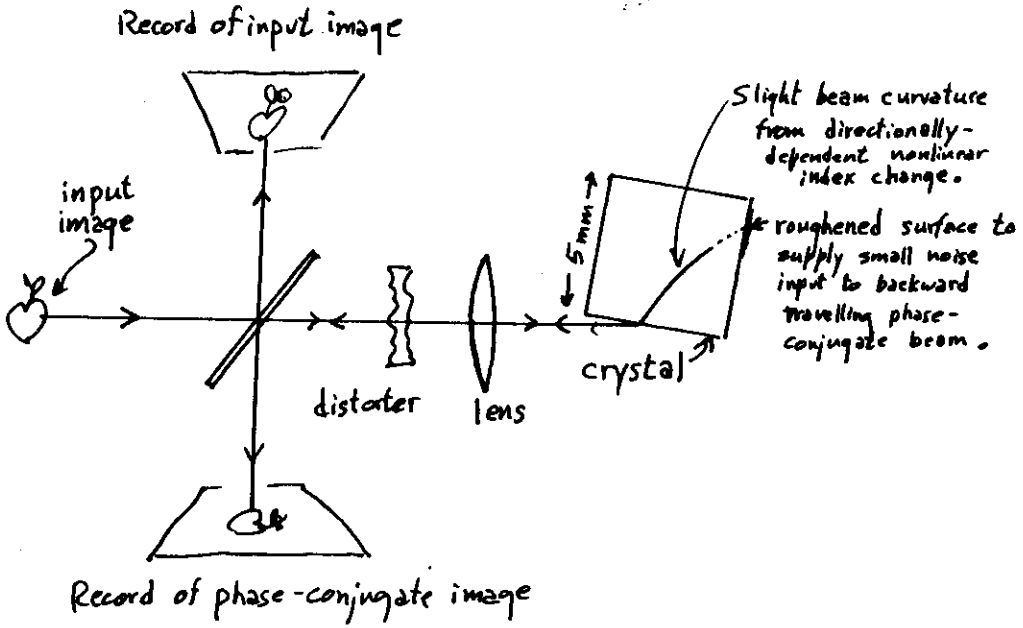

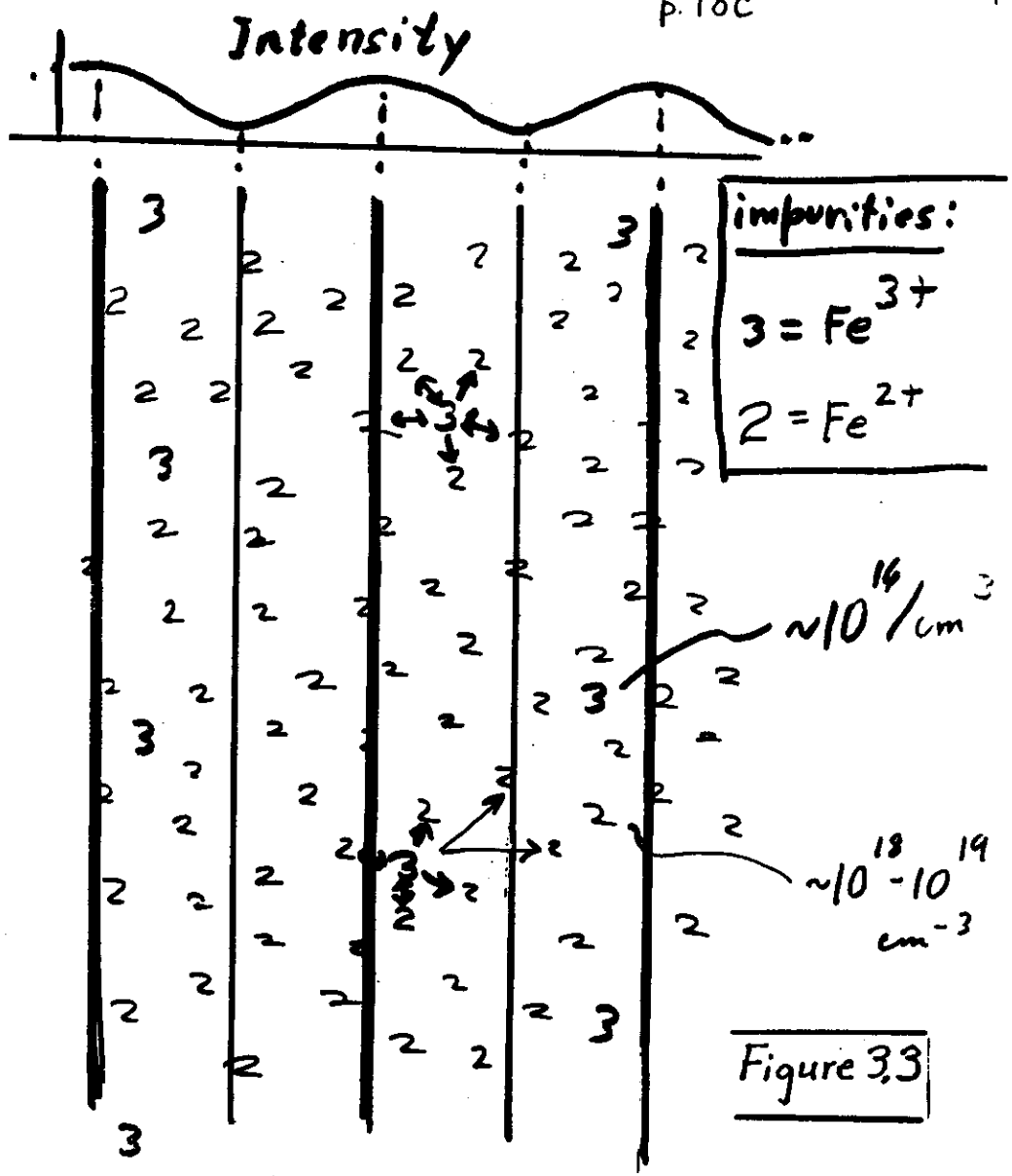

Figure 3.3

Charge hopping model for photorefraction in $BaTiO_3$ and $Bi_{12}SiO_{20}$.

p. 18d

Figure 3.4

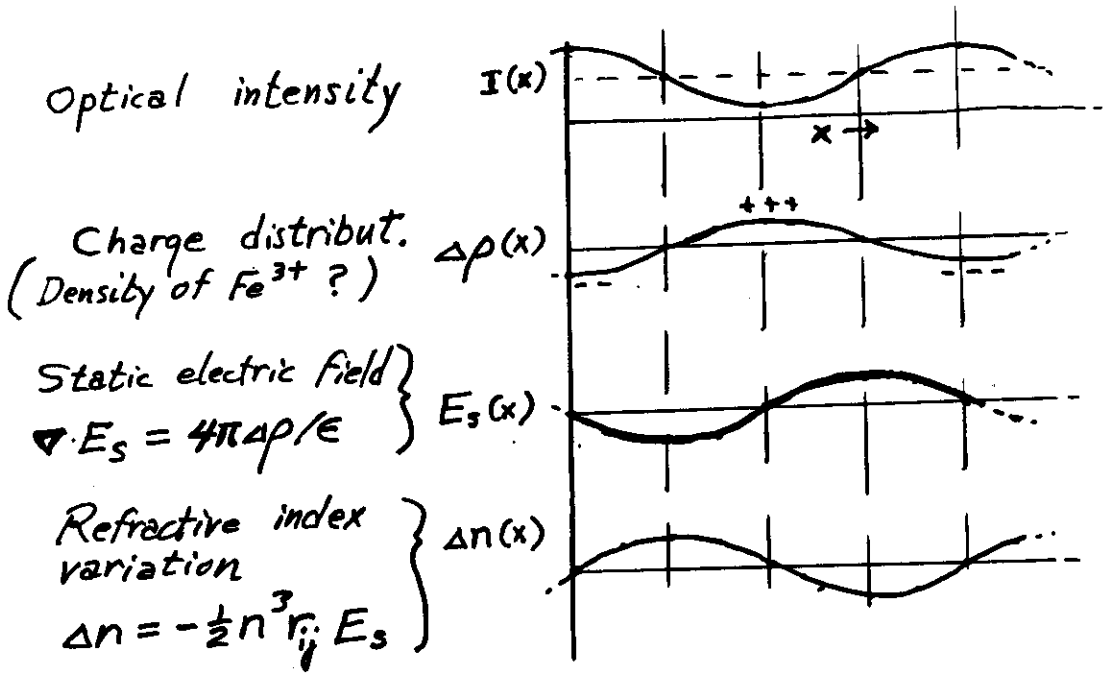

HOLOGRAM FORMATION BY THE PHOTOREFRACTIVE EFFECT

$$\Delta\varepsilon_{ij}=\varepsilon_{ik}R_{k\ell m}E_m\varepsilon_{\ell j} \tag{3.1}$$

where ε_{ik} is the unperturbed optical dielectric tensor, $R_{k\ell m}$ is the usual electro-optic tensor that is usually contracted to the r_{ij} notation ($r_{62}=R_{xyy}=R_{yxy}$, etc.), and the Coulomb electric field is related to the charge density amplitude W at wavevector k_i (in Fig. 3.5) by Poisson's equation (in esu)

$$ik_iE_i=4\pi WqN_o/\varepsilon_o \tag{3.2}$$

where q is the charge value of the hopping charges whose average density is N_o, and ε_o is the static dielectric constant.

With the spatial index variation represented by (3.1), the scattering of any additional beam (or one of the writing beams) can be calculated by the standard methods of holographic analysis. This analysis shows that if a weak cw beam traverses a strong cw pump beam at the same frequency, over half the angles in a photorefractive crystal, then the weak beam experiences exponential growth. (Over the other half of angles, it experiences exponential decay.) This is because the spatial variation of Δ_{ij} is not in (spatial) phase with the optical intensity variations caused by the two superposed beams. (See Refs. 1 and 31, and also Appendix VIII for details.)

When optical pulses of much higher power but short (~nsc) duration are used to write and read photorefractive gratings, it appears that the analysis of Fig. 3.5 remains essentially unchanged, at least for barium titanate.[29] The potential of photorefractive materials for high speed optical processing has not yet been explored and it promises much.

The result of the holographic analysis to obtain the steady-state phase-conjugate field reflectivity of Eqn. (1) in the geometry of Fig. 1.4, when the alteration to the E, G, and H beams can be neglected, is strikingly simple:

$$K=\omega n^3r_{eff}k_BTkLm[4cq(1+k^2/k_D^2)].)^{-1} \tag{3.3}$$

p.19b

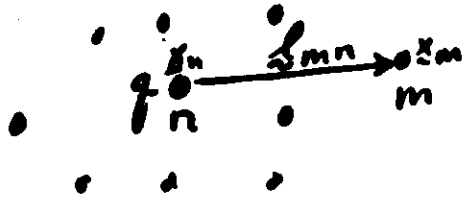

Figure 3.5

W_n = probability that q is at site n

I_n = optical intensity at n

ϕ_n = electrostatic potential at n

$$\frac{dW_n}{dt} = -\sum_{\substack{\text{neighbors}\\ m}} D_{nm} W_n I_n e^{-\frac{\phi_n - \phi_m}{2k_BT}} + \sum_m D_{mn} W_m I_m e^{-\frac{\phi_m - \phi_n}{2k_BT}}$$

To create "grating" pattern of charges;

use $I_n = \bar{I} + Re\, G e^{i\underline{K}\cdot\underline{x}_n}$

To solve, try $W_n = \bar{W} + Re\, W e^{i\underline{K}\cdot\underline{x}_n}$

$\phi_n = \phi_{on} + Re\, \phi e^{i\underline{K}\cdot\underline{x}_n}$

Find for $\phi_{on} = 0$:

$$\frac{dW}{dt} = -\sum_m D(\underline{\ell}_{mn})\bar{W}\bar{I}\left[w + w\cdot\frac{k_D^2}{K^2} + m\right]\left(1 - e^{i\underline{K}\cdot\underline{\ell}_{mn}}\right),$$

$w \equiv W/\bar{W} \quad m \equiv G/\bar{I}$

$$k_D^2 \equiv \frac{\bar{W}N_0q^2}{\epsilon\epsilon_0 k_BT}$$

Here r_{eff} is the effective electro-optic constant for the given beam directions and polarizations, and k_D is the screening wavevector defined in Fig. 3.5. For interior write-beam angles less than ~one radian in efficient materials, $k<k_D$. The magnitude of the modulation index m is less than unity. In $BaTiO_3$, $r_{eff} \sim 10^{-9}$ m/V, (depending on geometry) so the possibility of large gain is evident for effective interaction lengths L of only a few mm.

The cw gain $e^{\kappa L}$ experienced by a weak probe beam counter-propagating along a stronger pump beam in $BaTiO_3$ when both waves are extraordinary follows from (3.1) with Fig. (3.5) and simplifies in the usual case where $k>>k_D$ and the r_{42} term dominates to

$$\kappa = 4\pi N^2 q r_{42} N_0 \sin^2\theta\cos\theta/\epsilon_o(\theta) \text{esu}, \tag{3.4}$$

when the beams lie in the zx plane at angle θ to the z axis. The static dielectric constant ϵ_o varies with this angle, being ~100 at $\theta=0$ and ~4300 at $\theta=\pi/2$. One estimates from (3.4) with $N_o \sim 3\times10^{16}$ cm^{-3} that κ is maximum at $\theta \sim 26°$ where

$$\kappa \sim 8 \text{ cm}^{-1}. \tag{3.5}$$

(It is likely that the higher-gain samples have $N_0 \sim 10^{17}$ cm^{-3}.) Therefore, the backscattered beam can grow from the small noise present to attain intensity of the order of the input beam with L~1 cm, as observed. The observed phase-conjugate nature of this backscatter follows from arguments similar to those in Section 2 applying to stimulated Brillouin backscattering.[28]

4. Use Of Optical Beam Phase Conjugation In Physical Measurement

Optical beam phase-conjugation has been of value in physical measurement of (1) electronic and excitonic properties of atoms, molecules, and crystals, (2) thermodynamic properties, especially thermal conductivities, and (3) nuclear motions (vibration, rotation, etc.) in molecules, liquids, and crystals. The advantage of phase-conjugation beam geometries, especially among various four-wave mixing geometries, are several in each of

these areas. We review each area below.

4.1. Measurement of Electronic Excitations.

Most useful application of phase-conjugation to electronic measurements have been the following.

4.1.1. Electron and hole transport.

When two beams, called 1 and 2, interfere spatially in a medium, a spatial modulation, or "grating", of the optical intensity exists. This grating moves or is stationary depending on whether the beam frequencies are different or the same. When the radiation is near the bandgap frequency, free or bound electron-hole pairs are created so as to create a spatially varying density of these objects. This is illustrated schematically in Fig. 4.1. A reading beam labelled 3 is aligned so as to scatter phase-matched (i.e., as specified in Fig. 4.1) into the beam 4, which is essentially phase-conjugate to the beam 2. The refractive index variations arise from the newly-created electron-hole plasma. Their magnitude reflects the density of excitations and, for unbound electrons and holes, their effective masses. The decay of the grating reflects the mobilities of the particles and their recombination processes. How this decay varies with grating period and direction gives a fairly complete picture of the diffusion of the excited particles, especially when viewed in an external electric field. Because of the wide acceptance angle of the phase-conjugate geometry, a wide range of grating wavevectors can be studied simultaneously, often an advantage in accuracy and simplicity of measurement. See Ref. 1 for references and details.

4.1.2. Excited ion polarizability.

Similarly as do excited electron-hole pairs change the refractive index, so do stationary excited ions, such as the laser ions in ruby or Nd:YAG. Phase-conjugation has yielded the first measurements of this index change, and the altered optical polarizability

Fig. 4.1 Schematic of phase-conjugation by excitation grating.

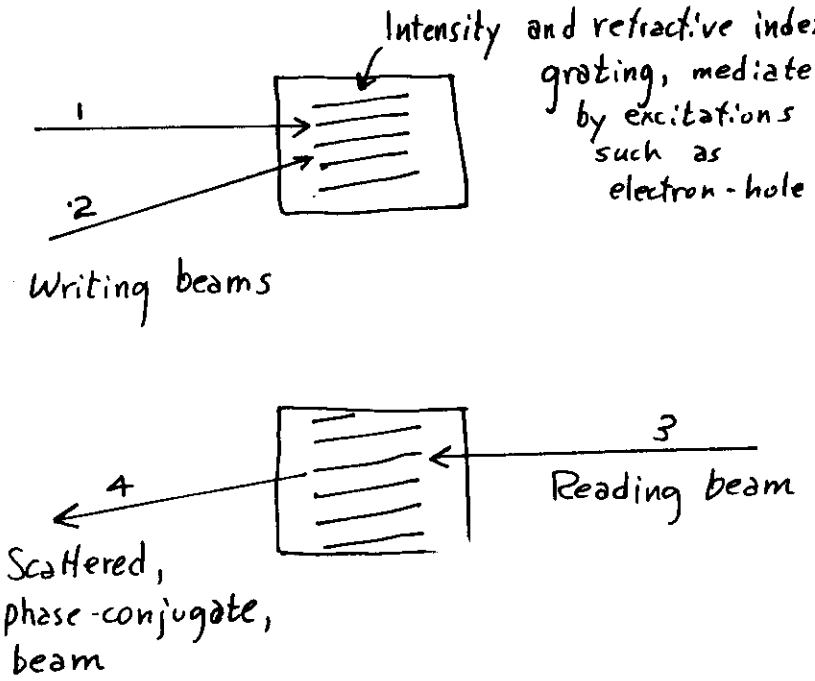

of excited ion states. See Ref. 30, which is attached as Appendix X, for details.

4.1.3. Exciton migration.

Spatial diffusion of excited ions in solids causes a dependence on grating wavevector k of the decay rate of the refractive index grating they cause. By measuring beam polarization states in cw phase-conjugation, a sensitive, self-calibrating measure of the k-dependence has been devised. It is the result of interference between scattering from the two gratings that can exist simultaneously in cw phase conjugation. This is illustrated in Fig. 4.2. Details are given in Appendix X.

4.1.4. Measurement of photorefractive parameters.

The discussion of Section 3 above, and the theory outlined there, make it clear that the dependence of phase-conjugate signals and their decays on beam angles and polarization can yield the necessary impurity parameters to calculate essentially any optical interaction. These impurity parameters include the densities of filled and empty trap sites, whether electron migration occurs in the conduction or valence bands (or both), the optical cross-section for ionizing a trap, and the mobilities and lifetimes of excited carriers. Examples of such measurements are described in Ref. 31.

4.1.5. Doppler-free 1 photon spectroscopy.

When phase-conjugation by degenerate four-wave mixing is mediated by 1-photon resonance (energy levels spaced ~ħω) in a vapor, and the absorption length is not less than the beam interaction length, the reflectivity shows a Doppler-free resonance.[32] Results using this technique are reviewed in Ref. 33.

4.1.6. Doppler-free 2 photon spectroscopy.

The most accurate measurements of level spacings in the excited $5D_{3/2}$ manifold of rubidium vapor have been made using the phase-conjugate beam geometry which

16

17

Fig. 4.2. Precise comparison of decay rates τ_a, τ_b * of two gratings of different wavevectors k_a, k_b

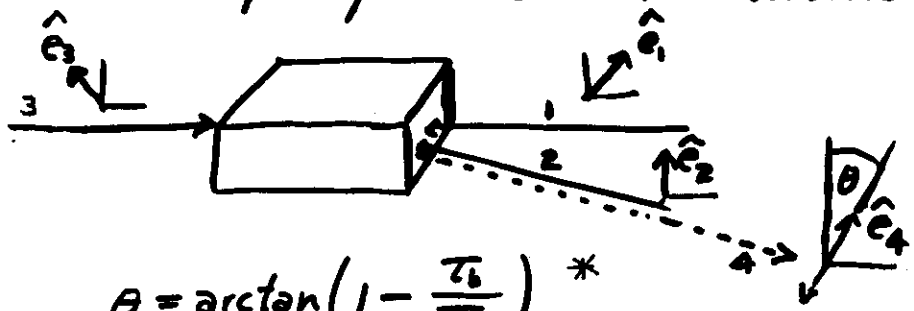

$$\theta = \arctan\left(1 - \frac{\tau_b}{\tau_a}\right) \quad *$$

$$k_b = |\vec{k}_2 - \vec{k}_3| \qquad \text{(all beams cw at } \omega\text{)}$$

$$k_a = |\vec{k}_2 - \vec{k}_1|$$

Scattered optical field amplitude $\vec{E}_4 = \vec{E}_a + \vec{E}_b$

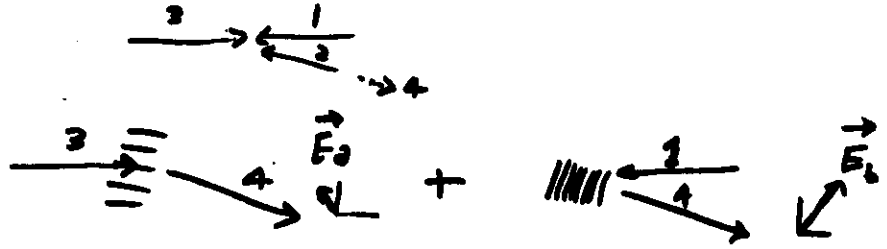

* Exponential decay of gratings assumed.

exhibits Doppler-free resonances for much the same reason as does 2-photon absorption from counter-propagating beams. A typical result is illustrated in Fig. 4.3.

4.1.7. Measurements of atomic collisions in vapors.

When absorption lengths are much shorter than the interaction length L of phase-conjugate beams at 1-photon resonance in a vapor, the polarization dependence of the conjugate signal in the wings of the resonance (where the absorption length has become longer than L) shows surprising behavior that reflects the rate at which collisions transfer the atom between magnetic sub-levels. In this case it was observed, as calculations predicted, that a refractive index grating is formed without optical intensity variations, but with spatial variations in the state of elliptical polarization of the light only. These results are summarized in Ref. 34 and attached as Appendix XII.

4.2. Measurement of Thermodynamic Properties.

When a medium is slightly absorbing, a spatial variation in optical intensity causes a spatial variation in temperature, and thereby, a spatial variation in refractive index. The transient decay of a phase-conjugate signal becomes a very simple and direct way of measuring the thermal conductivity of any nearly transparent substance,[11] as illustrated in Fig. 4.4. Other thermally-induced changes, such as solvent concentration can also be measured this way. Thermal contact and barrier problems are eliminated. Details of such measurements are given in Appendix V.

4.3. Measurements of Excitations of Nuclear Motions in Molecules, Liquids and Crystals by Raman-Induced Phase Conjugation (RIPC)

Non-degenerate phase-conjugation affords another technique of coherent laser spectroscopy that is comparable in many respects to Coherent Anti-Stokes Raman Scattering (CARS), Stimulated Raman gain spectroscopy and other similar techniques. As such it affords a way to study the same nuclear motions as might be studied by these

p. 23b

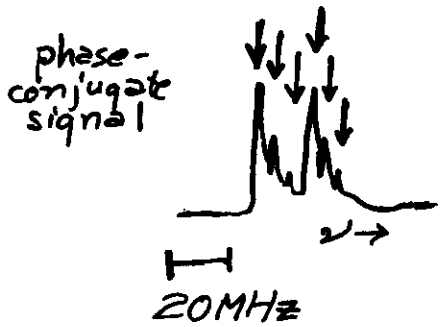

$5S-5D_{3/2}$ transition of ^{85}Rb
P = 2m Torr
Bloch, Ducloy, and Giacobino
(J. Phys. B. 14, L819 ('81))

Fig. 4.3

Doppler-free two-photon resonances in phase-conjugation signal.

p. 23c

Figure 4.4

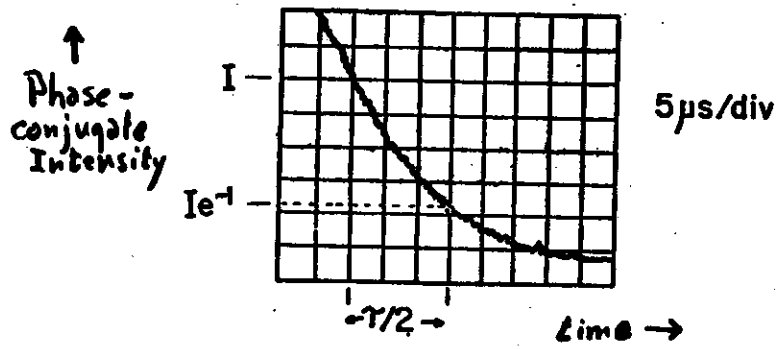

Decay of phase-conjugation mediated by thermally-induced index changes.

$$\tau = \frac{\rho C_p}{\lambda k^2}$$ in simple liquids.

τ may be partly determined by relaxation phenomena in cyclohexane and other isomeric liquids, by interdiffusion rates in liquid mixtures, by critical fluctuations near transition temperatures, and other thermodynamic modes.

other techniques, and it offers some interesting trade-offs in noise and sample accessibility problems. We call this technique "Raman-Induced Phase Conjugation" or RIPC.

Figure 4.5 illustrates how a Raman resonance may be observed by RIPC. This resonance has a non-Lorentzian line-shape in general which can be made to coincide with the spontaneous Raman lineshape by proper choice of beam polarizations. However, the complex forms of the lineshapes give useful data on the ratio of the Raman line strength to the strength of a uniform background of optical Kerr effect which is more easily measured absolutely. Details of the theory of these lineshapes is given Ref. 12 which is attached as Appendix VI.

A brief comparison of the geometries, advantages and disadvantages of RIPC, CARS, and three other techniques is given in Fig. 4.6.

Fig. 4.5. Typical arrangement for observing Raman resonance by Raman-induced phase-conjugation. For special choice of polarizations of E_1 and E_2, Kerr-effect background is absent.

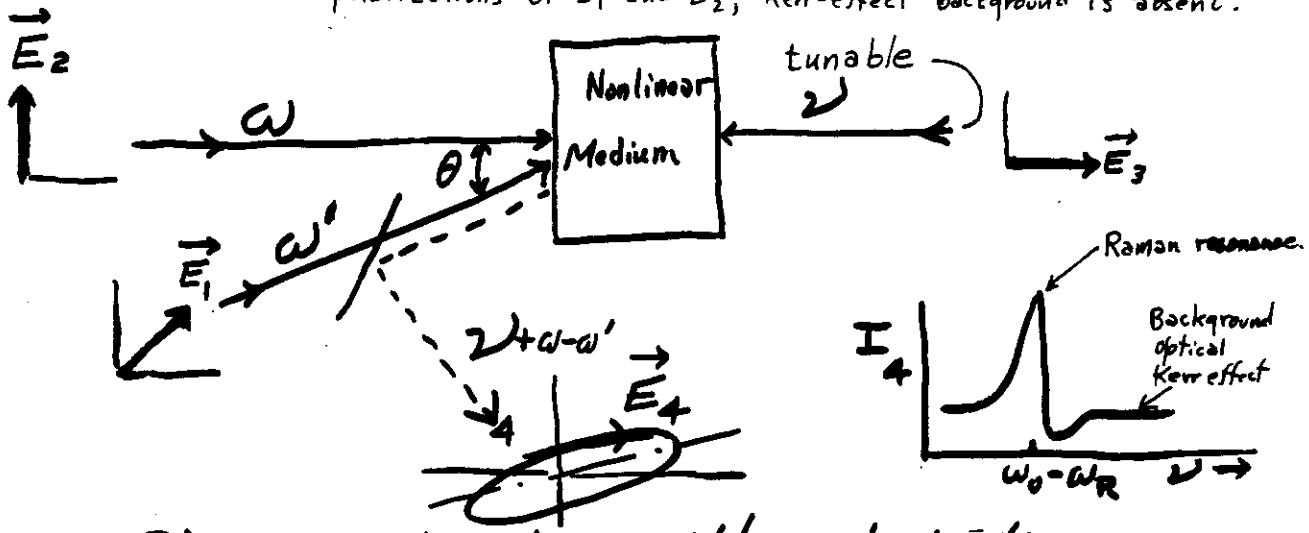

Phase-conjugation with polarization and frequency shift.

For $\nu=\omega$, $\vec{E}_4(\theta)$ gives medium symmetry and spatial dispersion of nonlinearity.

Summary of most-used techniques of coherent laser spectroscopy (FOR RAMAN AND BRILLOUIN SPECTRA)

Figure 4.6

1. Stimulated Raman gain spectroscopy

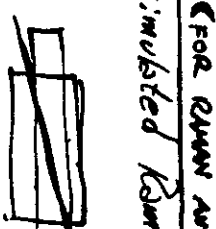

- High background signal, sensitive
- Two laser fluctuations.

2. Coherent anti-Stokes Raman scattering (CARS)

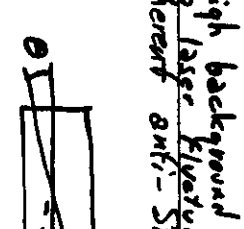

- Critical phase-matching θ.

3. Raman-induced Kerr effect

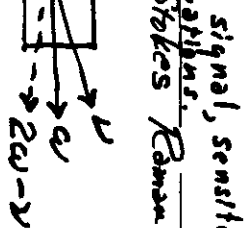

- Sensitive to stray birefringence.
- Can't handle birefringent crystals well.

4. Two-beam interferometry

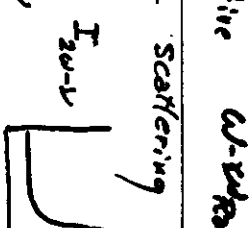

- High background, sensitive to inhomogeneity, laser fluctuations.

5. Raman-induced phase conjugation (RIPC)

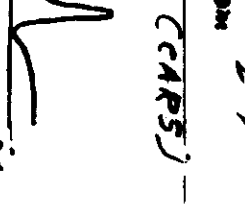

- 16 combinations of polarizations.
- Non-critical phase-matching

References

1. Optical Phase Conjugation, ed. by R.A. Fisher (Academic Press, New York, 1983).
2. R.W. Hellwarth, Journ. Opt. Soc. Am., 68, 1050 (1978).
3. B.Ya.Zel'dovich, V.V. Shkunov, Sov. J. Quant. Elect. 7, 610 (1977).
4. R.W. Hellwarth, J. Opt. Soc. Am. 67, 1 (1977).
5. D.A.B. Miller, S.D. Smith, and A. Johnston, Appl. Phys. Lett. 35, 658 (1979).
6. D.M. Bloom and G.C. Bjorklund, Appl. Phys. Lett. 31, 592 (1977).
7. S.M. Jensen and R.W. Hellwarth, Appl. Phys. Lett. 33, 404 (1978).
8. R.W. Hellwarth, IEEE Journ. Quant. Elect. QE-15, 101 (1979).
9. S. Saikan and H. Wakata, Opt. Lett. 6, 281 (1981).
10. J. Nilsen, N.S. Gluck, and A. Yariv, Opt. Lett. 6, 380 (1981).
11. G. Martin and R.W. Hellwarth, Appl. Phys. Lett. 34, 371 (1979).
12. S.K. Saha and R.W. Hellwarth, Phys. Rev. A 27, 919 (1983).
13. A. Ashkin, G.D. Boyd, J.M. Dziedzic, R.G. Smith, A.A. Ballman, H.J. Levinstein, and K. Nassau, Appl. Phys. Lett., 9, p. 72, (1966).
14. J.P. Huignard, J.P. Herriau, Appl. Phys. Lett., 29, 591, (1976).
15. A.M. Glass, G.E. Peterson, and T.J. Negran, pp. 15-26, Laser Induced Damage in Optical Materials: 1972, ed. by A.J. Glass and A.H. Geunther, (Nat'l Bur. of Standards Special Publ. 372).
16. W. Phillips, J.J. Amodei, and D.L. Staebler, RCA Rev. 23, pp. 94-109, (1972).
17. F.S. Chen, J. Appl. Phys., 38, p. 3418 (1967).
18. F.S. Chen, Jour. Appl. Phys., 40, p. 3389 (1969).
19. J.J. Amodei, Appl. Phys. Lett., 18, p. 22 (1971).
20. Juan J. Amodei, RCA Review, 32, p. 185 (1971).

21. L. Young, W.K. Y. Wong, M.L.W. Thewalt, and W.D. Cornish, Appl. Phys. Lett., 24 (1974), p. 264.
22. W.D. Cornish, M.G. Moharam, and L. Young, Appl. Phys. 47, p. 1479, (1976).
23. W. Kaiser and M. Maier, Laser Handbook vol. 2, ed. by F.T. Arecchi and E.O. Schulz-Dubois (North Holland, Amsterdam 1972).
24. B.Ya. Zel'dovich, V.I. Popovichev, V.I. Ragul'skii, and F.S. Faizullov, Sov. Phys. JETP 15, 109 (1972).
25. D.T. Hon, Opt. Lett. 5, 516 (1980).
26. J. Feinberg and R.W. Hellwarth, Opt. Lett. 5, 519 (1980); 6, 257 (1981).
27. J. Feinberg, Opt. Lett. 7, 486 (1982).
28. T. Chang and R.W. Hellwarth (to be published).
29. L.K. Lam, T.Y. Chang, Jack Feinberg, and R.W. Hellwarth, Opt. Lett. 6, 475 (1981).
30. D.S. Hamilton, D. Heiman, Jack Feinberg, and R.W. Hellwarth, Opt. Lett. 4, 124 (1979).
31. J. Feinberg, D. Heiman, A.R. Tanguay, and R.W. Hellwarth, J. Appl. Phys. 51, 1297 (1980).
32. P.F. Liao, D.M. Bloom, N.P. Economou, Appl. Phys. Lett. 32, 813 (1978).
33. M. Ducloy, Adv. in Sol St. Phys. XXII, pp. 35-60 (1982).
34. S.N. Jabr, L.K. Lam, and R.W. Hellwarth, Phys. Rev. A 24, 3264 (1981).

Appendix I

Generation of time-reversed wave fronts by nonlinear refraction*

R. W. Hellwarth

Electronics Sciences Laboratory, University of Southern California, University Park, Los Angeles, California 90007

(Received 2 September 1976)

We describe a nonlinear method for generating, nearly instantaneously, a time-reversed replica of any monochromatic-beam wave pattern. The method employs the interaction of the incident beam, of arbitrary wave front, with counter-propagating plane "pump" waves in a homogeneous, transparent, nonlinear medium. Media are shown to exist in which time-reversed waves can be generated with high efficiency using available laser pump sources.

I. INTRODUCTION

For any electromagnetic wave that propagates through an inhomogeneous, nonabsorbing, medium (having no permanent magnetism), there can exist in principle a time-reversed replica of this wave. This means, for example, than an appropriately patterned but irregular wave front can travel through a randomly inhomogeneous medium and emerge as a coherent uniform wave front, providing it is a replica, reversed in time, of a coherent beam that is deformed by the same inhomogeneous medium. Here we propose a new method for generating, nearly instantaneously, the time-reversed replica of any monochromatic beam. Our method employs the nonlinear refraction present in any medium and is realizable with existing laser sources.

It is well known to be possible to generate a time-reversed wave by nonlinear effects. Zeldovich *et al.*[1] showed experimentally that a nearly "time-reversed" wave was produced by stimulated Brillouin scattering (SBS) in the backward direction of a ruby laser beam whose phase front had been deformed by an inhomogeneous medium. This wave was not perfectly time reversed as it was slightly downshifted in frequency by the acoustic frequency. Nosach *et al.*[2] used SBS to restore the coherence of a laser beam that had been amplified by an inhomogeneous amplifying medium. Recently, Yariv has proposed to "undo" the distortion of images transmitted by multimode optical fibers by parametric mixing in an acentric crystal.[3] He has shown that the mixed wave would be a time-reversed version of the propagated wave that, upon further propagation in the fiber, would evolve back into the original pattern at the entrance face of the fiber.[3] This mixing process could also be used to produce an unguided, time-reversed beam. In either case, limitations are placed on the beam-acceptance angles in this process by "phase-matching" requirements on waves that can mix efficiently in the crystal. In the case of the technique using nonlinear refraction, which we discuss below, neither a frequency shift nor phase-matching need play a role, thus allowing a more accurate time-reversed replication than is possible with SBS or parametric mixing. Also, on the basis of nonlinear optical coefficients known to date, the effect we discuss here can be produced with less laser pump power than either of the other effects.

In Sec. II we will show how, in the presence of counter-propagating pump waves, a beam will cause the generation of its time-reversed wave by the nonlinear refraction which exists in any medium. In Sec. III we show that the pump power levels required for efficient time-reversed generation are well within the capability of available sources. We also suggest a simple experimental arrangement for demonstrating the generation of a time-reversed wave by nonlinear refraction.

II. THEORY

Consider a monochromatic electromagnetic beam that has a complex wave front and is incident from the left on a transparent slab of nonlinear dielectric, as shown in Fig. 1. We assume that this beam has an electric field $\mathrm{Re}E_i(\mathbf{r})e^{-i\omega t}$ whose complex amplitude $E_i (i = x, y, z)$ is known at every point $\mathbf{r}$ in space. We will derive the amplitude $F_i(\mathbf{r})$ of the field radiated by the nonlinear electric polarization density $\mathrm{Re}P_i^{NL}(\mathbf{r})e^{-i\nu t}$ that is created in the nonlinear medium by the interaction of this beam with strong forward and backward plane waves at frequency ω_0 that also exist in the medium. That is, we assume the following electric field to be impressed in a homogeneous nonlinear medium:

$$\mathrm{Re}[E_i(\mathbf{r})e^{-i\omega t} + G_i e^{i\mathbf{k}_0\cdot\mathbf{r}-i\omega_0 t} + H_i e^{-i\mathbf{k}_0\cdot\mathbf{r}-i\omega_0 t}]. \tag{1}$$

By virtue of the (third-order) nonlinear susceptibility that exists in any medium, we have, at $\nu = 2\omega_0 - \omega$,

$$P_i^{NL} = X_{ij}E_j. \tag{2}$$

Here, as throughout, the summation convention is used for repeated space indices, and

$$X_{ij} = 6c_{ijkl}(-\nu, -\omega, \omega_0, \omega_0)G_k H_l, \tag{3}$$

where the c_{ijkl} are the nonlinear susceptibility coefficients defined by Maker and Terhune[4] and which are known, at least approximately, for many materials.[5] We will call the oppositely traveling plane waves at ω_0

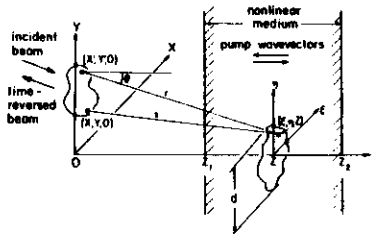

FIG. 1. Schematic and nomenclature for calculation of time-reversed wave fields.

the "pump" waves, as their amplitudes determine the magnitude of the nonlinear susceptibility X_{ij}.

Now we wish to calculate the electromagnetic field amplitude F_i generated at a point (x, y, z) far in front of the medium by P_i^{NL}, and show that, when $\omega = \omega_0$, F_i is proportional to the complex conjugate E_i^* of the incoming wave front at the same point. That is, the generated wave is the "time-reversed" wave. We can, without loss of generality, take the transverse frontal plane, in which we will demonstrate this relation, to be at $z = 0$, as shown in Fig. 1. For simplicity we will assume that, even though the nonlinear medium exists only between $z_1 < z < z_2$ (see Fig. 1), the linear refractive indices are the same inside and outside the medium. (Corrections for reflection and refraction at dielectric interfaces can be made later.) The incident wave amplitude at a point (ξ, η, z) inside the nonlinear medium may then be written simply in terms of its "initial" amplitude at the point $(x', y', 0)$. We assume these two points to be separated by a distance r much larger than a wavelength. The Fresenel-Kirchoff diffraction formula gives

$$E_i(\xi, \eta, z) = -ik \int\int dx'\,dy' E_i(x', y', 0) K e^{ikr}/(2\pi r), \tag{4}$$

where $k = n_1\omega/c$, n_1 being the refractive index for this wave, and $K = (1 + \cos\theta)/2$, θ being the angle between the ray along r and the z axis, as shown in Fig. 1. The nonlinear polarization density, which results from (4) substituted in (2), will radiate to give an electric field amplitude F_i at the point $(x, y, 0)$ in its far field:

$$F_i(x, y, 0) = q^2 \int_{z_1}^{z_2} dz \int\int d\xi\, d\eta T_{ij} X_{jk} E_k^*(\xi, \eta, z) e^{iqs}/s. \tag{5}$$

Here $q = n_2\nu/c$, n_2 being the refractive index for the radiated wave at ν, and s is the distance between $(x, y, 0)$ and (ξ, η, z). The operator T_{ij} takes the transverse part of the vector source, which is essentially its projection on a plane perpendicular to the incident beam.

After substituting (4) into (5), one finds that the integral over ξ and η can be performed nearly exactly under conditions which are commonly obtained in practice. To see this, we expand the phase function in powers of [the transverse incident-beam coordinates (ξ, η) divided by the distance z between the radiating and initial planes]

$$qs - kr = \Delta k z + \tfrac{1}{2}(q\rho^2 - k\rho'^2)/z + (k\mathbf{x}' - q\mathbf{x}) \cdot \boldsymbol{\xi}/z + \tfrac{1}{2}\Delta k \sigma^2/z + O[k\sigma^4/z^3]. \tag{6}$$

Here, $\Delta k = q - k$ and $\mathbf{x}$, $\mathbf{x}'$, and $\boldsymbol{\xi}$ are two-dimensional vectors, whose coordinates are (x, y), (x', y'), and (ξ, η), and whose magnitudes are ρ, ρ', and σ, respectively. The first two terms in the rhs of (6) are not functions of ξ and η; the next is the important term. So that we may neglect the terms in (6) of order σ^2 and higher, we will assume that the incident beam is contained inside a circle of radius d in the ξ, η plane, and that both of the following conditions are satisfied:

$$z \gg d^2\Delta k \tag{7}$$

and

$$z \gg kd^4/z^2. \tag{8}$$

It is seen that, since $\Delta k \sim k$, these conditions require that the nonlinear interaction region be a minimum distance from the initial plane at $z = 0$, but not so far as the Fraunhofer diffraction region. In performing the integral over ξ and η we will assume that $(rs)^{-1}$ does not vary with ξ and η within d and replace it by its average, which we call $(\overline{rs})^{-1}$. We treat K similarly, replacing it by $\bar{K}$. Then, with (7) and (8), the integral over ξ and η in (5) gives a delta function. When (4) for E_i^* is substituted in (5), the (x', y') integral may be performed trivially to yield

$$F_i(x, y, 0) = 2\pi i q^2 k^{-1} \int_{z_1}^{z_2} dz\, e^{i\Delta kz}\, \xi(z)\, T_{ij} X_{jk} E_k^*\left(\frac{q}{k}x, \frac{q}{k}y, 0\right), \tag{9}$$

where $\xi = \bar{K}z^2/\overline{rs}$. We have assumed that the product $G_k H_l$ of the amplitudes of the strong, oppositely traveling, pump waves at ω_0 was independent of ξ and η at given z, at least over the area of the incident beam E_i. However, the amplitudes G_i and H_i (and hence, X_{ij}) may still vary with z and affect the integral in (9).

The important consequence of (9) is that F_i is proportional to E_k^* at the same point (if $k = q$), or at a nearby point (if $k \neq q$), in space. That is, if $k = q$, a time-reversed or phase-conjugate wave is generated in this process. When $k \neq q$, a magnified and displaced replica of this wave results. There are no phase-matching requirements here, so a quite divergent beam can be "time reversed." We proceed to estimate the beam powers that would be necessary to obtain a given efficiency of generation of the time-reversed wave.

III. NUMERICAL EXAMPLE

To estimate the pump-wave powers necessary to produce a desired time-reversed wave, consider the practical case where (1) the incident beam is nearly colinear with the pump beams ($\theta \ll 1$), (2) $k = q$, and (3) the pump amplitudes do not vary appreciably in the region of the nonlinear medium where they overlap the incident beam. Then $\xi \sim 1$, $\Delta k = 0$, $T_{ij} \sim \delta_{ij}$, and (9) reduces to

$$F_i(\mathbf{r}) = 2\pi i k L X_{ij} E_j^*(\mathbf{r}). \tag{10}$$

where $L = z_2 - z_1$ is the thickness of the nonlinear medium, and $\mathbf{r}$ is assumed to be far enough in front of the medium so that conditions (7) and (8) are satisfied. From (10) we see that the ratio R of conjugate-wave power to incident-wave power is

$$R = I_G I_H \beta^2 L^2, \tag{11}$$

where

$$\beta = |96\pi^2 c^{-2} \omega c_{ijkl} f_i^* e_j^* X_{kl} h_l|. \tag{12}$$

here, f_i, e_i, g_i, h_i are the complex, normalized, polarization vectors of the waves ($e_i = E_i/|E_j^* E_j|^{1/2}$, etc.), and I_G and I_H are the intensities of the forward and backward pump waves. We have assumed that the time-reversed wave has an intensity small enough so as not to perturb appreciably the other wave intensities, i.e., $R \ll 1$.

For CS_2, one of the most optically nonlinear of

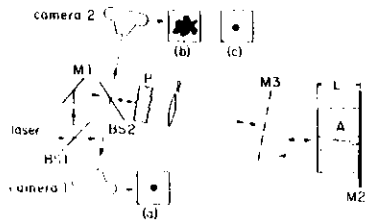

FIG. 2. Schematic diagram of apparatus described in text for observing generation of a time-reversed wave by nonlinear refraction in medium A.

liquids, $c_{xxxx}(-\omega, -\omega, \omega, \omega) \sim 2 \times 10^{-12}$ esu.[5] At 6943 A this would imply by (12) that $\beta \sim 6 \times 10^{-3}$ cm/MW. Grischkowsky and Armstrong have observed that for ω near the $^2P_{1/2}$ resonance in rubidium vapor, the c coefficient (and β) was nearly four orders of magnitude greater, implying $\beta \sim 30$ cm/MW near 7950 A.[6] With this latter figure as an example, we see from (11) that to obtain 10% conversion to a time-reversed wave ($R = 0.1$) in a 10 cm length of medium, the pump intensities required would be $I_G \sim I_H \sim 1$ kW/cm^2. The 2 mm diameter dye-laser beam of several kilowatts, which was used in Ref. (6) to observe the nonlinear index, would certainly satisfy this requirement.

In order to demonstrate the generation of a time-reversed wave with a single monochromatic laser source, one might employ an arrangement as shown in Fig. 2. A single-mode monochromatic laser source is directed into the nonlinear medium A. The mirror M2 reflects this beam back through the medium creating forward and backward plane-pump waves of nearly the same amplitude. Beam splitter BS1 and mirror M1 direct a portion of the laser source through a phase-distorting plate P and a focusing lens ℓ into the pumped region of the medium. Cameras 1 and 2 record the incident and backscattered beam patterns at beam splitter BS2. Camera 1 should show the "single-mode" pattern as in inset (a). If the nonlinear medium is removed and a back-reflecting mirror M3 placed at the focal point of lens ℓ, a distorted pattern, caused by double-passing P, will be recorded by camera 2 as indicated in inset (b). However, in the presence of the pumped nonlinear medium, camera 2 should record the same single-mode pattern (c) as recorded by camera 1. That is, the back-scattered beam is re-formed by plate P to have a smooth phase front and appear to be the time-reversed image of the incident beam.

In an experimental arrangement such as in Fig. 2, the linear refractive index of the medium A may not match the index outside its front surface. In this case, the length L of the medium must be long enough so that condition (8) is met for most of the interaction volume when the comparison plane $z = 0$ is considered to be just inside the entrance surface of the medium (i.e., $z_1 = 0$ in Fig. 1). Then the time-reversed wave front will have become well formed before exiting the medium A and continue back toward lens ℓ as a time-reversed replica (except for the small reflections at the dielectric interface which can be eliminated by coatings).

ACKNOWLEDGMENT

I would like to thank V. Wang for stimulating discussions on phase-conjugation processes.

*Supported by National Science Foundation Grant No. ENG 75 19335.

[1] B. Ya. Zel'dovich, V. I. Popovichev, V. V. Ragul'skii, and F. S. Faisullov, "Connection between the wavefronts of the reflected and exciting light in stimulated Mandel'stam–Brillouin scattering," Sov. Phys. JETP Lett. 15, 109–113 (1972).
[2] O. Ya. Nosach, V. I. Popovichev, V. V. Ragul'skii, and F. S. Faisullov, "Cancellation of phase distortions in an amplifying medium with a 'Brillouin mirror,'" Sov. Phys. JETP Lett. 16, 435–438 (1972).
[3] A. Yariv, "On transmission and recovery of 3-dimensional image information in optical waveguides," J. Opt. Soc. Am. 66, 301–306 (1976).
[4] P. W. Maker and R. W. Terhune, "Study of optical effects due to an induced polarization third-order in the electric field strength," Phys. Rev. 137, A801–A818 (1965).
[5] R. W. Hellwarth, *Third-Order Optical Susceptibilities of Liquids and Solids* (Pergamon, New York, 1976).
[6] D. Grischkowsky and J. A. Armstrong, "Self-defocusing of light by adiabatic following in rubidium vapor," Phys. Rev. Lett. 6, 1566–1570 (1972).

Minimum power requirements for efficient four-wave mixing and self-focusing of electromagnetic beams in glasses and fluids

R. W. Hellwarth
Departments of Electrical Engineering and Physics, University of Southern California, Los Angeles, California 90089-0484

(Received 12 September 1984)

We derive general expressions for the efficiency of cw phase conjugation by degenerate four-wave mixing and for the threshold power P_{cr} for cw self-trapping of coherent electromagnetic beams in fluids and glasses in which these effects arise predominantly from driven nuclear motions (molecular vibrations, molecular reorientation, elastic deformations, etc.). Apart from their dependence on beam frequency ω, medium temperature T, and refractive index n, these expressions are functions only of the integrated (polarized and depolarized) light scattering strengths versus scattering angle in the medium and the attenuation coefficient α. There is no other dependence on the scattering mechanism. When attenuation is entirely due to scattering, the expressions simplify and suggest that unprecedented low powers (in the microwatt regime for microwaves) can produce self-focusing and strong phase conjugation, as well as other beam mixing effects, when beam geometries are optimized in the scattering medium. In this case we find, for example, $P_{cr} \sim nk_BT\omega^2/c\alpha$ (k_B is Boltzmann's constant and c is the velocity of light) provided that there is significant beam diffraction in length α^{-1}. Our results also apply to some other media such as electron plasma.

AWR235 1985 PACS numbers 42.65.Bp 42.65.Gv

I. INTRODUCTION

The connection between spontaneous inelastic scattering of electromagnetic waves and coherent nonlinear propagation effects has long been exploited in nonlinear optics. Recently, Smith, Ashkin, and Tomlinson[1] demonstrated that a liquid suspension of 234-nm latex spheres in water, designed for high scattering ($\alpha \sim 15$ cm^{-1}), had a remarkably high nonlinear index ($\sim 10^5$ times that of CS_2) at the 515-nm argon laser wavelength. They observed cw phase-conjugation efficiency of order 0.5% using degenerate four-wave mixing with two 50-mW pump beams in the "artificial Kerr medium."[1] Ashkin, Dziedzic, and Smith[2] demonstrated cw self-focusing of 515-nm beams in less than the attenuation length $\alpha^{-1}(\sim 2$ mm) in similar suspensions, observing a threshold power of order 1 W, independent of beam diameter as is expected if the refractive index change equals a nonlinear index n_2 times the optical intensity I. They noted importantly that n_2 was proportional to the attenuation α cm^{-1} due to scattering.[2] Smith, Maloney, and Ashkin[3] estimated the constant of proportionality in terms of the difference between the refractive indices of a suspended particle and the liquid, finding satisfactory agreement with experiment. We generalize their expression in the course of this paper, in which we study the question: what limits, if any, are placed on the phase-conjugation efficiency and self-focusing thresholds of a fluid or glass that scatters light with arbitrary angular asymmetry and depolarization function, by virtue of the competition between the nonlinear coupling (proportional to the scattering strength) and the negative effects of the beam attenuation from the same scattering. We obtain a general expression for all components of the third-order nonlinear optical susceptibility tensor in terms of integrated (over frequency) scattering cross sections alone, independent of the scattering mechanism. Using this expression in standard treatments, we conclude that the same cw nonlinear effects will be found in any fluid or glass, having the same depolarized and polarized scattering coefficients $\sigma_\perp(\theta)$ and $\sigma_\parallel(\theta)$ cm^{-1}, regardless of the scattering mechanism, be it orientational or vibrational fluctuations, opalescence, concentration fluctuations in mixtures, aerosols,[4] etc. For example, efficient phase conjugation of 1-cm radiation is predicted with pump beam intensities less than a picowatt per square centimeter.

Here, we show that any transparent medium in thermal equilibrium at temperature T which attenuates an electromagnetic beam more by scattering than by absorption will phase conjugate a beam by degenerate four-wave mixing,[5] achieving power reflectivity R of order unity with relatively small pump powers. Specifically, we will show that, in such scattering with the usual beam configuration of Fig. 1, and with pump intensities I_1 and I_2 low enough so that R does not exceed ~ 0.5,[6]

$$R = \xi_1 \eta^2 I_1 I_2 / I\bar{I} \ , \tag{1}$$

where ξ_1 is a dimensionless function of the degree of depolarization and anisotropy of scattering only, which we will show is of order unity when light scattering is isotropic (but possibly orders-of-magnitude larger for anisotropic scatter-

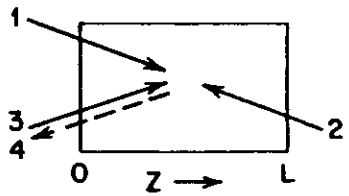

FIG. 1. Schematic of beam geometry for phase conjugation by degenerate four-wave mixing.

ing);

$$I_0 = n^2 k_B T \omega^2 / c^2 \ , \tag{2}$$

where n is the refractive index, k_B Boltzmann's constant, ω the electromagnetic beam (angular) frequency, c the velocity of light in vacuum, and

$$\eta = \gamma_{\rm re}^2 e^{-\alpha L/2}(1 - e^{-\alpha L})/L^2 \tag{3}$$

achieves its maximum value of unity when the interaction length L in the scattering medium is equal $2\alpha^{-1}$ (i.e., two attenuation lengths), where α is the intensity attenuation coefficient for beams of frequency ω. This may be expressed as the sum of the parts α_a arising from absorption and σ arising from scattering:

$$\alpha = \alpha_a + \sigma \ . \tag{4}$$

Note that σ, sometimes called the total scattering cross section per unit volume, equals the fraction of photons scattered per unit length to photons which are generally of slightly different frequency. When the scattered photons have frequencies differing from ω by shifts of order $\pm\Delta$, the response time of the phase-conjugating mirror, or of the self-focusing, will be of order Δ^{-1}.

From (1) we expect to achieve efficient phase conjugation in scattering media with lower intensities at longer wavelengths. For example, (1) predicts pump intensities of order 10^{-4} W/cm^2 for strong conjugation of 10-μm radiation, and predicts intensities of order 10^{-13} W/cm^2 for conjugating 1-cm microwave radiation. Realization of media with convenient scattering lengths α^{-1}, and having $\alpha_a < \sigma$, should be possible. For example, liquid chloroform has an absorption length ~ 6 mm at the carbon dioxide laser wavelength of 10.6 μm, and, being a polar liquid, should be capable of suspending enough micron-size rods (e.g., gold) to attenuate such a beam in less than 6 mm by scattering from orientational fluctuations. A convenient interaction length L of several millimeters or less in such a suspension should achieve phase conjugation with efficiencies approaching those in (1), at heating rates $2\alpha_a I_1$ much less than are met in dye lasers. The response time of such a medium will be the orientational relaxation time of the scattering rods, which should be, for example, of the order-of-magnitude of milliseconds for micron-size rods.[7]

We also show that, assuming the critical power P_{cr} for self-focusing of monochromatic linearly polarized radiation is given by $5.14\, c^2/(\omega^2 n n_2)$,[8] then

$$P_{cr} = \frac{1.24 n k_B T \omega^2 \xi_2}{c\sigma} \ , \tag{5}$$

where ξ_2 is a dimensionless function of scattering anisotropy and depolarization only, which equals unity for isotropic polarized scattering (the case studied in Refs. 1–3). From (5) we would expect for example, to produce self-focusing of X band (3 cm) microwaves from a 2-m-diam antenna, in such a medium having $\sigma = 5$ km^{-1}, with 14 μW of power.

II. THEORY

We will consider only fluids and glasses. These have the simplest, though nontrivial symmetry. To establish (1) for such media we first write the usual formula for the complex phase-conjugate-amplitude reflectivity r, which is proportional to $\eta\chi^{(3)}/\alpha$.[5] We then relate the appropriate third-order nonlinear susceptibility $\chi^{(3)}$ to the real scalar response functions $a(t, \bar{\Sigma})$ and $b(t, \bar{\Sigma})$ which describe nuclear motion in the Born-Oppenheimer regime in which $\chi^{(3)}$ is negligibly affected by electronic excitations. (Purely electronic nonlinearities contribute negligibly to $\chi^{(3)}$ in the regime of interest here.) It is well known that the a and b functions can be determined from the exponential "Raman" gain at frequency ω that is stimulated by a "pump" beam at frequency ν, if specified at all ω and for all relative beam directions and polarizations.[9] It is also well known that this Raman gain is linearly related to ordinary Raman scattering cross sections.[10] We will show that the nonlinear $\chi^{(3)}$ that governs cw phase conjugation is proportional to a weighted average $\bar{\sigma}$, depending on beam polarization, of ordinary Raman scattering cross sections at angles θ and $\pi - \theta$. The "isotropic scattering" limit, where these cross sections depend only on beam polarization, and not otherwise on the scattering wave vector $\bar{k}$, has been treated previously.[9] Here, we will sometimes be interested in media caused to be highly scattering by particles having size of the order of a wavelength, for which we must extend the theory to anisotropic scattering. Since α is also proportional to σ in the media of interest here, the maximum magnitude of the reflectivity $r \propto \chi^{(3)}/\alpha$ does not depend on the scattering mechanism, and we find the simple limit of (1).

We consider the plane-wave description of phase conjugation by degenerate four-wave mixing depicted in Fig. 1 and assume the angle between beams 1 and 3 to be much less than one radian. The optical field $\mathcal{E}_i$ ($i = x,y,z$) in the medium can be represented by

$$\mathcal{E}_i(\bar{X}t) = \mathrm{Re}\{e_{i1}E_1 \exp(i\bar{k}_1\cdot\bar{X} - \alpha z/2) + e_{i2}E_2\exp[i\bar{k}_2\cdot\bar{X} - \alpha(L-z)/2] + e_{i3}E_3\exp(i\bar{k}_3\cdot\bar{X} - \alpha z/2) + e_{i4}E_4\exp(i\bar{k}_4\cdot\bar{X} + \alpha z/2)\} \ . \tag{6}$$

The complex polarization vectors (which must be proper vectors of the linear dielectric tensor) are normalized so that $e_{i1}^* e_{i1} = 1$, etc. (Repeated space indices are assumed to be summed throughout.) Using the usual convention, the component of the nonlinear polarization density $\mathcal{P}_i^{\rm NL}(\bar{X},t)$ along vector e_{i4} that generates the phase conjugate wave E_4 has complex amplitude

$$P_4 = 6\chi^{(3)} E_1 E_2 E_3^* \exp[i(\bar{k}_1 + \bar{k}_2 - \bar{k}_3)\cdot\bar{X} - \alpha(L+z)/2] \ . \tag{7}$$

where, in terms of the usual nonlinear susceptibility tensor c_{ijkl}

$$\chi^{(3)} = c_{ijkl}(-\omega,\omega,\omega,-\omega) e_{i4}^* e_{j1} e_{k2} e_{l3}^* \ . \tag{8}$$

In the absence of $\chi^{(3)}$, E_1, E_2, E_3, and E_4 are constants. With $\chi^{(3)}$, transient and steady-state (cw) solutions for these amplitudes have been found in a variety of approximations, with and without nonlinear components other than (7) which may be pertinent.[5] For our purposes it will suffice to

assume the conjugate wave E_4 disturbs the others negligibly, nor do they disturb each other. This approximation has been found to be accurate for power reflectivities $R = |r|^2 = |E_4/E_3|^2$ up to ~ 0.5.[4] We also consider only the steady-state solution quantitatively, for which Maxwell's equations give directly[5]

$$r = -\tfrac{3}{2}i\pi\omega\chi^{(3)}E_1E_2\pi/(\tfrac{1}{2}nc\alpha) \quad . \tag{9}$$

A useful expression of the part of the third-order polarization density $\mathscr{P}_i^{NL}$ arising from nuclear motions in fluids and glasses is obtained by noting that it is the quantum average $\langle \chi_{ij}(\bar{x},t)\mathscr{E}_j(\bar{x},t)\rangle$ calculated to third order in $\mathscr{E}$, using the time-dependent interaction potential

$$-\tfrac{1}{2}\int d^3x'\,\mathscr{E}_i(\bar{x}',t)\chi_{ij}(\bar{x}',t)\mathscr{E}_j(\bar{x}',t)$$

(in esu). Clearly $\mathscr{P}_i^{NL}(\bar{x},t)$ will have only terms parallel to $\mathscr{E}_i(\bar{x},t)$ and $\mathscr{E}(\bar{x}',t')(t'<t)$, the only vectors available. This average results in a $\mathscr{P}_i^{NL}$ of the form

$$\mathscr{P}_i^{NL}(\bar{x},t) = \int_{-\infty}^{\infty}dt'\int d^3x'\{\mathscr{E}_i(\bar{x},t)\mathscr{E}_j^2(\bar{x}',t')a(t-t',\bar{x}-\bar{x}') + \mathscr{E}_i(\bar{x}',t')\mathscr{E}_j(\bar{x},t)\mathscr{E}_j(\bar{x}',t')b(t-t',\bar{x}-\bar{x}')\} \quad . \tag{10}$$

The functions a and b may be calculated directly from the quantum average, or its hydrodynamic or classical limits, in the tradition of Brillouin, Born, and Placzek. For our purposes it is more useful to use (10) to obtain both an expression for $\chi^{(3)}$ and for the stimulated gain function, thereby linking $\chi^{(3)}$ to the spontaneous scattering functions. Inserting (6) in (10) and identifying P_4, one has, by comparing with (7), that

$$\begin{aligned}24\chi^{(3)} = {} & (42,13)\{2A_0(13)+B_0(23)\}\\ & +(41,23)\{2A_0(23)+B_0(13)\}\\ & +(43,12)\{B_0(13)+B_0(23)\}\end{aligned} \quad , \tag{11}$$

where $(42,13) = e_4^*e_2e_1e_3^*$, etc., and $A_0(13)$ represents the Fourier transform

$$A_0(\bar{k}) = \int_{-\infty}^{\infty}dt\int d^3x\exp(i\Delta t - i\bar{k}\cdot\bar{x})a(t,\bar{x}) \tag{12}$$

evaluated at $\Delta = 0$ and $\bar{k} = \bar{k}_1 - \bar{k}_3$. Similarly $B_0(23) = B_0(\bar{k}_2 - \bar{k}_3)$, etc.

In the regime of interest here, where the light scattering is predominantly to frequency shifts much smaller than both $k_BT/\hbar$ and the laser frequency ω itself, the coefficients in (11) are related to the total polarized and depolarized differential light scattering cross sections per unit volume $\sigma_\parallel(\theta)$ and $\sigma_\perp(\theta)$ at scattering angle θ (and its complement $\bar{\theta} = \pi - \theta$) by the relation (A8) derived in the Appendix. Substituting (A8) in (11) gives

$$24\chi^{(3)} = c^4\bar{\sigma}/(\omega^4k_BT) \quad , \tag{13}$$

where

$$\begin{aligned}\bar{\sigma} = {} & (42,13)\{\sigma_\parallel(\theta)-2\sigma_\perp(\theta)+\sigma_\perp(\bar{\theta})\}\\ & +(41,23)\{\sigma_\parallel(\bar{\theta})-2\sigma_\perp(\bar{\theta})+\sigma_\perp(\theta)\}\\ & +(43,21)\{\sigma_\perp(\theta)+\sigma_\perp(\bar{\theta})\}\end{aligned} \quad . \tag{14}$$

Using this result in (9) for the amplitude reflection r, and taking the absolute square to obtain the phase-conjugate power reflectivity R, gives the result (1) with

$$\xi_1 = (\tfrac{3}{2}\pi^2\bar{\sigma}/\tfrac{2}{3}\sigma)^2/27. \tag{15}$$

Note, from the angle dependence (A3) of the scattering cross section, we have that the total scattering cross section per unit volume σ (the scattering attenuation coefficient) is related to the differential cross sections by the integral over solid angle Ω:

$$\sigma = \int d\Omega\,[\sigma_\perp(\theta)(1+\cos^2\phi)+\sigma_\parallel(\theta)\sin^2\phi] \quad . \tag{16}$$

where ϕ is the angle between one possible incident (linear) polarization vector and the direction of scattering.

When the scattering particles are much smaller than a wavelength, the polarized and depolarized scattering cross sections (per unit volume per unit solid angle) $\sigma_\parallel$ and $\sigma_\perp$ are constants independent of scattering angle θ, and (16) gives the familiar expression $8\pi(\sigma_\parallel+2\sigma_\perp)/3$. When all beam polarizations are linear and parallel in this "isotropic" scattering limit, (15) gives ($\rho = \sigma_\perp/\sigma_\parallel$)

$$\xi_1 = [\tfrac{1}{2}\pi/(9+18\rho)]^2 \quad , \tag{17}$$

nearly unity for the interesting case of scattering from orientational fluctuations in fluids, for which $\rho = \frac{1}{4}$.

The change in refractive index (n_2) for a linearly polarized plane wave is easily seen from (10) to give[3] where

$$n_2 = 8\pi^2[A_0(0)+B_0(0)]/n^2c \quad . \tag{18}$$

With the relations (A8) this may be expressed as

$$n_2 = \frac{3\sigma c^4}{8\xi_2 nk_BT\omega^4} \quad , \tag{19}$$

where the parameter

$$\xi_2 = 3\sigma/[8\pi\sigma_\parallel(0)] \quad , \tag{20}$$

which is a function of scattering depolarization and anisotropy only, becomes unity for isotropic polarized scattering, the case studied in Refs. 1–3. The exact expressions (19) and (20) reduce to the approximate expression (4) of Ref. 3 for a suspension of small spherical particles, in the limit where ξ_2 approaches unity and the refractive index of the particles is close to that of the suspending liquid. It is (19) and (20) that give directly our result (5) for the threshold power for self-focusing or self-trapping of a Gaussian beam when the attenuation length α^{-1} is much larger than the distance in which normal diffraction becomes significant.

We note that any nonlinear effect in transparent fluids or glasses that arises mainly from nuclear motions and can be described with the nonlinear susceptibility tensor $\chi_{ijkl}(-\omega,\omega,\omega,-\omega)$, can be predicted from light scattering data by using (A8) to evaluate the nonlinear polarization density (10). To obtain the time dependence of such effects, the details of the frequency dependence of the light scattering must also be known. Saturation effects (i.e., $\chi^{(n)}$ for $n>3$) cannot be obtained from light scattering and must be considered separately for each material.

There are other classes of scattering media, such as an electron plasma, or a multicomponent plasma of charged particles, for which the nonlinear polarization density is approximately of the form (10). Since the relation (A1) does not depend on the type of excitations responsible for the scattering, the results we have derived here apply to these other media as well.

In conclusion, we have derived expressions (1) for the efficiency of cw phase conjugation by degenerate four-wave mixing, and (5) for the threshold of cw self-trapping of beams in a fluid or glass, in which electronic transitions and nonlinearities have no effect on light propagation (and also in certain plasma), and by which light is scattered with arbitrary function of scattering angle and state of scattered polarization. The results suggest that these and other nonlinear effects can be produced with unprecedented low powers with proper beam geometry in any medium in which beam attenuation arises more from scattering than from absorption.

ACKNOWLEDGMENTS

We would like to acknowledge the support of the Air Force Office of Scientific Research through Contract No. F49620-83-C-0045 and of the National Science Foundation under Grant No. ECS-8114754.

APPENDIX

When a material in thermal equilibrium is transparent enough so that there is a well-defined differential scattering cross section $d^2\sigma_{\alpha\beta}/d\Omega\,d\omega$ [per unit volume per unit solid angle per (angular) frequency interval] to scatter a photon from proper polarization state $e_{\alpha i}$ and wave vector $\bar{k}_\alpha$ to proper state $e_{\beta f}$ and wave vector $\bar{k}_\beta$, then[3,10]

$$\frac{d^2\sigma_{\alpha\beta}}{d\Omega\,d\omega_\beta} = \frac{g_{\alpha\beta}\hbar\omega_\alpha\omega_\beta^3n_\alpha n_\beta}{I_\alpha 8\pi^3c^2[1-\exp(-\hbar(\omega_\alpha-\omega_\beta)/k_BT)]} \quad , \tag{A1}$$

where $g_{\alpha\beta}$ is the stimulated exponential gain per unit length experienced by the β beam due to the presence of intensity I_α in the α beam. $|\bar{k}_\alpha| = n_\alpha\omega/c$, etc., $\hbar = h/2\pi$.

If one uses Eq. (10) to calculate the stimulated gain $g_{\alpha\beta}$ in a fluid or glass, one finds[12] ($\mathcal{I}_\alpha = n_\alpha c|\mathscr{E}_\alpha|^2/8\pi$)

$$g_{\alpha\beta} = \mathrm{Im}\,\pi\omega_\beta D_\Delta(\alpha\beta)|\bar{k}_\alpha|^2/n_\beta c \tag{A2}$$

where

$$D_\Delta(\alpha\beta) = 2A_\Delta(\alpha\beta)|e_{\beta f}^*e_{\alpha i}|^2 + B_\Delta(\alpha\beta)(1+|e_{\beta f}e_{\alpha i}|^2) \quad . \tag{A3}$$

Here, $\Delta = \omega_\alpha - \omega_\beta$ is the Stokes shift and the argument $(\alpha\beta)$ signifies $\bar{k} = \bar{k}_\alpha - \bar{k}_\beta$. Substituting (A2) in (A1) gives for the Born-Oppenheimer regime in fluids and glasses

$$\frac{d^2\sigma_{\alpha\beta}}{d\Omega\,d\omega_\beta} = \frac{\hbar\omega_\alpha\omega_\beta^3\,\mathrm{Im}D_\Delta(\alpha\beta)}{\pi c^4[1-\exp(-\hbar\Delta/k_BT)]} \quad . \tag{A4}$$

The usual integrated differential polarized scattering cross section is defined for scattering angle θ in optically inactive media by

$$\sigma_\parallel(\theta) = \int_0^\infty d\omega_\beta(d^2\sigma_{\alpha\beta}/d\Omega\,d\omega_\beta) \quad , \tag{A5}$$

in which both incident and scattered polarizations are "π," i.e., perpendicular to the scattering plane. The depolarized cross section $\sigma_\perp(\theta)$ is defined similarly, with one polarization perpendicular to, and the other lying in, the scattering plane. Note that, for optically active media, one may need to employ the cross sections for right-to-right and right-to-left circularly polarized beams; this was one motivation for writing (A1) to (A4) for arbitrary proper polarizations.

From (A3) we see that, for optically inactive fluids and glasses,

$$\sigma_\perp(\theta) = \int_{-\infty}^{\infty}\frac{d\Delta\hbar\omega_\alpha\omega_\beta^3\,\mathrm{Im}B_\Delta(\bar{k}_\Delta)}{\pi c^4[1-\exp(-\hbar\Delta/k_BT)]} \quad , \tag{A6}$$

where we have recognized that $\bar{k}$ is, in general, a function of the scattered frequency ω at fixed scattering angle θ. We can neglect this dependence because all shifts Δ of interest here are less than ω_0. Since $B_\Delta(\bar{k})$ is a function only of the magnitude of $\bar{k}$ we can therefore use $B_\Delta(k_0)$ in (A6), where $k_0 = |\bar{k}_\alpha - \bar{k}_\beta|_{\Delta=0}$.

Strongly scattering media of interest here also scatter mainly to shifts Δ much less than both $k_BT/\hbar$ and ω. Since the Kramers-Kronig relation between the real and imaginary parts of A_Δ (and B_Δ) gives ($\mathrm{Re}A_0 = A_0$)

$$A_0 = \int_{-\infty}^{\infty}\mathrm{Im}A_\Delta\,d\Delta/\pi\Delta \quad , \tag{A7}$$

and similarly for B_0, we have from (A6) that ($\omega = \omega_\alpha$)

$$\sigma_\perp(\theta) \cong \omega^4k_BTB_0(k_0)/c^4 \quad . \tag{A8}$$

The relation (A8) also holds for $\sigma_\parallel(\theta)$ but with $B_0(k_0)$ replaced by $2[A_0(k_0)+B_0(k_0)]$. These are the desired relations between the differential scattering cross sections and the nonlinear coefficients in (11) which we need to write the important relations (13) and (14).

[1] P. W. Smith, A. Ashkin, and W. J. Tomlinson, Opt. Lett. 6, 284 (1981).
[2] A. Ashkin, J. M. Dziedzic, and P. W. Smith, Opt. Lett. 7, 276 (1982).
[3] P. W. Smith, P. J. Maloney, and A. Ashkin, Opt. Lett. 7, 347 (1982).
[4] A. J. Palmer, Opt. Lett. 5, 54 (1980).
[5] *Optical Beam Phase Conjugation*, edited by R. A. Fisher (Academic, New York, 1983).
[6] Generalizations of Eq. (1) to include pump beam depletion exist. These predict, for example, gain ($R > 1$) as has been observed in a variety of systems (see Ref. 5). However, no general treatment exists that takes into account self-focusing, optical Kerr effect and the other nonlinear effects expected to become strong when $R > 1$.
[7] F. Perrin, J. Phys. Radium 7, 1 (1956).
[8] R. Y. Chiao, E. Garmire, and C. H. Townes, Phys. Rev. Lett. 2, 138 (1965), *ibid.* 14, 1056(E) (1965).
[9] R. W. Hellwarth, J. Cherlow, and T. T. Yang, Phys. Rev. B 11, 964 (1975).
[10] R. W. Hellwarth, Phys. Rev. 130, 1850 (1963).
[11] P. D. Maker and R. W. Terhune, Phys. Rev. 137, A801 (1965).
[12] R. W. Hellwarth, *Progress in Quantum Electronics* (Publisher, location, 1977), Vol. 5, Pt. 1.

Appendix III

23

Generation of time-reversed waves by nonlinear refraction in a waveguide[a)]

S. M. Jensen and R. W. Hellwarth

Electronics Sciences Laboratory, University of Southern California, Los Angeles, California 90007
(Received 12 May 1978; accepted for publication 19 June 1978)

We have generated, essentially instantaneously, a time-reversed replica (phase-conjugate) of a monochromatic optical wave (at 6943 Å) by directing the wave into a CS_2-filled waveguide where it interacts via the third-order nonlinear susceptibility with counterpropagating pump waves of the same frequency. This method is shown to have advantages over a similar replication process which has been observed with unguided waves in an infinite homogeneous medium.

PACS numbers: 42.30.Va, 42.65.Jx, 42.65.Cq

The time-reversed replica of any essentially monochromatic electromagnetic image-bearing beam can be generated by the nonlinear interaction, in a unbounded transparent medium, of the beam with two counterpropagating "pump" waves at the same frequency.[1-6] This replication (or "phase-conjugation") process, which is a form of "degenerate four-wave mixing", has been previously studied with unguided beams (free waves) in "infinite" media.[3-6] Here, we report the generation of the time-reversed replica of an optical beam by coupling it into a dielectric waveguide where it interacts with the counterpropagating pump waves through nonlinear refraction. We find, as has been predicted,[7] that (1) the pump power required is much less than for free waves, (2) the guided pump waves can be multimode without spoiling the fidelity of replication (in fact, the beam to be replicated can serve as one of the pump waves), (3) the alignment of the beams entering the guide is not critical, and (4) the only requirement on the guiding structure is that it not attenuate or scatter any of the beams too drastically.

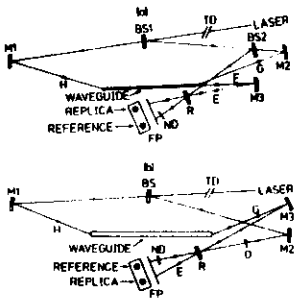

FIG. 1. Schematic of apparatus discussed in text. (a) Three-beam arrangement with pump beams G and H interacting in CS_2-filled hollow glass waveguide with beam F to generate its time-reversed replica E. Isolation is supplied by a 30-nsec time delay TD. Beamsplitter BS1 reflects 55%. Mirrors M1, M2, and M3 have radii of 1, 1, and 0.5 m, respectively, and focus the beams on to the ends of the 80-cm-long guide. About 8% of beam G is split by BS2 to form F. (b) Two-beam arrangement whereby image-bearing beam G interacts in the aforementioned guide with beam H to generate its time-reversed replica E. Mirrors M1 and M3 have radii of 36 cm and focus the beams onto the ends of the waveguide. Beamsplitter BS reflects 55%, and R reflects 75% while transmitting 24%.

Our first experimental arrangement, shown in Fig. 1(a), employed two pump beams, G and H, focused into opposite ends of a dielectric waveguide which consisted of a 0.4-mm i.d. by 80-cm-long glass tube filled with liquid CS_2. An input (image-bearing) beam F was focused into the same end of the guide as was beam G. All beams originated from the same Q-switched ruby laser. The beamsplitter R directed a beam E backscattered along F onto photographic plate FP where it was compared with a reference fraction of beam F [as shown in Fig. 2(a), upper plate] to verify that it was a time-reversed replica of beam F. A critical test was the replication, recorded in Fig. 2(a), of the fringes formed from the interference between reflections from parallel front and back surfaces of beamsplitter BS2. The absence of polarization scrambling (checked also with a polarizer) and of phase distortions in the replicated beam are reflected in the fidelity and high contrast ratio of the fringes replicated. In Fig. 2(a) the reference beam energy was 0.42 times that of the input F beam, showing that the energy in the replica E was about 0.4 that in F. Here, a 20-nsec laser pulse supplied about 35 kW peak power to each pump wave. The replica beam E disappeared when either pump wave was absent, as shown in the lower plate of Fig. 2(a). The F, G, and H beams were focused to spots at the guide entrance which were much

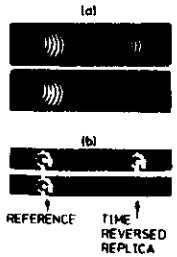

FIG. 2. Photographic images produced on Polaroid 410 film at film plate FP (see Fig. 1) by a single laser pulse. (a) Upper plate is from same arrangement but with beam H blocked. (b) Upper plate is from arrangement of Fig. 1(b); lower plate is from same arrangement but with beam H blocked.

a)Supported by the Air Force Office of Scientific Research under Grant No. 78-3479.

 0003-6951/78/3305-0404$00.50

smaller than the guide i.d., so that nearly all of each beam (except for ~2% dielectric reflection) was coupled into the guide. The G and H beams entered at about 10° to the guide axis. They emerged from the guide in hollow conical beams whose dimensions showed that about 10^4 transverse modes had been excited by each beam. (The total number of bound transverse modes was ~10^6.) Efficiency of replication was greatest when the forward pump beam G was adjusted so as to enter the guide within the cone of the exiting H beam.

In another experimental arrangement shown in Fig. 1(b), there was no third beam F; the pump beam G itself was observed to be replicated (phase conjugated) by its nonlinear interaction with a counterpropagating H beam when both are focused into the guide. A beam E backscattered along G was directed on to film plate FP by the partial reflector R, where it was compared with a reference fraction of the G beam, as in the upper plate of Fig. 2(b). That the backscattered E beam was essentially a phase-conjugate or time-reversed replica of the G beam was verified by placing various objects in the G beam [at position O in Fig. 1(b)] and observing their replicas in the E-beam patterns.

The reference beam patterns differed somewhat from those of the replicas because the film plate FP was not at the same effective distance from the object O for each beam. For example, one can see diffraction fringes in the reference beam pattern in Fig. 2(b) where none exist in the replica (E-beam) pattern, which replicates beam G very near the object O. The reference-beam fraction was 0.21 in this instance, showing that the replica energy was ~0.2 of that in beam G. Here, the G and H beams were 20-nsec pulses of about 25 kW peak power.

The efficiency, or effective reflectivity R, of the replication process may be defined as the ratio of the power in the replica beam to that in the beam being replicated. In both the geometries of Fig. 1, the efficiency R would rise with increasing pump power to about 0.5 before other nonlinear processes would intervene to spoil replication.

According to theory,[7] when $R < \frac{1}{2}$ in either geometry of Fig. 1,

$$R \cong \beta^2 L^2 P_G P_H \theta_{GH}/S^2, \tag{1}$$

where L and S are the length and area of the guiding region, respectively, P_G and P_H are the powers of the G and H beams, respectively, and θ_{GH} is the fraction of the energy in the G beam that is phase conjugate to the H beam inside the guide. If g_b and h_b are the complex amplitudes of excitation of guide mode b by the G and H beams, respectively,[7]

$$\theta_{GH} = |\Sigma_b g_b h_b|^2/\Sigma_c|g_c|^2\Sigma_d|h_d|^2. \tag{2}$$

If all beams are linearly polarized along the x axis, the coefficient β in Eq. (1) is given in esu in terms of the conventional nonlinear susceptibility tensor[8] $c_{ijkl}(-\omega_s, -\omega, \omega, \omega)$ by

$$\beta = |96\pi^2 c^{-2} n^{-2} \omega c_{xxxx}(-\omega, -\omega, \omega, \omega)|, \tag{3}$$

where n is the linear refractive index of the guide material on axis and ω is the angular frequency of the beams. When polarizations are not parallel inside the guide, other components of c_{ijkl} are involved. For the CS_2 medium used here at 6943 Å, $\beta \sim 6$ cm/GW[-1] (neglecting acoustic contributions), and we estimate from Eq. (1) that $\theta_{GH} \sim 10^{-3}$ in our experiments.

To approach theoretical efficiency, our ruby-laser source had to give a stable output over the time (~4 nsec) required for light to traverse the optical guide. When we made the laser fail this criterion by permitting it to oscillate in several axial modes (spaced by 1/60 cm^{-1}) the replica beam E was not observed.

The pump powers required here were nearly an order of magnitude less than we required for comparable replication efficiency R for free (unguided) waves in CS_2.[4] Furthermore, the number of resolution elements in a beam that could be replicated in our guide is almost the number of guide modes (~10^5). This is orders of magnitude larger than the number of free-space modes replicated at quoted power levels.[3,4] Of course, with guides of smaller i.d., pump-power requirements could be further reduced [see Eq. (1)] with a corresponding loss in the number of resolution elements that could be replicated.

In summary, we have demonstrated the generation of time-reversed replicas (phase conjugation) of monochromatic image-bearing optical beams by the process of nonlinear refractive mixing in a waveguide with counterpropagating pump waves of the same frequency. With this process much less pump power is required, and the alignment and mode quality of the pump beams is much less critical than in the corresponding process with unguided beams.

[1] R. W. Hellwarth, J. Opt. Soc. Am. 67, 1 (1977).
[2] A. Yariv and D. M. Pepper, Opt. Lett. 1, 16 (1977).
[3] D. M. Bloom and G. C. Bjorklund, Appl. Phys. Lett. 31, 592 (1977).
[4] S. M. Jensen and R. W. Hellwarth, Appl. Phys. Lett. 32, 166 (1978).
[5] D. M. Bloom, P. F. Liao, and N. P. Economou, Opt. Lett. 2, 58 (1978).
[6] P. F. Liao, D. M. Bloom, and N. P. Economou (unpublished).
[7] R. W. Hellwarth, IEEE J. Quantum. Electron. (to be published).
[8] P. W. Maker and R. W. Terhune, Phys. Rev. A 137, 801 (1965).

IEEE JOURNAL OF QUANTUM ELECTRONICS, VOL. QE-15, NO. 2, FEBRUARY 1979

Appendix IV

Theory of Phase-Conjugation by Four-Wave Mixing in a Waveguide

ROBERT W. HELLWARTH, FELLOW, IEEE

(Invited Paper)

Abstract—We show that one can generate the time-reversed replica of an "input" monochromatic, image-bearing beam by coupling it into a waveguide where it interacts with counterpropagating multimode "pump" waves of the same frequency. The nonlinear electric polarization density that is third order in the propagating electric fields in the guide medium generates the replica by the process of "four-wave mixing." We show also that the input beam can serve simultaneously as its own pump beam. If the frequency ν of the backward pump beam is different from the frequency ω of the input beam, then the "phase-conjugate" to the input is generated at the entrance plane to the guide, and this radiates a replica of the input field, magnified by ω/ν, back along the input beam. The pump power required per resolution element to phase-conjugate a beam in a waveguide is orders-of-magnitude less than for the corresponding process with free (unguided) waves interacting in an infinite medium. Unlike the requirements for free waves, the pump waves do not need to be well aligned or single-mode to produce high fidelity in the replication process. Neither does the guiding structure or enclosed medium have to be precise in dimension or uniformity; the main requirements on the guiding structure being that it not attenuate the waves too heavily. Formulas are derived for the replication efficiency and fidelity in the various guided configurations. We also show how the process can be used: 1) to make a narrowband optical filter with a large acceptance solid angle; 2) to perform image-frequency conversion; 3) to obtain Raman and two-photon spectra of small samples; and 4) to achieve broadband optical amplification. We examine the conditions under which phase conjugation and these applications can be performed at several frequencies simultaneously. Limitations placed by the power-dependence of propagation constants are derived.

Manuscript received August 28, 1978. This work was supported by the Air Force Office of Scientific Research under Grant 78-3479 and the United States Army Research Office under Grant DAAG29-76-G-0295.

The author is with the Electronics Sciences Laboratory, University of Southern California, Los Angeles, CA 90007.

I. Introduction

THERE can exist in principle a time-reversed replica of any electromagnetic wave that propagates through an inhomogeneous, static, nonabsorbing medium having no permanent magnetism. Maxwell's equations are invariant to time reversal in this situation. This means, for example, that if a monochromatic wave exists whose electric field is $\mathrm{Re}\, \mathcal{E}(r) e^{-i\omega t}$ in a portion of a medium, there could also exist the time-reversed

0018-9197/79/0200-0101$00.75

replica Re $E(r)\,e^{i\omega t}$ in the same region. Since this replica also equals Re $E^*(r)\,e^{-i\omega t}$ (i.e., its amplitude is the complex conjugate of the original wave's amplitude) it is often called the "phase-conjugate" of the original wave. A wave at another frequency ν can also have its complex amplitude $F(r)$ be equal to $E^*(r)$ in one plane of space. Such a wave is also called a phase-conjugate to E. A phase-conjugate wave, once generated, has a wide variety of possible uses, such as restoration of the input beam after it has been distorted by passage through a randomly inhomogeneous medium [1], [2]. Several nonlinear optical effects, in a variety of configurations, have been demonstrated to be capable of generating excellent approximations to the phase-conjugate of a given wave [1]-[14]. It will be to a small subclass of potentially useful configurations that this paper will be devoted; namely, to the generation of a phase-conjugate of a free wave at the entrance plane of a waveguide, into which the wave is entirely coupled and in which it undergoes a form of "four-wave mixing" with counterpropagating pump waves. If the phase-conjugate wave generated is at the same frequency ω as the incident free wave, it will radiate a time-reversed replica back along the incident wave in front of the guide in that portion of space in which propagation is reversible. If the phase-conjugate is at a different frequency ν, it will resemble a time-reversed wave but with its field pattern magnified by (ω/ν) about the waveguide axis.

The nonlinear optical process of "four-wave mixing" which we will consider here to mediate the replication process (or phase-conjugation) in the guide is a process in which three waves (of amplitudes F, G, and H and frequencies ν, ω_G, and ω_H) mix via the third-order nonlinear susceptibility existing in any medium to generate a polarization density proportional to F^*GH and thereby generate a fourth wave at frequency $\omega = \omega_G + \omega_H - \nu$ [15]. When, as has often been the case experimentally, $\omega = \nu = \omega_G = \omega_H$, then the process has been called "degenerate four-wave mixing" [16]. We will show that, in order for this process to generate time-reversed replicas in the guide, two of these waves (the G and H waves) must be counterpropagating "pump" waves. The third F-wave then can be replicated in the fourth output wave. When the replication process involves "free" waves in an unbounded nonlinear medium, the pump waves must be nearly single-mode Gaussian beams which are precisely counterpropagating in order for the process to be of high fidelity [5], [6]. Yariv *et al.* [11] have pointed out also that, if one excites precisely the same single transverse mode in a waveguide with each of two counterpropagating pump waves, and if this pump mode does not change its shape along the guide, then a third wave launched in the guide will be replicated (phase-conjugated) with high fidelity.

In this paper we will study the replication process in a waveguide in which each of the two counterpropagating pump waves is comprised of more than one transverse guide mode, each exciting different transverse patterns in different relative amounts and phases than does the other as is most likely in practice. We find, among other things, that with multimode pumps, the replication process still has high fidelity, although with reduced efficiency from the case of single pump modes. However, as we will show, the efficiency with guided multimode pump beams can still be much higher than for free-wave phase-conjugation, with the added advantage that pump-beam alignment is no longer critical and acceptance solid angles become as large as the guide itself can accept.

In this paper, we will analyze two configurations by which phase-conjugation may be effected by four-wave mixing in a waveguide. The first, a "three-beam configuration," is illustrated schematically in Fig. 1(a). This is analogous to the free-wave configuration which employs three distinct beams: two counterpropagating pump beams G and H and an image-bearing input beam F.

The second configuration which we will analyze is the "two-beam configuration" illustrated in Fig. 1(b). This configuration has no analogue in free-wave interactions; here the image-bearing beam which is to be conjugated also serves as one of the pump beams. We will find that this configuration has several advantages and uses not shared by the first. The expectations of the theory we will present here for the high efficiency and fidelity of phase conjugation by both configurations has recently been confirmed experimentally [14]. The plan of this paper is as follows.

In Sections II–VI we analyze the configuration of Fig. 1(a) for the case that all beams have the same frequency ω. In Section II, we construct, and obtain a formal solution for, the equations for the E-beam generated in the guide. We assume a nonlinear polarization density that is cubic in the optical field, use the slowly varying envelope approximation for the E-beam, and assume the F-, G-, and H-beams are negligibly altered by the process. In Section III we show that terms which spoil phase-conjugation tend to cancel, and cancel more effectively the longer the guide, the higher the number of modes in the F-beam being replicated, and the more imperfect the guide; the basic criterion for phase-conjugation in this case being that at least one of the beams (F, G, and H) be well guided. In Section IV a formula for the fraction of the generated E-beam power that is not phase-conjugate to the F-beam is derived, and it is noted that this fraction is very much less than unity for conditions commonly met in practice. The efficiency of the replication process is shown in Section V to be proportional to the product of the following: the pump intensities, the square of the effective length of the guide, the inverse of the square of the cross-sectional area, the fraction of the H-beam that is phase-conjugate to the G-beam, and the square of a nonlinear susceptibility coefficient. In Section VI, it is pointed out that in an ideal guide which must have mode degeneracies, phase-conjugation can still take place by careful choice of polarization if the nonlinear medium is of high-enough symmetry.

The second "two-beam" configuration for phase-matching illustrated schematically in Fig. 1(b), is considered in Section VII where it is found that only a simple modification of the theory for the first case is required. A further generalization of the theory is given in Section VIII where the frequencies of the four waves being mixed are all allowed to be different. Phase conjugation still results. The potential usefulness of this case for realizing a tunable narrowband optical filter with a very large acceptance solid angle is analyzed. The application of two-frequency phase-conjugation to image-frequency conversion is examined in Section IX where the number of resolution elements that can be converted for a given change of image wavelength is derived. The absence of image conversion is also possible, and the conditions under which several frequencies can be made to generate phase-conjugate waves independently of each other, i.e., without appreciable interference in the guide, as derived in Section X. In Section XI we note that, because multiple-frequency phase-conjugation is sensitive to resonances in the nonlinear medium, and because the interaction volume in a waveguide can be quite small, the configurations of either Fig. 1(a) or (b) could be used for small-sample spectroscopy, of either Raman or two-photon resonances. Then in Section XII we describe how the configurations of Fig. 1 act as a broadband optical transistor. In Section XIII we derive the power dependence of the mode-propagation constants for the four waves involved and discuss how this dependence affects phase-conjugation. A summary of the salient features of phase conjugation by four-wave mixing in waveguides follows in Section XIV.

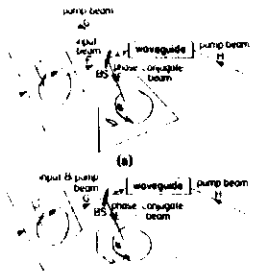

Fig. 1. Schematic illustrations of two arrangements for generating an optical beam E which is the phase-conjugate to an input image-bearing beam, by the process of "four-wave mixing" in a waveguide with counterpropagating pump beams G and H: (a) A three-beam configuration in which a separate beam F is phase-conjugated, thus producing an image replica as indicated. (b) A two-beam configuration in which the phase-conjugate of one pump beam G is generated.

II. Separate Image and Pump Beams

In the configuration illustrated in Fig. 1(a) for generating the time-reversed replica of a separate image-bearing monochromatic beam F, three waves (F and two pump waves G and H) are launched in a cylindrical optical waveguide to produce a total impressed electric field

$$E_i(t) = \mathrm{Re}\,[F_i(r) + G_i(r) + H_i(r)]\,e^{-i\omega t}; \quad i = x, y, z. \tag{1}$$

Inside the waveguide, we may express each of the three complex field-amplitude functions in terms of the normal-mode functions of the guide as follows. Hereafter repeated mode incides $(a, b, c \cdots)$ or space indices $(i, j, \cdots = x, y, z)$ are assumed to be summed unless otherwise stated.

$$F_i = e_{ai}(x, y)\, f_a \exp(ik_a z - \tfrac{1}{2}\alpha z) \tag{2a}$$

$$G_i = e_{ai}(x, y)\, g_a \exp(ik_a z - \tfrac{1}{2}\alpha z) \tag{2b}$$

$$H_i = e_{ai}(x, y)\, h_a \exp(-ik_a z + \tfrac{1}{2}\alpha z), \tag{2c}$$

where the guide attenuation coefficient is α.

The transverse mode functions e_{ai} and e_{bj} of any two modes a and b obey the orthogonality relation

$$\int dx\, dy\, e^*_{ai} e_{bi} = \delta_{ab}. \tag{3}$$

The eigenvalue u_a^2 associated with the function e_{ai} is assumed to be the same for forward and backward modes. The propagation vector k_a of mode a satisfies

$$k_a^2 + u_a^2 = n^2\omega^2/c^2, \tag{4}$$

where n is the refractive index of the medium in the guide at its axis.

The complex amplitude P_i^{NL} of the nonlinear polarization density has a term which is a backward wave at frequency ω that is proportional to F_i^*, and hence may possibly generate the phase-conjugate to the F-wave. In terms of the nonlinear susceptibility tensor c_{ijkl} defined by Maker and Terhune [15] (and sometimes called $\chi^{ijkl}_{(3)}$ or χ^{NL}_{ijkl}),

$$P_i^{NL} = 6c_{ijkl}(-\omega, -\omega, \omega, \omega)\, F_j^* G_k H_l. \tag{5}$$

We assume that the backward wave generated by this nonlinear polarization has the form

$$\mathrm{Re}\,\Sigma_a b_a(z)\, e_{ai}(x, y) \exp(-ik_a z - i\omega t + \tfrac{1}{2}\alpha z), \tag{6}$$

where $b_a(z)$ varies slowly with the distance z along the guide. We assume further that the generation of this wave does not disturb appreciably the other fields. Then Maxwell's equations for the coefficients b_a may be easily integrated to obtain

$$b_a(0) - b_a(L) = \left(\frac{12\pi\omega}{icn}\right) f_b^* g_c h_d \int_0^L dz \exp(i\Delta kz - \tfrac{1}{2}\alpha z) \cdot \iint dx\, dy\, c_{ijkl} e^*_{ai} e^*_{bj} e_{ck} e_{dl}, \tag{7}$$

where the guide is assumed to extend from $z = 0$ to L, and the boundary condition $b_a(L) = 0$ is appropriate. Here

$$\Delta k \equiv k_a - k_b + k_c - k_d \tag{8a}$$

$$\cong (u_a^2 + u_c^2 - u_b^2 - u_d^2)/2k, \tag{8b}$$

where $k \equiv n\omega/c$. The frequency arguments of c_{ijkl} are assumed to be as in (5) unless otherwise stated. We now proceed to examine the conditions under which the solution (7) for $b_a(0)$ gives a time-reversed replica of the F-wave.

III. Conditions for Replication

It will become evident that, in order for the backward-generated B-wave of (7) to be approximately a time-reversed replica of the input F-wave when all waves are guided, all terms on the right-hand side (RHS) of (7) must be negligible except those for which either

$$a = d \quad \text{and} \quad b = c \tag{9}$$

or

$$a = b \quad \text{and} \quad c = d. \tag{10}$$

These are clearly among the largest in (7), because both the (x, y) integral is large and also the z-integral is maximum in these cases. Let us examine the constraints placed on experiment by the condition that other terms are small.

First, note that the terms (9) in (7) give a contribution to b_a that is proportional to ih_a (plus a fluctuating correction) and these constitute mainly a nonlinear correction to the refractive index experienced by the H-wave. This correction is small compared to other index corrections (of order $|H|^2H$ and $|G|^2H$) whose effects we shall consider in Section XIII. The terms arising from condition (10) contribute amounts $\tilde{b}_a$ to the backward-generated amplitude at the guide entrance ($z = 0$) which may be written (with no implied summation)

$$\tilde{b}_a = \Sigma_c \frac{12\pi\omega l}{icn} f_a^* \gamma_{ac} g_c h_c, \tag{11a}$$

where the "effective" guide length l is defined as

$$l \equiv \int_0^L \exp\left(-\frac{1}{2}\alpha z\right) dz \tag{11b}$$

and

$$\gamma_{ac} \equiv \Sigma_{ijkl} \int dx\, dy\, c_{ijkl} e_{ai}^* e_{aj}^* e_{ck} e_{cl}. \tag{12}$$

In the next section we shall show that (11) implies that b_a is generally nearly a constant times f_a^*, i.e., is the desired phase-conjugate. Here we discuss the conditions on the guide geometry which make all the terms except those of (9) and (10) negligible.

The main condition for high fidelity of replication is that the guide be imperfect enough, or asymetrical, or its interior be birefringent or inhomogeneous enough, that none (or few) of its modes are degenerate. That is, the k_a values may be assumed to be randomly spaced in any given small range. We see then from (8b) that, for terms in (7) not included in (9) or (10), it is generally true that

$$\Delta k > \pi^2/kS \tag{13}$$

where S is the cross-sectional area of the guide. If high mode numbers are excited, the inequality (13) is a strong one. (In practice high mode numbers may always be excited by arranging the input coupling appropriately.) But (13) implies that Δkl is larger than unity, and generally much larger, provided that there is significant guiding of at least one of the beams entering the guide. For significant guiding of near-axial beams, l must be at least several diffraction lengths:

$$l >> S/\lambda. \tag{14}$$

With (13) this gives the desired result for "mixed" terms not included in (9) and (10):

$$\Delta kl >> 1. \tag{15}$$

Several factors help suppress these mixed terms. For these terms the z-integral in (7) is both reduced because of (15), and fluctuates in sign to give a further reduction by a factor on the order of the square root of the number of well-guided modes involved. Also most mixed terms have a vanishing, or nearly vanishing transverse x-y mode overlap integral in (7), as one can see by trying rectangular waveguide modes in the x-y integral there.

In summary, terms in (7) other than (9) and (10) will be relatively small if the waveguide performs significant guiding and has few mode degeneracies. The unwanted terms are smaller for longer effective guide length l, for a higher number of modes excited by the input or pump beam, and for more guide irregularities and mode mixing. These make the unwanted terms add more incoherently while the wanted terms (10) add coherently, generating more closely perfect phase conjugation, as we see in the next section. "Ideal" configurations, such as those with single-mode pump beams, could also produce time-reversed replicas of high fidelity, as we discuss in Section VI. In Section XIII we discuss limits on phase-conjugation placed by the power dependence of the wavevector mismatch Δk.

IV. Fidelity of Replication

The solution (11) gives the main portion of the backscattered wave which, when radiated from the front ($z = 0$) plane of the guide, will lie outside the cone of the backward-pump (H) beam. It is evident from (11) that if

$$d_a \equiv \gamma_{ac} g_c h_c \tag{16}$$

did not vary with mode-index a, then $\tilde{b}_a$ would be a perfect "phase-conjugate" to f_a and would generate a time-reversed replica of the F-beam in front of the guide. However, the actual mode-to-mode variation in d_a causes only the fraction

$$\theta_{pc} \equiv |\tilde{b}_a f_a|^2/(f_b^* f_b \tilde{b}_c^* \tilde{b}_c) \tag{17}$$

of the backscattered energy to be the phase-conjugate to f_a. That this fraction is generally close to unity may be seen by writing (17) as

$$\theta_{pc} = |\langle d_a \rangle|^2/\langle |d_a|^2 \rangle \tag{18}$$

where the average of any quantity m_a that is a function of mode-index "a" is defined by

$$\langle m_a \rangle \equiv \Sigma_a\, m_a |f_a|^2/\Sigma_b |f_b|^2. \tag{19}$$

The variations in d_a are small because γ_{ac} in (16) varies little. For a rectangular, weakly guiding, dielectric waveguide in which only modes of one linear polarization are excited

$$\gamma_{ac} \to c_{xxxx}\xi/S, \tag{20}$$

where $\xi = 1$ for all pairs (a, c) of modes except either: 1) when the modes have one of their two space indices matching, whence $\xi = 3/2$, or 2) when the modes are the same, whence $\xi = 9/4$. However, not only are the variations in the d_a small in (18), but the weighting function $|f_a|^2$ often varies little in practice. In the case where all of the F modes excited by the incident image beam have the same energy ($|f_a| = |f_b|$, etc.), but arbitrary phase, then (18) shows that $\theta_{pc} = 1$, and the backscattered beam is a perfect phase conjugate. Model calculations show that when the mode energies vary, θ_{pc} differs from unity by a term which is of the order of the inverse of the number of modes excited times the rms energy variation. In conclusion, the interaction considered here of monochromatic guided waves produces a backscattered wave that approximates well the phase conjugate of an incident wave, of which it creates thereby a useful time-reversed replica.

V. Efficiency of Replication

The ratio R of energy in the phase-conjugate portion of the backscattered wave to the energy in the forward F-wave conjugated is

$$R = |f_a \tilde{b}_a|^2/(f_b f_b^*)^2. \tag{21}$$

This is also essentially the ratio of powers in the conjugated and F-wave, if the guide modes excited are not near cutoff. We will assume that the F-wave excites a number N of guide modes and that $N >> 1$. Then, to evaluate (21) we use

$$\Sigma_a |f_a|^2 \gamma_{ac} \cong \bar{\gamma} \Sigma_a |f_a|^2 \tag{22}$$

where γ_{ac} has been replaced by an average value which, according to (20), we may approximate by

$$\bar{\gamma} = c_{xxxx}/S, \tag{23}$$

its value for modes (a, c) in a rectangular guide that have no common indices. The relation (22) errs by a term of order N^{-1} which model calculations show has a small coefficient of order the rms fluctuation in $|f_a|^2$. We shall not belabor this here as it is intuitively clear that the accuracy of (22) is sufficient for our purpose.

With (22), (23), and (11) in (21), we have for the fraction of the F-beam replicated

$$R \sim \left| \frac{12\pi\omega l c_{xxxx} E_a h_a}{ncS} \right|^2. \tag{24}$$

It is instructive to rewrite (24) in terms of the energy fraction θ_{GH} of the forward-pump (G) wave which is the phase conjugate to the backward-pump (H) wave:

$$\theta_{GH} = |g_a h_a|^2/(g_b g_b^* h_c h_c^*). \tag{25}$$

At $z = 0$ the power P_G in the G-wave is $ncg_a g_a^*/8\pi$ and the power P_H in the backward H-wave is $nch_c h_c^*/8\pi$ (for modes not near cutoff). From (2), the product $P_G P_H$ does not vary with z in the guide. With this (24) becomes

$$R \sim \beta^2 l^2 \theta_{GH} P_G P_H/S^2 \tag{26}$$

where

$$\beta \equiv \left| \frac{96\pi^2\omega^2 c_{xxxx}}{n^2 c^2} \right|. \tag{27}$$

We have assumed that all polarizations are parallel and are not scrambled by accidental coupling among guide modes. Phase conjugation should occur just as well with scrambling, but a modified value of the nonlinear susceptibility coefficient c_{xxxx} would have to be used. If pump and probe beams are not parallel polarized, terms containing c_{xxyy}, etc., may be needed in (27).

The relation (26) neglects terms in b_a that are of higher order (than first) in f_a and is useful for $R \leq 0.5$. The higher order terms probably can lead to real gain ($R > 1$) in the backscattered wave, without spoiling its conjugate property, as occurs in phase-conjugation by degenerate four-wave mixing without guiding [5] - [10], and in a guide if both pump beams are in the same single mode ($g_c = g_c = g\delta_{cd}$) [11].

Note that (26) is very similar to the expression that applies to free-space (unguided) phase-conjugation except that the plane-wave-pump beam intensities have been replaced by P_G/S and P_H/S and the factor $\theta_{GH}(\leq 1)$ is appended. However, now the effective interaction length l is not limited by diffraction but by attenuation in the guide. One can expect, as has been recently demonstrated [14], that a time-reversed replica can be generated in a waveguide with much less pump power than is required with unguided waves, even though in practice the pump beams are multimode and have an overlap factor θ_{GH} that is much less than unity. As an example, consider liquid CS_2 at 6943 A for which $\beta \sim 0.01$ cm/MW [5]. With $\theta_{GH} \sim 10^{-2}$, $l \sim 1$ m, $S \sim 10^{-4}$ cm^2, $R \sim 10^{-2}$, we see that a pump power of order 100 W is required. We proceed to consider other guide configurations in which phase-conjugation occurs usefully for a variety of applications.

VI. Ideal-Guide Configurations

It is of interest for high efficiency R to obtain a high pump-overlap factor Θ_{GH} in (26). This could only be done in a guide perfect enough to make precise pump-mode patterns excitable throughout its entire length. In such a guide, there would be potentially troublesome mode degeneracies that would allow terms other than those of (9) or (10) to be large and spoil the fidelity of the phase configuration process. In most long ($l >> S/\lambda$) practical guides, imperfections remove these degeneracies and suppress the unwanted terms, as explained in Section III, but at the cost of making Θ_{GH} low. Therefore we consider here an ideal-guide configuration which may produce both $\Theta_{GH} \sim 1$ and high replication fidelity, although fabrication of such a guide may be difficult. Here, degeneracies are dealt with as follows.

In an ideal guide fabricated of isotropic media, whose cross section has low symmetry about the guide (z) axis, mode degeneracies are mainly "polarization degeneracies." That is, $u_a = u_b$, while for example $\hat{\varepsilon}_a = \hat{x}f(x, y)$ and $\hat{\varepsilon}_b = \hat{y}f(x, y)$, except for small fringe fields.

If, in such a guide, both pump beams and the probe beam are x-polarized, the c_{ijkl} tensor in (7) will not mix in other degenerate polarizations and will generate an x-polarized phase-conjugate wave. One may see this as follows.

For isotropic media, the nonlinear susceptibility tensor in (7) has the form [15]

$$c_{ijkl} = c_1\delta_{ij}\delta_{kl} + c_2\delta_{il}\delta_{jk} + c_3\delta_{ik}\delta_{jl}. \tag{28}$$

Clearly, if $j = k = l = x$, so must the scattered-mode polarization index i be x; degenerate modes of other polarizations are not excited or mixed in. Once degeneracies are removed, the z-integral in (7) suppresses terms other than those of (9)

and (10) and phase-conjugation follows as in the previous discussion.

VII. Two-Beam Conjugation

Another interesting configuration in an imperfect guide is one in which the forward-pump and probe beams are a single multimode beam G superposed in the guide on the multimode backward pump H as in Fig. 1(b). The part of the resulting nonlinear polarization density that is relevant here is obtained by replacing F_j^0 by G_j^0 in (5); and the resulting mode amplitudes of the backward generated wave are obtained by replacing f_b^0 by g_b^0 in (7). The arguments of Sections III-VI go through unchanged, except for those substitutions, and (26) becomes an estimate of the energy fraction of the forward (pump and probe) G-beam that appears in the phase-conjugate wave at low efficiencies ($R \lesssim 0.5$).

With this configuration, one might want to keep the pump-overlap fraction θ_{GH} small in order to reduce the fraction of the backward pump that emerged in the cone of the phase-conjugate wave. A corresponding penalty in efficiency R would then be paid. An advantage of this configuration, aside from mechanical simplicity, is that the power in the conjugated wave is a larger fraction of the total power involved (in all beams) for a given θ_{GH}, P_G, and P_H. Also the fact that the power in the conjugated wave is proportional to the square of the power of the beam being conjugated, rather than to the first power, may have advantages in some applications. Recent experiments verify that this configuration is effective in producing high fidelity replicas, and is a potentially useful configuration in which the frequency of the phase-conjugate wave is shifted from that of the wave being conjugated [14].

VIII. Properties as Wide-Angle Narrowband Filter

Up to this point we have discussed only the case where all beams involved in the replication process are at the same frequency ω. However, if the input F-beam frequency in the configuration of Fig. 1 is varied, replication will still occur in a small band centered about the pump frequencies. Since the acceptance angle of either metallic or dielectric waveguides is large ($\sim$ steradians), the replication process can act as a narrowband optical filter for waves impinging from any angle within a wide range. Such wide-angle narrowband filters at laser frequencies are difficult to realize by other methods. We examine here the spectral response of such a filter, and ways by which its center frequency can be tuned.

Suppose for generality that the monochromatic forward (G) and backward (H) pump beams in the guide of Fig. 1(a) have different frequencies ω_G and ω_H, and the probe (F) beam is at a third frequency ν. Then our previous analysis may be repeated, but with $c_{ijkl}(-\omega, -\nu, \omega_G, \omega_H)$ in (5), in which the mixed frequency ω of a possible backward wave generated by the nonlinear polarization becomes

$$\omega = \omega_G + \omega_H - \nu. \tag{29}$$

Equation (7) is altered by reinterpreting c_{ijkl} as just mentioned, and by noting that, instead of (8), one has for the relevant terms with $a = b, c = d$

$$\Delta k = 2\pi(\omega_G - \nu)/c - \tfrac{1}{2}cn^{-1}\left[u_a^2(\omega_G^{-1} - \nu^{-1}) + u_c^2(\omega_G^{-1} - \omega_H^{-1})\right] \tag{30}$$

to order (u^2/k^2). We will assume that the pump modes are of low enough order so that the u_c^2 term in (30) can be neglected. Then following the arguments of Sections II-V again leads to the following generalization of (26):

$$R \sim \beta^2 P_G P_H \theta_{GH} l^2 S^{-2} \phi \tag{31}$$

in which the frequency arguments of the c_{ijkl} coefficient in β are modified as above. Here, ϕ is the phase mismatch reduction factor

$$\phi \equiv \left| \int_0^L \exp\left(i\Delta kz - \frac{1}{2}\alpha z\right) dz/l \right|^2 \tag{32}$$

in which Δk is given by (30). (It is assumed that u_a^2 does not vary significantly for the rays involved.) The function is a bell-shaped function of $u = \nu - \omega_G$ which does not change its quality as the guide length L and attenuation α vary. The full width at half maximum (FWHM) of this function varies between $\Delta\omega$ (when $\alpha L >> 1$) and 2.8 $\Delta\omega$ (when $\alpha L << 1$) where

$$\Delta\omega \equiv \frac{c}{nl}\left\{1 - (\psi/2n)^2 + O\{\psi^4\}\right\} \tag{33}$$

for a ray entering the guide at angle ψ to its axis. Here it is assumed that $\psi < \pi$, so it is seen that the bandwidth for all rays is of the order of twice the axial mode spacing ($c/2nl$) of an optical cavity whose length is the same as the effective guide length l defined in (11).

The center of the band of replicable frequencies can be tuned by tuning the pump frequencies $\omega_G = \omega_H$ in unison. However, as we show below, phase-conjugation can occur within the same bandwidth (33) about $\nu \sim \omega_G$ even when $\omega_G \neq \omega_H$. Having the backreflected phase-conjugate E-beam at a frequency ω differing from ν by (29) can improve filter characteristics. For example, a dichroic beamsplittler could then be employed that avoids the factor of 4 reduction in replica intensity that results when an ordinary 50 percent beamsplittler is used to separate the E- and F-beams, as in Fig. 1.

Two-frequency operation of phase-conjugation in a guide also allows the possibility of image conversion (in frequency) and spectroscopy of small samples, as we discuss next.

IX. Image-Frequency Conversion

The analysis in the preceding section suggested the possibility of generating an E-wave as in Fig. 1(a) whose amplitude in the entrance plane of the guide is proportional to the complex conjugate of the F-beam amplitude, but whose frequency is different from that of the F-beam, according to (29). The E-wave emerging from the front of the guide would no longer be exactly a time-reversed replica of the F-wave but would be a magnified (by ν/ω) version of it which would still reproduce the incident image at the detection plane P in Fig. 1. We derive here the maximum number of resolution elements that

can be successfully replicated in this process of "image conversion."

Suppose that the variation in the pump-mode indices u_c^2 is less than the variation in u_a^2 in (30), as will generally be the case because the probe carries an image while the pump need not. Suppose also that the input probe F-beam is centered about the guide axis, exciting modes whose indices range up to a maximum value u_{am}^2. The axial F-rays experience a bandpass for replication centered about $\nu \sim \omega_G$ (where $\phi \sim 1$) with a bandwidth (32). The skew F-rays with larger values of u_a^2 will also be well replicated until their phase mismatch Δkl approaches π. This sets a limit N_F on the number of incident F-modes that can be replicated which is given by the number of eigenvalues u_a^2 that are less than u_{am}^2:

$$N_F \sim Su_{am}^2/4\pi. \tag{34}$$

Estimating u_{am}^2 by equating Δk of (30) to π/l, one obtains for the maximum number of resolution elements at ω_G that can be replicated at the shifted frequency ω_H

$$N_F \sim k_0^2 S\,\Delta\omega/|\omega_H - \omega_G|, \tag{35}$$

where $k_0^2 \equiv n^2\omega_G\omega_H/c^2$.

In this case, the pump modes need not be tightly guided, and one can increase N_F by increasing the guide area S up to the point where a typical image ray entering at angle $\sim u_{am}/k$ to the axis experiences several bounces in the effective length l: i.e., S can be increased to order $l^2u_{am}^2/k^2$. However $l \leq 2/\alpha$. Substituting these limits in (35) gives an estimate for the theoretical upper limit on N_F, the number of resolution elements that can be replicated with fidelity in a guide:

$$(N_F)_{max} \sim \omega_G\omega_H/(\omega_G - \omega_H)^2. \tag{36}$$

Of course, with free (unguided) waves, one can always defeat phase mismatch by having a short enough interaction region (too short for any waves to be guided). Making up for the small length l and large area S with more beam power enables one in principle to obtain image conversion of arbitrarily large N_F over any frequency range $\omega_G - \omega_H$ with unguided waves.

However, in practice, the lower power requirements that result from using guided waves may still make guiding the preferred configuration for image conversion when condition (35) is not too restrictive.

X. Multiple Frequency Conjugation

The converse of the case of the previous section is also of interest, that is, where sets of pump and probe beams of two or more different frequencies are present simultaneously and replicating independently of each other. We derived in the previous section the conditions under which two frequencies interact to perform image conversion. We follow similar reasoning here to determine when they interact negligibly while replicating.

Suppose that each beam of Fig. 1(a) contained several discreet incommensurate frequencies: $\omega_F, \omega_G, \omega_H = \omega, \nu$, etc., all separated from one another by much more than c/l. It is sufficient to consider the interaction of each pair of frequencies separately; we suppose that only ν and ω are present in each beam. That is, (1) becomes a sum of terms for each frequency. Following again the subsequent analysis, one finds that the only mixed-frequency terms whose phase mismatch is possibly small enough to cause intermixing are the terms for which $\omega_G = \omega_F = \nu$ and $\omega_H = \omega_E = \omega$, the same terms which we considered in the previous section for image-frequency conversion. The wavevector mismatch is again given by (30), and to keep this mismatch large enough to avoid intermixing, one sees that it is sufficient to excite such high-order guide modes that

$$\tfrac{1}{2}cn^{-1}|u_a^2 - u_c^2||\omega^{-1} - \nu^{-1}|l > \pi. \tag{37}$$

This is easily accomplished by having the pump beams, which excite c-modes, nearly axial while the input F-beams enter the guide at an angle around $\theta \sim u_c c/\nu$ large enough so that $u_a^2 >> u_c^2$ and (37) is satisfied. That is

$$\theta^2 > \left|\frac{\Delta\omega}{\nu - \omega}\right| 2\pi n \tag{38}$$

which can be easily fulfilled in practice.

In summary: 1) if pump (G, H) and probe (F) beams all contain the same set of well-separated discreet frequencies; 2) if the pump beams are near axial; and 3) if probe beams consist of rays which enter the guide at angles θ to the axis which satisfy (38), then replication will take place at each frequency independently without intermixing.

XI. Small-Sample Spectroscopy

It is evident that the image-conversion efficiency R of (31) varies when both the frequency ν of the forward (F and G) beams and the frequency ω of the backward (E and H) beams are tuned. If ϕ in (31) can be kept of order unity in this process (as we found could be done when few guide modes are excited) and if then, this variation is due only to the variation in the nonlinear coefficient $c_{ijkl}(-\omega, -\nu, \omega, \nu)$ involved in β. This coefficient has resonances when $|\omega - \nu|$ is near a "Raman" excitation frequency ω_R of the guide medium or walls, as well as when ω or ν are near an absorption frequency, or when $\omega + \nu$ is nearly a two-photon resonance, and when either 3ω, 3ν, $|2\omega \pm \nu|$, or $|2\nu \pm \omega|$ are near a three-photon resonance. The spectroscopic information to be gained by observing phase-conjugation as a function of forward- and backward-beam frequencies is evident. Here we consider briefly its application to Raman spectroscopy. The other forms may be treated similarly. We find that spectra of small, ($\sim$ nanoliter) samples should be obtainable in this manner.

Suppose that, when $\nu - \omega \sim \pm\omega_R$, c_{ijkl} is mainly the imaginary term that characterizes the Raman susceptibility at resonance. Assuming all polarizations are parallel ($i = j = k = l = x$), an examination of (27) shows that β is then half the commonly used peak stimulated Raman gain constant (power gain per cm per pump intensity). These gain constants are typically of order 1 cm/GW for allowed Raman transitions in liquids. For a small-diameter optical guide ($S \sim 10^{-7}$ cm^2), the small number of accessible guide modes will allow Θ_{GH} to be at least 0.1. Assuming a length $l \sim 100$ cm, or a sample volume of 10^{-5} cm^3, we have from (31) that pump powers of 1 W will

produce $R \sim 10^{-2}$. With CW dye lasers and phase-locked detection, $R \sim 10^{-6}$ should be easily detectable, so that Raman resonances of dilute solutions or gases in microliter quantities should be observable with this technique. Sample heating should be manageable because of the rapid cooling possible with such high surface-to-volume ratio.

XII. Broadband Optical Transistor

As has been shown by Yariv *et al.* [11], when the G- and H-pump waves in the configuration of Fig. 1(a) excite only the same single transverse mode of the guide, then the E-beam can experience a power gain over the input F-beam power without loosing its phase-conjugate property ($b_c \propto f_c^*$). However, it is doubtful that this property holds for the multimode pump beams of main concern here. There are, however, other ways to achieve what is effectively linear gain, or "optical transistor" action by phase-conjugation in a waveguide. Consider, for example, the configuration of Fig. 1(b) which is known experimentally to produce $R = P_E/P_G \sim 0.2$ with high fidelity replication [5]. According to (7) the E-beam amplitude is proportional to the G-beam amplitude, and from (26) one sees that the beam powers are related by

$$P_E = \xi P_G^2 P_H, \tag{39}$$

when $P_E \leq 0.5 P_G$. Here ξ is an obvious combination of constants. Clearly (39) holds the possibility $P_E/P_H >> 1$, that is, power gain exists, when $P_H << P_G$. The extra energy in P_E must come from the G-beam, so the H-beam serves to switch much larger powers than its own from the G- to the E-beams.

The amplifier bandwidth in this configuration can be much larger than that ($\sim c/l$) in the configuration considered by Yariv *et al.* [11]. Here the bandwidth is governed by $\Delta k < \pi/l$ through the function ϕ in (31). From the discussion in Section IX it is evident that the bandwidth can approach the value of the input frequency itself, making the device a broadband amplifier with spatially distinct input and output channels: that is, a sort of "optical transistor." Similar action is possible with the configuration of Fig. 1(a).

XIII. Power Dependence of Mode-Propagation Constants

The third-order nonlinear optical susceptibility

$$c_{ijkl}(-\omega, -\nu, \nu, \omega)$$

which is responsible for the generations of a phase-conjugate wave also causes an intensity-dependent change in the mode propagation constants k_a. Using the mode decompositions (2) and (6) in the expression for the total third-order polarization density, one can identify the leading corrections to the k_a. These corrections are first order in the powers P_G and P_H of the G- and H-beams. (We assume that the E- and F-beam powers are much smaller.) Let us consider, for definiteness, the degenerate case ($\omega = \nu$) with all fields being linearly polarized in the x-direction and having mode amplitudes b_a, f_a, g_a, and h_a which vary slowly with z. Then, for example, one finds the derivative $-2ik_a db_a/dz$ arising from the $\nabla^2 E$ term in Maxwell's equation to be partly compensated by a term in the nonlinear polarization density

$$b_a 24\pi\omega^2 c^{-2} c_{xxxx} \Sigma_c (|g_c|^2 + |h_c|^2)/S, \tag{40}$$

which clearly represents a correction

$$\Delta k_{a,E} = (P_G + P_H)\beta/S \tag{41}$$

to the propagation constant k_a for the backscattered wave. Here β is the same coefficient as in (27) which describes the strength of phase-conjugation, and S is the guide cross-sectional area as before. Similarly, the mode-propagation constants for the F-, G-, and H-beams experience the following corrections:

$$\Delta k_{a,F} = (P_G + P_H)\beta/S \tag{42}$$

$$\Delta k_{a,G} = (\tfrac{1}{2}P_G + P_H)\beta/S \tag{43}$$

$$\Delta k_{a,H} = (P_G + \tfrac{1}{2}P_H)\beta/S \tag{44}$$

to lowest order in the pump beam powers.

The main question which arises in connection with the nonlinear nature of the mode-propagation constants is: how much do they affect the phase-conjugation process? Substituting (41)–(44) in (8) shows that the nonlinear terms cause a wavevector mismatch which is, to lowest order in the pump fields

$$\Delta k^{NL} = \tfrac{1}{2}(P_H - P_G)\beta/S \tag{45}$$

for the configuration of Fig. 1(a) with $\omega = \nu$. This mismatch will be unimportant to phase-conjugation when $\Delta k^{NL} < l^{-1}$. Comparison of (45) with (26) shows that the nonlinear propagation effects are easily made unimportant by arranging

$$\frac{(P_G - P_H)^2}{P_G P_H} < \frac{1}{R}, \tag{46}$$

where, if P_G and P_H are varying with z due to absorption, one should use their values averaged over the first l cm of the waveguide in the numerator of (46).

When the frequencies of the forward and backward beams are unequal, but (29) is satisfied, then the relation (45) remains unaltered, provided that neither frequency is near a resonance and β is taken to be the single-frequency coefficient of (27), which is the same evaluated at either ν or ω. Again the nonlinear phase mismatch need not be troublesome if $P_G \sim P_H$.

The analysis of nonlinear propagation constants may be repeated for the configuration of Fig. 1(b). This is equivalent to substituting the G-wave in place of the F-wave, and the alterations (41), (43), and (44) apply. When substituted into (8), these give for the nonlinear contribution to the wavevector mismatch

$$\Delta k^{NL} = \tfrac{1}{2}P_H\beta/S, \tag{47}$$

again, whether or not forward and backward wave frequencies are equal. Here, clearly, phase mismatch will limit the effective reflectivity R of the phase-conjugation process to a lower value than is possible with the configuration of Fig. 1(a). However, the possibility of transistor action in (39) is not spoiled.

XIV. Summary and Conclusions

We have analyzed two ways by which optical beams can be coupled into a waveguide and interact there so as to generate the time-reversed replica, or phase-conjugate, of one of the beams. We showed that these guided "four-wave mixing" schemes, illustrated in Fig. 1, are superior in the following ways to the corresponding arrangements that have been used to generate a phase-conjugate beam by interaction of "free" unguided beams in an infinite medium: 1) The pump power required in the guide is orders-of-magnitude less. 2) Unlike for unguided beams, the two counterpropagating pump beams can be multimode without spoiling the fidelity of the replica. 3) Unlike for unguided waves, the pump beams need not be carefully aligned with respect to each other. 4) Unlike for unguided waves, a multimode pump beam will itself be replicated (i.e., serve as both pump- and image-beams) in the presence of a counterpropagating pump beam in the guide. 5) The medium in the guide and the guiding structure itself need not be perfectly homogeneous or ideal. The only requirement on the guiding structure is that it not attenuate beams too drastically in relation to the required nonlinear interaction length. These predictions have been recently verified experimentally.

We have shown that a phase-conjugate beam can be generated that is either at the same frequency as the input beam being conjugated or not, depending on the values of the pump frequencies. When the frequencies are not the same, "image-conversion" can result, i.e., the creation of a (magnified or demagnified) image replica at one frequency of another at a (higher or lower) frequency. Conversely, several frequencies can be replicated simultaneously without "image-conversion" or crosstalk between the frequencies if certain conditions are satisfied.

We have also shown how the frequency dependence of the replication process can be used to realize a narrowband optical filter with a large solid angle of acceptance.

Because the efficiency of the phase-conjugation process exhibits Raman and two-photon resonances as the frequency offset between the beams is varied, the process has potential for laser spectroscopy of very small volumes of material or of the surface excitations in the waveguide.

Linear power gain of one wave in the guide in response to another is possible over a very broad bandwidth, in a manner resembling transistor action.

The inevitable power-dependence of the guide propagation constants is found not to seriously limit the phase-conjugation process in the waveguide.

In conclusion, phase-conjugation by four-wave mixing in a waveguide holds great promise for many beam-processing and spectroscopic applications.

Acknowledgment

The author would like to thank S. M. Jensen, R. L. Abrams, V. Wang, A. Yariv, H. Davies, and D. L. Coutu for many stimulating discussions.

References

[1] B. Y. Zel'dovich, V. I. Popovichev, V. V. Ragul'skii, and F. S. Faisullov, "Connection between the wavefronts of the reflected and exciting light in stimulated Mandel'stam-Brillouin scattering," *Sov. Phys. JETP Lett.*, vol. 15, pp. 109–113, 1972.

[2] O. Y. Nosach, V. I. Popovichev, V. V. Ragul'skii, and F. S. Faisullov, "Cancellation of phase distortions in an amplifying medium with a 'Brillouin mirror,'" *Sov. Phys. JETP Lett.*, vol. 16, pp. 435–438, 1972.

[3] A. Yariv, "On transmission and recovery of 3-dimensional image information in optical waveguides," *J. Opt. Soc. Amer.*, vol. 66, pp. 301–306, Apr. 1976.

[4] P. V. Avizonis, F. A. Hopf, W. D. Bomberger, S. F. Jacobs, A. Tomita, and K. H. Womack, "Optical phase conjugation in a lithium formate crystal," *Appl. Phys. Lett.*, vol. 31, pp. 435–437, Oct. 1977.

[5] R. W. Hellwarth, "Generation of time-reversed wavefronts by nonlinear refraction," *J. Opt. Soc. Amer.*, vol. 67, pp. 1–3, Jan. 1977.

[6] D. M. Bloom and G. C. Bjorklund, "Conjugate wave-front generation and image reconstruction by four-wave mixing," *Appl. Phys. Lett.*, vol. 31, pp. 592–594, Nov. 1977.

[7] S. M. Jensen and R. W. Hellwarth, "Observation of the time-reversed replica of a monochromatic optical wave," *Appl. Phys. Lett.*, vol. 32, pp. 166–168, Feb. 1978.

[8] D. M. Bloom, P. F. Liao, and N. P. Economou, "Observation of amplified reflection by degenerate four-wave mixing in atomic sodium vapor," *Opt. Lett.*, vol. 2, pp. 58–60, Mar. 1978.

[9] A. Yariv and D. M. Pepper, "Amplified reflection, phase-conjugation, and oscillation in degenerate four-wave mixing," *Opt. Lett.*, vol. 1, pp. 16–18, July 1977.

[10] P. F. Liao, D. M. Bloom, and N. P. Economou, "cw optical wavefront conjugation by saturated absorption in atomic sodium vapor," *Appl. Phys. Lett.*, vol. 32, pp. 813–815, June 1978.

[11] A. Yariv, J. Au Yeung, D. Fekete, and D. M. Pepper, "Image phase compensation and real-time holography by four-wave mixing in optical fibers," *Appl. Phys. Lett.*, vol. 32, pp. 635–637, May 1978.

[12] R. W. Hellwarth, "Theory of phase conjugation by stimulated scattering in a waveguide," *J. Opt. Soc. Amer.*, to be published.

[13] V. Wang and C. R. Giuliano, "Correction of phase aberrations via stimulated Brillouin scattering," *Opt. Lett.*, vol. 2, pp. 4–6, Jan. 1978.

[14] S. M. Jensen and R. W. Hellwarth, "Generation of time-reversed waves by nonlinear refraction in a waveguide," *Appl. Phys. Lett.*, vol. 33, pp. 404–405, Sept. 1978.

[15] P. W. Maker and R. W. Terhune, "Study of optical effects due to an induced polarization third-order in the electric field strength," *Phys. Rev.*, vol. 137, pp. A801–A818, Feb. 1965.

[16] R. L. Carman, R. Y. Chiao, and P. L. Kelley, "Observation of degenerate stimulated four-photon interaction and four-wave parametric amplification," *Phys. Rev. Lett.*, vol. 17, pp. 1281–1283, Dec. 1966.

Appendix V

Infrared-to-optical image conversion by Bragg reflection from thermally induced index gratings

G. Martin and R. W. Hellwarth

Electronics Sciences Laboratory, University of Southern California, Los Angeles, California 90007
(Received 10 November 1978; accepted for publication 4 January 1979)

We have observed efficient reproduction at visible wavelengths of 1.06-μ images. We employed a phase-matched four-wave mixing process in which three waves at ν, ν, and ω mix to generate a fourth wave at ω, with no resonant conditions on either frequency. The image conversion was seen with each of the 14 liquids tried as a nonlinear medium and also with a glass. Thermal index changes were the dominant mechanism.

PACS numbers: 42.80.Qy, 42.65.Jx, 42.40.Kw, 42.30.Va

It is well known that three beams of wave vectors $\mathbf{k}_F$, $\mathbf{k}_G$, and $\mathbf{k}_H$ and frequencies ν, ν, and ω, respectively, will generate a beam of frequency ω via the (third-order) nonlinear polarization density set up in any transparent medium.[1] This process is often called "four-wave mixing." The strength of this generated signal is enhanced many orders of magnitude if the input beams are "phase matched," that is, if the magnitude k_E of the vector defined by

$$\mathbf{k}_E \equiv \mathbf{k}_G - \mathbf{k}_F + \mathbf{k}_H \tag{1}$$

is such that

$$k_E = n_\omega \omega / c, \tag{2}$$

where n_ω is the refractive index at frequency ω. Here, we show that, for the nearly counterpropagating beam geometry of Fig. 1 (and even for ω much different from ν) the input wave vector $\mathbf{k}_F$ (and beam $\mathbf{k}_E$) can rotate by many diffraction angles without spoiling phase matching over a typical beam interaction length ($\sim$ mm). This suggests, as the experimental results we report show, that an infrared image in the F beam can be frequency shifted by four-wave mixing to yield an optical image in the H beam that is a (demagnified) replica of the F image; the mixing process produces infrared image conversion.

In terms of holography concepts, this process is analogous to a volume hologram reconstructed at a shorter wavelength. The optical H (read) beam is Bragg reflected [according to Eqn. (1) and (2)] from a transient index grating formed in the nonlinear medium by spatial beats between the infrared F (image) and G (reference) beams. Such effects have been observed for plane-wave beams in geometries other than that of Fig. 1.[2,3] However, it has not been previously appreciated that Bragg reflection of beam H at a considerably different wavelength from that of the F and G beams can occur over a wide enough range of image-beam angles so as to yield useful image conversion (provided the geometry of Fig. 1 is employed). We shall derive below the beam powers required to convert an image of a given number of resolution elements over a given frequency shift with a given efficiency. First, we describe the image conversion as we have observed it.

As shown schematically in Fig. 1, the infrared "write" beams F and G originated from a repetitively Q-switched Nd : YAG laser oscillator. This produced 15-nsec pulses at up to 20 pps of about 4 mJ energy each. The green "read" beam H originated from a portion of the Nd : YAG oscillator output that was frequency doubled by a CD*A crystal at several percent efficiency. The angle ϕ_0 between the infrared F and G beams was arbitrarily fixed near 15°, and the green H beam adjusted near 176° to the G beam until phase matching optimized the output E-beam image intensity. The beam diameters were about 1 mm inside the 2-mm-long sample cell. Good images of around 10^3 resolution elements were formed, of comparable intensities to the input images, for all sample liquids tried as well as for a glass sample (an infrared filter plate). The pure liquid samples tried were carbon disulphide, water, methanol, acetone, trichloroethylene, cyclohexane, 1-2 dichloroethane, ethanol, hexane, carbon tetrachloride, glycerol, isopropyl alcohol, benzene, and toluene. A typical optical image of a nine-hole pattern cut in a plate is shown in Fig. 2, alongside the input infrared image carried by the F beam.

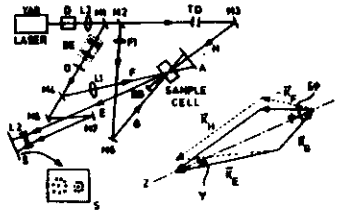

FIG. 1. Schematic of apparatus used to observe up-converted phase-conjugated images, and of the phase-matching diagram for the waves involved. (Angles shown are discussed in text.) Infrared beam F, bearing the image of object O, beats with infrared beam G and visible beam H in sample to generated visible phase-conjugate replica-beam E which is observed (alongside reference fraction of F) at S. D is a frequency doubler, BE a beam expander, $F1$ is a 532-nm blocking filter, BB is a beam block, A is an aperture, S is a screen or film paper, TD is a variable time delay, and O is a hole pattern. Mirror $M1$ is a 50% 1.06-μ reflector (4% in the green), $M2$, $M4$, and $M6$ reflect 99% at 1.06 μ (4% in the green) while $M3$, $M5$, and $M7$ are 99% reflectors in the visible. $L1$ is a 500-mm lens, $L2$ is a ($-$)200-mm diverging lens, and $L3$ is a 1000-mm main focusing lens.

 0003-6951/79/060371-03$00.50

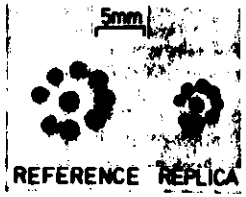

FIG. 2. Photographic images of the infrared-image (reference) beam F and the phase-conjugated (replica) beam E obtained by placing ordinary photographic print paper at the observation plane S in Fig. 1. The reference image is made by the green light from the 4% reflectance of $M1$ in Fig. 1, the print paper being insensitive to the infrared. The Fresnel fringes seen on the reference beam pattern should be, and are, absent from the phase-conjugate pattern at the plane of observation.

To see whether the refractive index grating established by the infrared beams persisted measurably in time, the green H pulse was delayed up to 30 nsec with respect to the infrared pulse. For the first several nsec of delay, the image energy increased to a maximum, then stayed constant for the longer delay times obtainable. This persistence of the grating was seen in all samples. In order to determine the persistence times, 20 mW of a 515-nm cw argon-ion laser beam was used to supply the G beam in place of the green pulse. The image E beam was monitored by a photomultiplier and displayed on a scope. Exponential delay times of the order of microseconds were observed in all samples. These times were consistent with those calculated for the index grating to decay by thermal diffusion, except in cyclohexane and 1-2 dichloroethane. (The thermal conductivity of the glass has not yet been measured). The latter two liquids are the only ones whose molecules have an optically and thermally excitable isomer of different optical polarizability. In these the possibility of an isomer-concentration grating exists in addition to the thermal index grating. In CS_2 the grating of partially reoriented molecules is also expected to contribute 1–10% of the observed signal. Direct evidence for this was inconclusive. The persistence time of this "reorientation" grating ($\sim$ psec) is too short to be measured in our experiments. Many other physical mechanisms exist which can mediate the image-conversion process efficiently, such as photorefractive effects and impurity-ion excitation in solids.[4–12]

The number N of image resolution elements that can be converted by the geometry of Fig. 1 is approximately the solid angle Ω_p in which $\mathbf{k}_E$ is phase matched divided by the diffraction solid angle Ω_d. Phase matching is obtained when $\Delta k \equiv |k_E - n_\omega \omega/c| \lesssim \pi/l$. Here, l is the effective length over which the nonlinear polarization is generated; it is set by beam overlap geometry, sample length, or the infrared absorption length, whichever is least. An examination of the geometry of Fig. 1 shows $\mathbf{k}_E$ is unchanged when $\mathbf{k}_F$ is rotated about the symmetry (z) axis of the k-vector diamond. That small deviation $\delta\phi$ of ϕ (about its average value ϕ_0) which makes $\Delta k l = \pi$ is easily seen to be such that (for $\phi_0 \ll 1$) $\Omega_p \simeq 2\pi\phi_0\delta\phi \simeq 4\pi^2/(k_F l\,|1 - k_F/k_E|)^2$. Taking the diffraction solid angle of the input beam to be $4\pi^2/k_F^2 A$, where A is the beam area, we have for the number N of phase-matched image resolution elements

$$N \simeq A k_F / l\,|1 - k_F/k_E|. \tag{3}$$

As k_F approaches k_E this number approaches infinity, reflecting the fact that for degenerate four-wave mixing of the geometry of Fig. 1 phase matching is satisfied for all input beam angles (and the generated E wave is the time-reversed replica of the F wave). Furthermore, as $l \to 0$, one has the case of a plane hologram, for which all angles can be replicated, and for which the reading of a complex image at a shifted frequency often has been demonstrated.[1–4] For a volume interaction such as in our experiments, where $k_F = \frac{1}{2}k_E \sim 6\times10^5$ cm^{-1}, $A \sim 10^{-2}$ cm^2, and $l \sim 2$ mm, we expect $N \sim 10^6$. Moreover, by decreasing the absorption length at ν, N can be increased without increasing pump-beam powers, as we see below.

Although several physical mechanisms seem to be involved in the nonlinear index that produces the image conversion in some of our experiments, a useful estimate of the conversion efficiency in these experiments can be obtained by assuming that the F and G beams create a transient spatial "grating" of temperature variation[3,4,9,10] whose wave vectors are near $\mathbf{q} = \mathbf{k}_G - \mathbf{k}_F$. It is sufficient for our purposes to consider only the case where the fractional rate of change in time of the amplitude of this grating is less than the frequency of sound of wave vector q. Then, acoustic waves equalize pressure everywhere in the medium nearly instantaneously, and the variation $\theta(\mathbf{x},t)$ in temperature throughout the sample obeys the diffusion equation

$$\rho C_p \dot{\theta} - \lambda \nabla^2\theta = (\alpha n c/4\pi)\,\mathrm{Re}[\mathbf{G}\cdot\mathbf{F}^* \exp(i\mathbf{q}\cdot\mathbf{x})], \tag{4}$$

where ρ is the mass density, C_p is the specific heat (at a constant pressure) per unit mass, λ is the thermal conductivity, α is the loss (Np/cm) of the medium (at ν), n is the refractive index (at ν), and G and F are the time-varying amplitudes of the G and F beams (at ν), respectively.

The thermal grating couples to the electromagnetic field via the nonlinear polarization density $\mathbf{p}^{\mathrm{NL}}$ created by the variation in refractive index with temperature:

$$\mathbf{p}^{\mathrm{NL}}(\mathbf{x},t) = \mathrm{Re}[(n\chi/2\pi)\theta(\mathbf{x},t)\mathbf{H}\exp(i\mathbf{k}_H\cdot\mathbf{x} - i\omega t - \tfrac{1}{2}\mu s)], \tag{5}$$

FIG. 2. Photographic images of the infrared-image (reference) beam F and the phase-conjugated (replica) beam E obtained by placing ordinary photographic print paper at the observation plane S in Fig. 1. The reference image is made by the green light from the 4% reflectance of M 1 in Fig. 1, the print paper being insensitive to the infrared. The Fresnel fringes seen on the reference beam pattern should be, and are, absent from the phase-conjugate pattern at the plane of observation.

tor output that was frequency doubled by a CD*A crystal at several percent efficiency. The angle ϕ_0 between the infrared F and G beams was arbitrarily fixed near 15°, and the green H beam adjusted near 176° to the G beam until phase matching optimized the output E-beam image intensity. The beam diameters were about 1 mm inside the 2-mm-long sample cell. Good images of around 10^3 resolution elements were formed, of comparable intensities to the input images, for all sample liquids tried as well as for a glass sample (an infrared filter plate). The pure liquid samples tried were carbon disulphide, water, methanol, acetone, trichloroethylene, cyclohexane, 1-2 dichloroethane, ethanol, hexane, carbon tetrachloride, glycerol, isopropyl alcohol, benzene, and toluene. A typical optical image of a nine-hole pattern cut in a plate is shown in Fig. 2, alongside the input infrared image carried by the F beam.

To see whether the refractive index grating established by the infrared beams persisted measurably in time, the green H pulse was delayed up to 30 nsec with respect to the infrared pulse. For the first several nsec of delay, the image energy increased to a maximum, then stayed constant for the longer delay times obtainable. This persistence of the grating was seen in all samples. In order to determine the persistence times, 20 mW of a 515-nm cw argon-ion laser beam was used to supply the G beam in place of the green pulse. The image E beam was monitored by a photomultiplier and displayed on a scope. Exponential delay times of the order of microseconds were observed in all samples. These times were consistent with those calculated for the index grating to decay by thermal diffusion, except in cyclohexane and 1-2 dichloroethane. (The thermal conductivity of the glass has not yet been measured). The latter two liquids are the only ones whose molecules have an optically and thermally excitable isomer of different optical polarizability. In these the possibility of an isomer-concentration grating exists in addition to the thermal index grating. In CS_2 the grating of partially reoriented molecules is also expected to contribute 1–10% of the observed signal. Direct evidence for this was inconclusive. The persistence time of this "reorientation" grating ($\sim$ psec) is too short to be measured in our experiments. Many other physical mechanisms exist which can mediate the image-conversion process efficiently, such as photorefractive effects and impurity-ion excitation in solids.[6-11]

The number N of image resolution elements that can be converted by the geometry of Fig. 1 is approximately the solid angle Ω_p in which $\mathbf{k}_E$ is phase matched divided by the diffraction solid angle Ω_d. Phase matching is obtained when $\Delta k \equiv |k_E - n_\nu \omega/c| < \pi/l$. Here, l is the effective length over which the nonlinear polarization is generated; it is set by beam overlap geometry, sample length, or the infrared absorption length, whichever is least. An examination of the geometry of Fig. 1 shows $\mathbf{k}_E$ is unchanged when $\mathbf{k}_F$ is rotated about the symmetry (z) axis of the k-vector diamond. That small deviation $\delta\phi$ of ϕ (about its average value ϕ_0) which makes $\Delta kl = \pi$ is easily seen to be such that (for $\phi_0 \ll 1$) $\Omega_p \simeq 2\pi\phi_0\delta\phi \simeq 4\pi^2(k_F l\,|1 - k_F/k_E|)^{-1}$. Taking the diffraction solid angle of the input beam to be $4\pi^2/k_F^2 A$, where A is the beam area, we have for the number N of phase-matched image resolution elements

$$N \simeq Ak_F/l\,|1 - k_F/k_E|. \tag{3}$$

As k_F approaches k_E this number approaches infinity, reflecting the fact that for degenerate four-wave mixing of the geometry of Fig. 1 phase matching is satisfied for all input beam angles (and the generated E wave is the time-reversed replica of the F wave). Furthermore, as $l \to 0$, one has the case of a plane hologram, for which all angles can be replicated, and for which the reading of a complex image at a shifted frequency often has been demonstrated.[1-4] For a volume interaction such as in our experiments, where $k_F = \frac{1}{2}k_E \sim 6\times 10^4\ \mathrm{cm}^{-1}$, $A \sim 10^{-2}\ \mathrm{cm}^2$, and $l \sim 2$ mm, we expect $N \sim 10^6$. Moreover, by decreasing the absorption length at ν, N can be increased without increasing pump-beam powers, as we see below.

Although several physical mechanisms seem to be involved in the nonlinear index that produces the image conversion in some of our experiments, a useful estimate of the conversion efficiency in these experiments can be obtained by assuming that the F and G beams create a transient spatial "grating" of temperature variation[2,4,6,9] whose wave vectors are near $\mathbf{q} = \mathbf{k}_G - \mathbf{k}_F$. It is sufficient for our purposes to consider only the case where the fractional rate of change in time of the amplitude of this grating is less than the frequency of sound of wave vector q. Then, acoustic waves equalize pressure everywhere in the medium nearly instantaneously, and the variation $\theta(\mathbf{x},t)$ in temperature throughout the sample obeys the diffusion equation

$$\rho C_p \dot{\theta} - \lambda\,\nabla^2\theta = (\alpha nc/4\pi)\,\mathrm{Re}[\mathbf{G}\cdot\mathbf{F}^* \exp(i\mathbf{q}\cdot\mathbf{x})], \tag{4}$$

where ρ is the mass density, C_p is the specific heat (at a constant pressure) per unit mass, λ is the thermal conductivity, α is the loss (Np/cm) of the medium (at ν), n is the refractive index (at ν), and G and F are the time-varying amplitudes of the G and F beams (at ν), respectively.

The thermal grating couples to the electromagnetic field via the nonlinear polarization density $\mathbf{p}^{\mathrm{NL}}$ created by the variation in refractive index with temperature:

$$\mathbf{p}^{\mathrm{NL}}(\mathbf{x},t) = \mathrm{Re}[(nX/2\pi)\theta(\mathbf{x},t)\mathbf{H}\exp(i\mathbf{k}_H\cdot\mathbf{x} - i\omega t - \tfrac{1}{2}\mu s)], \tag{5}$$

where μ is the loss coefficient (at ω), s is the distance $(L - z)$ the H beam has traveled in the sample of length L, and $X \equiv (\partial n/\partial\theta)_p$ is the complex change in index (at ω) with temperature at constant pressure. It is a straightforward matter to calculate with Eq. (5) the amplitude $\mathbf{E}(0,t)$ of the generated wave at the front ($z = 0$) surface of the nonlinear medium, assuming that field amplitudes change very little within a wavelength or within a transit time L/c. It is also straightforward to solve for the important part of θ using Eq. (4) with the excellent approximation $\nabla^2\theta = -q^2\theta$.

A useful way to express the result is by the "grating efficiency" R defined as the ratio of E-beam power output (at $z = 0$) to H-beam power in (at $z = L$). In our experiments, the grating always decays very little in a time equal to the laser-pulse duration ($\sim 10^{-8}$ sec). Therefore, R will rise to a maximum while the F and G beams are on, and subsequently decay slowly (if the thermal mechanism dominates). For simplicity, we will give only this maximum R_m of R here, which is found from Eqs. (4) and (5) to be

$$R_m = TD^2 U_F U_G \eta. \tag{6}$$

Here, T is the transmission coefficient $\exp(-\mu L)$ at ω, U_F is energy per unit area in the F beam, U_G is the energy per unit area in the G beam, and η is the phase-mismatch factor which is defined as $|\int_0^L dx \exp(i\Delta kx/\alpha - x)|^2$ and which approaches unity when $\alpha L \gg 1$ and $\alpha \gg \Delta k$. The coupling coefficient D (area per energy) is defined as $-\omega X/\rho C_p$. The values of D for our materials range (in $\mathrm{cm}^2\,\mathrm{J}^{-1}$) from 130 (cyclohexane), 48 (CS_2), 46 (1-2 dichloroethane), and 33 (benzene) down to 27 (acetone), 16 (methanol), and 1.7 (water). (The value is unknown for the glass.)

Clearly, the pump power required to achieve a given efficiency is reduced by making the infrared absorption α large so that η approaches unity, while the optical absorption μ remains so small that the optical transmission T approaches unity. To this end, we added an infrared-absorbing dye (Kodak No. 14015 Q-switching dye) to 1-2 dichloroethane. Then, we have $T \sim \frac{1}{2}$, $\eta \sim 1$, and $D \sim 10^2$. With $U_G \sim 10^{-2}$ and $U_F \sim 10^{-3}\ \mathrm{J/cm}^2$, we expected $R_m \sim 5\times 10^{-3}$ and, in fact, observed such a high efficiency. This efficiency is comparable to that obtained by Stappaerts *et al.*[11] in up-converting an infrared image by resonant frequency summing in cesium vapor.

The efficiencies with the pure liquids (no dyes added) were three to four orders of magnitude lower. If $\alpha L \sim 10^{-2}$ for our 2 mm cell, this reduction would be expected from Eq. (6). Unfortunately, data on the absorption coefficients α of our media at 1.06 μ were lacking at the time this paper was written, but our observations were not unexpected.

For a thermal grating to mediate image conversion efficiently, the phase of F^*G in Eq. (4) cannot vary much while $|FG|$ is large, or during the grating-decay time (whichever time is shorter). However, we expect that materials will be found in which the index grating is both efficient and decays fast (compared to thermal gratings), thus relaxing beam-coherence requirements.

In summary, we have shown that four-wave mixing (or a volume hologram) of a certain geometry can produce useful image-frequency conversion, and can also provide a simple means to measure relaxation times longer than nanoseconds.

This work was supported by the U.S. Air Force Office of Scientific Research under Grant No. 78-3479 and by the National Science Foundation under Grant No. ENG78-04774.

[1] P.W. Maker and R.W. Terhune, Phys. Rev. 137, A801 (1965).
[2] R.G. Harrison, P. Key, V.I. Little, G. Magyar, and J. Katzenstein, Appl. Phys. Lett. 13, 253 (1968).
[3] P.Y. Key, R.G. Harrison, V.I. Little, and J. Katzenstein, IEEE Quantum Electron. QE-6, 641 (1970).
[4] M.E. Mack, Phys. Rev. Lett. 22, 13 (1969).
[5] H. Eichler and B. Kluzowski, Z. Angew. Phys. 27, 4 (1969).
[6] H. Eichler and B. Kluzowski, Z. Angew. Phys. 28, 306 (1970).
[7] F.S. Chen, J.T. LaMacchia, and D.B. Fraser, Appl. Phys. Lett. 13 223 (1968).
[8] H. Eichler, G. Enterlein, J. Munschau, and H. Stahl, Z. Angew. Phys. 31, 1 (1971).
[9] K.O. Hill, Appl. Opt. 10, 1695 (1971).
[10] R.I. Scarlet, Phys. Rev. Lett. 26, 364 (1971).
[11] H.J. Eichler, Opt. Acta 24, 631 (1977).
[12] J.P. Huignard and F. Micheron, Appl. Phys. Lett. 29, 591 (1976).
[13] E.A. Stappaerts, S.E. Harris, and J.F. Young, Appl. Phys. Lett. 29, 669 (1976).

Appendix VI

47

PHYSICAL REVIEW A VOLUME 27, NUMBER 2 FEBRUARY 1983

Raman-induced phase conjugation spectroscopy

S. K. Saha and R. W. Hellwarth
Departments of Physics and Electrical Engineering, University of Southern California, Los Angeles, California 90089-0484
(Received 25 October 1982)

Complete Raman spectra of transparent media are obtained with a single 10-nsec, 10-mJ, laser pulse by a new spectroscopic technique which exploits resonant behavior of nondegenerate four-wave mixing in the phase-conjugate geometry.

To obtain optical Raman (Brillouin, etc.) spectra of transient media, hot media (above 10^{-3} K), or static media exhibiting strong fluorescence, or to obtain spectral resolution of greater than 1 cm^{-1}, one must generally employ some form of coherent Raman spectroscopy (CRS). The most widely used CRS techniques employ two coherent sources whose frequencies are separated by nearly the Raman excitation frequency. These techniques include (1) stimulated Raman gain (loss) spectroscopy (SRS),[1-3] (2) coherent anti-Stokes Raman scattering (CARS),[4-8] (3) Raman-induced Kerr effect (RIKE),[4,5,7,9] and two-beam interferometry.[4,7,10]

Here we propose and demonstrate a new CRS technique that also employs coherent sources at only two frequencies. This is a form of four-wave mixing in which two beams at ω and at $\omega-\omega$ (or at $\omega+\omega$) mix with a third beam at ω to generate a fourth beam at $\omega-\omega$ (or at $\omega+\omega$). The generated beam is nearly phase conjugate to one of the beams at ω. This effect, which we call "Raman-induced phase conjugation" or RIPC has the following characteristics. (1) The Raman signal is generated as a coherent beam which is nearly phase conjugate to one of the incident beams. (2) Up to 16 independent combinations of beam polarizations are possible. (3) The Raman signal beam is not coincident with any input beam. (4) Phase matching among the four beams can be achieved for excitation frequencies in a wide range (many hundreds of cm^{-1}) for a given beam geometry. (5) Phase matching among the four beams can also be achieved, for given beam frequencies, for a wide range of input, or "image," beam angles, thus allowing an enhanced (or altered) phase-conjugate image at Raman resonance. This spatial resolution can be used to enhance spectral resolution or to focus on a particular region of the sample. (6) The wave vectors of excitations observed in RIPC are nearly $(2\omega\pm\omega)n/c$ where n is the refractive index. (7) If the input beam containing $\omega\pm\omega$ is broadband, and beam polarizations are properly adjusted, only Raman-shifted frequencies will be conjugated, and the usual nonresonant component will be absent. These properties allow Raman spectra to be recorded with single (~nsec) pulses. After describing our initial results and theory, we note how RIPC may be superior to all other CRS techniques in special situations, such as for hot, birefringent, and slightly tremulous media.

A typical experimental arrangement for recording (a large range of) the Raman spectrum with a single 10-nsec pulse by RIPC is shown in Fig. 1. Here a Raman vibration(s) of frequency ω in the medium S is excited by the simultaneous presence of the monochromatic beam 2 at ω and the spectral component of the broadband beam 3 that is within a Raman linewidth of $\omega-\omega$ (or of $\omega+\omega$ if the broadband source is at higher frequency than beam 1). This excitation varies the optical polarizability seen by monochromatic beam 1 (at ω), scattering a portion of it into beam 4, which becomes the signal at frequency $\omega-\omega$ whose phase front is nearly conjugate to that of beam 2 at the cell entrance plane. Some typical spectrometer traces of beam 4 are shown in Fig. 2. For these spectra the beams 1 and 2 were each 10-mJ, 10-nsec pulses from a frequency-doubled Nd:YAG laser, half of whose output was used to pump the Rhodamine 6G dye laser which supplied beam 3 with ~0.1-mJ, 8-nsec pulses of broadband radiation spanning about 500 cm^{-1}. The angle θ_{12} between beams 1 and 2 was ~40 mrad. Phase matching optimized the signal when beam 3 was at an angle of 1 to 3 mrad from the direction counter to beam 1 (depending on ω in the range 1000–3000 cm^{-1}). The observed signal spanning 300 cm^{-1} in Fig. 2(e) is well within the limit of 500 cm^{-1} set by phase matching. Also within limits is the image signal of Fig. 3 spanning ~30 mrad. The limits set by phase matching can be estimated as follows.

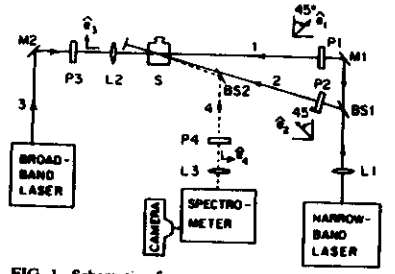

FIG. 1. Schematic of apparatus used to observe RIPC. Incident beams 1, 2, and 3 are polarized by polarizers $P1$, $P2$, and $P3$. Output signal beam 4 is analyzed by polarizer $P4$. Polarizations are either as shown (relative to the same plane in S) or modified as described in text. Incident beams were focused by lenses $L1$ (1-m focal length) and $L2$ (30-cm focal length) into the 1-cm long sample cell S.

Signals fall to half maximum whenever the magnitude Δk of the beam wave-vector mismatch $\Delta\vec{k}\equiv\vec{k}_1-\vec{k}_2+\vec{k}_3-\vec{k}_4$ exceeds either $2.8/L$ (when the absorption coefficient α times the interaction length L is less than 1) or α (when $\alpha L>1$). Consider nearly collinear and counterpropagating monochromatic beams at ω and ν ($\sim\omega-\omega$) aligned for perfect phase match ($\Delta k=0$) as in Fig. 1. Then, if only the angle of the input (image) beam 2 is varied by $\Delta\theta$ from the angle θ_{12} made with beam 1, the resulting Δk is ($k_2\equiv\omega n_2/c$, etc.)

$$\Delta k\sim|\tfrac{1}{2}k_2(k_2/k_4-1)\theta_{12}\Delta\theta|\ . \tag{1}$$

For the case of Fig. 3, we expect from (1) that $\Delta\theta$ within ±20 mrad will preserve phase matching. If, on the other hand, only the frequency ν of the pump beam 3 is varied by $\Delta\nu$ around perfect phase matching, one obtains

$$\Delta k\sim|(\theta_{34}^2-1+k_4/k_3)n_3\Delta\nu/c|\ , \tag{2}$$

where θ_{34} is the angle between beams 3 and 4. From this, we expect in the situation of Fig. 2(e) that phase matching is achieved for $\Delta\nu/2\pi c$ within the range ±200 cm^{-1}. These ranges are one to two orders of magnitude larger than are available in CARS spectroscopy.

The strength of the observed lines in Fig. 1 and the absence of background wave mixing off resonance in Figs. 1(a)–1(d) can be predicted from the dependence on the optical electric field $\vec{\mathcal{E}}(\vec{x},t)$ of that part $\vec{\mathcal{P}}^{(3)}(\vec{x},t)$ of the nonlinear optical polarization density that is third order in $\vec{\mathcal{E}}$. In liquids, gases, and glasses when the Born-Oppenheimer approximation is valid, i.e., when all optical frequencies are well below the electronic band edge, $\vec{\mathcal{P}}^{(3)}$ is of the form (with space argument $\vec{x}$ suppressed)[11,12]

$$\vec{\mathcal{P}}^{(3)}(t)=\tfrac{1}{2}\sigma\vec{\mathcal{E}}(t)\mathcal{E}^2(t)+\vec{\mathcal{E}}(t)\int_{-\infty}^{t}ds\,a(t-s)\mathcal{E}^2(s)+\int_{-\infty}^{t}ds\,b(t-s)\vec{\mathcal{E}}(t)\cdot\vec{\mathcal{E}}(s)\vec{\mathcal{E}}(s)\ . \tag{3}$$

Here σ is a real number measuring the instantaneous nonlinear electronic response or "hyperpolarizability" (that would be present if the nuclei were fixed), and $a(\tau)$ and $b(\tau)$ are nuclear response functions describing Raman-active excitations which alter the optical susceptibility. These "nuclear" terms may be thought of as of the linear form $\chi(t)\mathcal{E}(t)$ but with $\chi(t)$ modulated by nuclear motions (vibration, rotation, etc.) driven by the interaction potential $-\frac{1}{2}\chi\mathcal{E}^2(s)$ at past times.[11,12] In thermal media, the

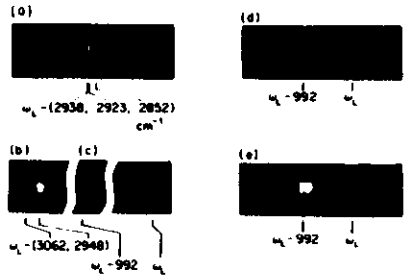

FIG. 2. Spectra taken with apparatus of Fig. 1. Samples S were (a) cyclohexane and (b)–(e) benzene. In (a)–(d) linear polarizers were fixed as shown in Fig. 1, but in (e) polarizer P_4 was rotated clockwise by $\theta\sim10°$ from direction shown. Spectra (d) and (e) were taken with lower grating order. The cross sections of the three Raman lines in (a) are comparable. The cross sections of the Raman lines in (b) and (c) are in the ratio 0.01:0.1:1, respectively. Spectra were recorded on Polaroid 410 film. From one to ten pulses were used for exposure depending on line strength.

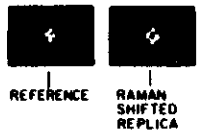

FIG. 3. Image replication. Images recorded on Polaroid 410 film at open exit slits of spectrometer when four-hole image plate was inserted adjacent to $P2$ in Fig. 1. Reference image obtained with plane mirror in place of cell S. This frequency-shifted replica was obtained with benzene in cell S and all beams as in Fig. 1. Image subtended 30 mrad at sample.

48

response functions $a(\tau)$ and $b(\tau)$ are related to the differential Raman scattering cross sections

$$d^2\sigma_i(\Delta)/d\Omega\, d\Delta$$

[$\text{cm}^{-1}\,\text{sr}^{-1}$ (rad/s)$^{-1}$] which give the probability per unit length for a photon to scatter from frequency ω to frequency $\nu=\omega-\Delta$ per unit (angular) frequency range per unit solid angle for scattered polarization either parallel ($i=\|$) or perpendicular ($i=\perp$) to the incident beam polarization. Defining the Fourier transforms

$$A_\Delta \equiv \int_0^\infty dt\, a(t)e^{i\Delta t}$$

and similarly for B_Δ, we have[11,12]

$$\text{Im}B_\Delta = \frac{\pi c^4}{\hbar\omega\nu^3}\frac{d^2\sigma_\|}{d\Omega\, d\Delta}(1-e^{-\hbar\Delta/kT}) \qquad (4)$$

and a similar relation with A_Δ and $\frac{1}{2}\sigma_\|-\sigma_\perp$ substituted for B_Δ and $\sigma_\perp$, respectively. Here kT is Boltzmann's constant times temperature. Because of the causal nature of $a(t)$ and $b(t)$ the real parts of A_Δ and B_Δ can be calculated from the imaginary parts (4) by the usual Kramers-Kronig integrals.[11] Given the Raman spectrum of a medium and the electronic hyperpolarizability σ, the nonlinear polarization density (3) is completely determined.

In our experiments $\vec{\mathcal{E}}$ in (3) is essentially the sum of three incident beams $\vec{\mathcal{E}}_1+\vec{\mathcal{E}}_2+\vec{\mathcal{E}}_3$ which give rise to a term in the polarization density $\vec{\mathcal{P}}^{(3)}$ which generates a fourth phase-conjugate beam $\vec{\mathcal{E}}_4$. Our results can be understood by assuming each beam is a plane wave:

$$\vec{\mathcal{E}}_1 = \text{Re}\vec{E}_1 e^{i(\vec{k}_1\cdot\vec{r}-\omega t}\,,$$

etc. If one takes from (3) the part $(\text{Re}\vec{P}_4 e^{i(\vec{k}_4\cdot\vec{r}-\omega t})$ of $\vec{\mathcal{P}}^{(3)}$ which generates the signal (phase-conjugate) beam one finds that[12] ($\mu\equiv\nu-\omega=-\Delta$, $A_\mu=A_{-\Delta}=A_\Delta^*$, $A_0\equiv A_{\Delta=0}$, etc.)

$$\vec{P}_4=\tfrac{1}{4}[\vec{E}_1\vec{E}_2^*\cdot\vec{E}_3(\sigma+B_0+2A_\mu)+\vec{E}_2^*\vec{E}_1\cdot\vec{E}_3(\sigma+B_0+B_\mu)+\vec{E}_3\vec{E}_2^*\cdot\vec{E}_1(\sigma+2A_0+B_\mu)]e^{i\Delta\vec{k}\cdot\vec{r}}\,. \qquad (5)$$

With the polarizers arranged as in Fig. 1, the effective polarization component is

$$P_{4h}\equiv\hat{h}\cdot\vec{P}_4=(B_\mu-2A_\mu)E_1E_2^*E_3/8\,,$$

where $\hat{h}$ is a horizontal unit vector. Since B_μ and A_μ are only large near Raman resonances, we observe in Figs. 2(a)–2(d) narrow lines when $\Delta\sim\omega$ and negligible signal far from resonance. If the linear polarizer $\hat{e}_4$ is oriented at $\pi/4+\theta$ from $\hat{e}_1$, then one finds from (5) that the effective component of $\vec{P}_4$ is $P_{4\theta}=P_{4h}\cos\theta+P_{4v}\sin\theta$, where

$$P_{4v}\equiv\hat{v}\cdot\vec{P}_4$$
$$=(\sigma+B_0+\tfrac{1}{2}B_\mu+A_\mu)E_1E_2^*E_3/4\,,$$

and $\hat{v}$ is a unit vertical vector (parallel to $\hat{e}_3$). Evident in P_{4v} is the nonresonant (constant) background term which is observed in Fig. 2(e) to interfere with the resonant B_μ and A_μ terms when $\Delta\sim\omega$. Since the output signal intensity is proportional to $|\hat{e}_4^*\cdot\vec{P}_4|^2$ in general, the details of this interference can be used to measure the parameters appearing in (5).[13]

If the incident beams are negligibly disturbed by the mixing process, the intensity I_4 of the phase-conjugate signal can be easily calculated from (5) in terms of the incident intensities I_1, I_2, and I_3. The result is often written in the form

$$I_4=\beta^2L^2I_1I_2I_3\,, \qquad (6)$$

where L is an effective interaction length (equal to the cell length in our case) and β is a nonlinear coefficient which depends on all beam polarizations and the parameters in (5). For example, the magnitudes of the signals seen in Figs. 2(c) and 2(d) may be estimated using the foregoing relations and the measured values for the 992-cm^{-1} line of benzene: 1.6×10^{-5} for $d\sigma_\|/d\Omega$, 1.2 cm^{-1} for the linewidth, and 0.02 for $\sigma_\perp/\sigma_\|$.[14,15] These give $\beta\sim1$ cm/GW at line center. For our beam intensities, this predicts $I_4/I_2\sim10^{-5}$, which is consistent with our observations.

We summarize the properties of RIPC as a Raman spectroscopic tool by considering the following task, for which RIPC appears to be better suited than any other technique. Suppose one wished to obtain the Raman spectrum of a crystal in a phase that only exists at temperatures ($\gtrsim10^3$ K) that are too high for spontaneous Raman spectra to be visible in the thermal background.[16,17] Suppose further that the dispersion of the refractive index is unknown so that the CARS signal could not be obtained without a very tedious search for the phase-matching angle. Suppose also that the crystal is birefringent. Then a probe beam having comparable ordinary and extraordinary components (necessary for RIKE) cannot be nulled by any practical polarizer to better than ~1%. This would make RIKE insensitive to any but the strongest Raman lines. Suppose further that the hot crystal is undergoing temperature fluctuations. Raman gain spectroscopy and two-beam interferometry, which rely on many seconds of processing of very stable beams, become

inapplicable. Noise-initiated single-pass stimulated Raman scattering (ordinary SRS) might produce a signal, but only at the strongest Raman line, and provided that the crystal is not damaged by self-focusing before threshold is reached. However, none of these impediments would prevent RIPC spectra, such as those in Fig. 2, from being obtained.

The authors would like to acknowledge the support of the Air Force Office of Scientific Research under Grant No. 78-3478 and of the National Science Foundation under Grant No. ECS-8114828.

[1]W. J. Jones and B. P. Stoicheff, Phys. Rev. Lett. 13, 657 (1964).
[2]R. W. Hellwarth, Phys. Rev. 130, 1850 (1963).
[3]A. Owyoung, in *Advances in Infrared and Raman Spectroscopy*, edited by R. Clark and R. Hestor (Heyden, London, 1979), Vol. 9.
[4]A. Owyoung, in *Chemical Applications of Nonlinear Spectroscopy*, edited by A. Harvey (Academic, New York, 1979).
[5]S. A. Akhmanov, in *Nonlinear Spectroscopy, Proceedings of the International School of Physics, "Enrico Fermi,"* edited by N. Bloembergen (North-Holland, Amsterdam, 1977).
[6]P. D. Maker and R. W. Terhune, Phys. Rev. A 137, 801 (1965).
[7]G. L. Eesley, J. Quant. Spectrosc. Radiat. Transfer 22, 507 (1979).
[8]J. L. Oudar, R. W. Smith, and Y. R. Shen, Appl. Phys. Lett. 34, 758 (1979).
[9]D. Heiman, R. W. Hellwarth, M. D. Levenson, and G. Martin, Phys. Rev. Lett. 36, 189 (1976).
[10]A. Owyoung and P. S. Percy, J. Appl. Phys. 48, 674 (1977).
[11]R. W. Hellwarth, J. Cherlow, T. T. Yang, Phys. Rev. B 11, 964 (1975).
[12]R. W. Hellwarth, in *Progress in Quantum Electronics*, edited by J. H. Sanders and S. Stenholm (Pergamon, New York, 1977), Vol. 5, Part 1.
[13]S. K. Saha and R. W. Hellwarth (unpublished).
[14]J. G. Skinner and W. G. Nilsen, J. Opt. Soc. Am. 58, 113 (1968).
[15]Y. Kato and H. Takuma, J. Chem. Phys. 54, 5398 (1971).
[16]P. Alain, J. P. Coutures, and B. Piriou, J. Raman Spectrosc. 8, 88 (1979).
[17]A. Owyoung, IEEE J. Quantum Electron. QE-14, 192 (1978).

Appendix VII

Generation of a time-reversed replica of a nonuniformly polarized image-bearing optical beam

G. Martin,* L. K. Lam, and R. W. Hellwarth

Electronic Sciences Laboratory, University of Southern California, Los Angeles, California 90007

Received November 19, 1979; revised manuscript received February 12, 1980

We demonstrate the generation of the time-reversed replica of an incident monochromatic image-bearing optical beam that is nonuniformly polarized. A form of degenerate four-wave mixing in liquid CS_2 of beams at 532 nm is employed. We discuss sources of distortion in the vector replica using standard theory of nonlinear beam interaction.

Introduction

The generation of a time-reversed replica (i.e., the phase conjugate) of a monochromatic, image-bearing optical wave has been demonstrated previously by a variety of techniques, but only for cases in which the wave has a known and uniform (usually linear) state of polarization.[1] Here we report the generation of a complete time-reversed vector replica (or phase conjugate) of an incident monochromatic image-bearing optical wave whose state of polarization has been altered by a nonuniformly birefringent window so that it is randomly nonuniform over the wave front.

We employ a kind of degenerate four-wave mixing process in which the incident wave is made to overlap two counterpropagating plane pump waves whose electric field vectors are rotating (circularly polarized) in opposite directions. Theory predicts that the wave generated by the resulting third-order nonlinear polarization in an isotropic medium is the desired time-reversed vector replica, provided that the incident and pump waves are mutually temporally coherent where they overlap in the nonlinear medium (CS_2).[2]

The earliest demonstration of the generation of a time-reversed replica of a uniformly polarized optical wave (i.e., scalar phase conjugation) was by Kogelnik, who used standard holographic methods of still photography.[3] The first demonstration of nearly instantaneous scalar phase conjugation, by Stepanov *et al.*, employed a degenerate four-wave mixing process that was described as a kind of transient holography.[4]

Our experimental arrangement for conjugating a nonuniformly polarized wave is described below. This arrangement is similar to one proposed by Zel'dovich and Shkunov[5] for conjugating a wave front of uniform but arbitrary polarization. The theory of this vector-image conjugation is outlined in the section on theory, and the area of applicability of this process is described in the discussion section.

Experiment

The experimental arrangement we have employed to study vector-wave phase conjugation is shown schematically in Fig. 1. A linearly polarized optical pulse of ~15-nsec duration and ~1-MW peak power at 532-nm wavelength is generated by a frequency-doubled Nd:YAG laser. This wave is split into three beams by beam splitters BS1 (35% reflecting) and BS2 (50% reflecting) of Fig. 1. The two beams from BS2 form counterpropagating pump waves G and H, which are circularly polarized (counterrotating) by quarter-wave plates Q1 and Q2 and focused into the interaction region at C by lenses L1 and L2. The 100% reflecting dielectric mirrors M1 and M2 do not affect the polarizations of G and H.

The wave that is split off by beam splitter BS1 is linearly polarized at angle ϕ to the vertical by polarizer P2 and expanded by telescope BE to a diameter of about 2 cm. This beam F illuminates the object O and

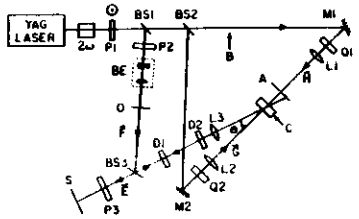

Fig. 1. Schematic of apparatus for observing (at plane S) backscattered images of incident beam F from region C. The backscattering is caused either by an ordinary mirror at C or by nonlinear mixing of the incident image-bearing beam F with counterpropagating plane pump beams G and H in liquid CS_2 (contained in a 2-mm-long cell at C). The role of the various optical elements is discussed in the text.

Reprinted from Optics Letters, Vol. 5, page 185, May, 1980

is then directed by mirror BS3 through phase distorter D1 and polarization distorter D2 and is focused by lens L3 into region C in the nonlinear medium (CS_2), where it crosses the counterpropagating pump beams at an angle of about 4°. All three beams (F, G, and H) have a diameter of ~0.3 mm in the cell, where they overlap for the entire 2-mm length of the cell.

The phase-conjugate image is observed behind beam splitter BS3 and is recorded on photographic print paper at observation plane S, which is approximately the same distance from the interaction region as is object O.

Figure 2 compares photographic records at plane S of waves backscattered from the incident image-bearing beam F either by a plane mirror at position C (column I) or by the phase-conjugation process when the cell of CS_2 is at C (column II). The pictures of rows a, b, and c of Fig. 2 were taken without polarizer P3 under the following conditions:

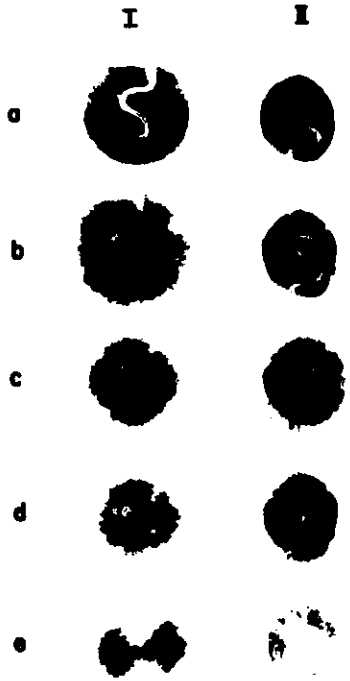

Fig. 2. Backscattered images recorded at plane S (Fig. 1). The images of column I were backscattered from beam F by an ordinary plane mirror at C (the focal plane of lens L3 of Fig. 1). The images of column II were backscattered from beam F by nonlinear mixing with the counterpropagating plane pump waves in liquid CS_2 (as depicted in Fig. 1). Various conditions of phase and polarization distortion, as well as incident and backscattered beam polarizations, result in the images shown here in rows a–e, as is explained in the text. The backscattered fraction from nonlinear mixing was of the order of 1%. These images were recorded on FSC polycontrast G photographic printing paper. Images in column I are averages of a few shots. Images in column II are averages of about 50 shots.

Picture Ia is the mirror-reflected image of object O (a bent wire) with the distorting plates D1 and D2 removed. (The image is inverted because of the presence of focusing lens L3.) Picture IIa is the phase-conjugate image with the CS_2 cell at position C and distorters D1 and D2 absent. Pictures Ib and IIb are the corresponding images but with phase distorter D1 in place. Pictures Ic and IIc are the corresponding images when both phase distorter D1 and polarization distorter D2 are in place. The cross superposed on this image arises from polarization distorter D2, which consisted of four quadrants of quarter-wave retarding plastic, each of a different orientation. Pictures Id, Ie, IId, and IIe are taken with linear polarizer P3 placed as indicated in Fig. 1: first, in row d, with its axis aligned parallel to the initial polarization set by P2 of image-bearing beam F, and then, in row e, aligned 90° to this direction.

Comparison of the pictures in column I of Fig. 2 with those in column II shows that our arrangement for phase conjugation not only restores phase distortions created in an image-bearing beam but also corrects polarization scrambling. To check the degree of the polarization restoration of image-bearing beam F, we oriented the F-beam polarizer P2 at different angles ϕ to the vertical and in each case measured the fraction of the phase-conjugate wave polarized orthogonal to the input direction (e.g., we measured the ratio of intensities in pictures IIe and IId). We found the ratio to be less than 1:100 for all cases. Beam restoration was observed to deteriorate as the pump-beam polarizations were altered from circular.

Theory

Our experimental conditions are expected from theory to produce a quite accurate time-reversed vector replica of a nonuniformly polarized incident wave of amplitude $F_i(\mathbf{x})$, $i = x,y,z$. This can be seen from the expression in esu (valid for small replication efficiencies) for the vector amplitude $E_i(\mathbf{x})$, $i = x,y,z$, of the backscattered wave at positions $\mathbf{x}$ in front of the region of nonlinear beam interaction[2]:

$$E_i(\mathbf{x}) = 12\pi i\omega(nc)^{-1}LT_{ij}c_{jklm}F_k^*(\mathbf{x})G_lH_m. \quad (1)$$

Here the summation over repeated space indices (j, k, l, m) is assumed. The waves are all at angular frequency ω in a nonlinear medium having refractive index n and nonlinear susceptibility tensor c_{jklm} evaluated at the four frequency arguments $(-\omega, -\omega, \omega, \omega)$. The incident wave $F_k(\mathbf{x})$ overlaps two counterpropagating pump waves (whose vector amplitudes G and H in the interaction region have spatial components G_l and H_l) over an effective interaction length L. The tensor T_{ij} yields the projection of any vector onto the plane transverse to the F and E beams.

For isotropic media and optical wavelengths such as we employ, the c_{ijkl} tensor has the form

$$c_{ijkl} = a\delta_{ij}\delta_{kl} + b\delta_{ik}\delta_{jl} + c\delta_{il}\delta_{jk}, \quad (2)$$

where the coefficients a, b, and c may exhibit temporal and spatial dispersion. When the nonlinear polarization arises from a nonpropagating physical change, such as the electronic and molecular reorientation mechanisms that will predominate in our CS_2 medium, then symmetry requires that $b = c$. For CS_2, a variety of existing measurements gives values (appropriate to 532 nm) $b = c \sim 4 \times 10^{-13}$ esu and $a \sim 8 \times 10^{-14}$ esu to within 10%, provided that electrostrictive and thermal effects can be neglected.[6]

If the angle θ between beams F and G (see Fig. 1) is much less than unity, and if $|b - c| \ll |b + c|$, then one finds from Eqs. (1) and (2) that having G and H oppositely circularly polarized gives the desired result that $E_i \propto F_i^*$ to order θ^2. Of course, a real beam will not be perfectly circularly polarized, so assume for the purpose of evaluating Eq. (1) that

$$\mathbf{G} = (\hat{e}_R + \epsilon\hat{e}_L)G \quad (3)$$

and

$$\mathbf{H} = (\hat{e}_L + \delta\hat{e}_R)H, \quad (4)$$

where $\hat{e}_R$ and $\hat{e}_L$ are the complex unit vectors representing right and left circular rotations, respectively, of the optical electric vector [equaling $(\hat{x}' \pm i\hat{y}')/2^{1/2}$ for waves directed along $\pm\hat{z}'$] and the fractions ϵ and δ of "wrong" polarization are assumed to be much less than unity. Substituting Eqs. (2)–(4) in Eq. (1) gives (in vector notation) for the backscattered field

$$\mathbf{E} = 12\pi i\omega(nc)^{-1}L[(a + \tfrac{1}{2}b + \tfrac{1}{2}c)\mathbf{F}^* + \tfrac{1}{2}f\mathbf{K}]GH. \quad (5)$$

Here the error field $\mathbf{K}$ is defined as $\hat{x}F_y - \hat{y}F_x$ so it is orthogonal to the desired conjugate part $\mathbf{F}^*$. The error coefficient f is

$$f = (b + c)\{|\sin^2\theta + (1 + \cos^2\theta)(\epsilon + \delta)|F_x^*F_y^* + i(\delta - \epsilon)\cos\theta\,(F_x^*F_x^* - F_y^*F_y^*)|/F^2 - (b - c)\cos\theta\,(F_x^*F_x^* + F_y^*F_y^*)/F^2, \quad (6)$$

in which we have omitted terms higher than first order in ϵ and δ. In Eq. (5), terms in the coefficient of F^* that are fractionally smaller by terms of the order of ϵ, δ, θ^2, and $(b - c)/b$ have also been neglected.

The power fraction $|f/(b + c + 2a)|^2$ of the "wrong" polarization of the backscattered beam is seen to have terms of the order of (1) the power fractions ϵ^2 and δ^2 of wrong polarization in the pump beams, (2) the broken symmetry ratio $|(b - c)/(b + c)|^2$, and (3) $\sin^4\theta$, as well as the three cross terms of the order of the square root of the product of any two of the above. It is seen to be experimentally feasible to keep the fraction of wrong polarization generated (at any place $\mathbf{x}$ in the phase front) well below 1%, as we observed.

Discussion

One can interpret the three terms in the nonlinear susceptibility Eq. (2) acting in Eq. (1) to produce the backscattered field E as a superposition of four gratings of linear refractive index off which the beams G and H scatter to generate E. The four gratings are (1) beam G scattering off the scalar grating $\mathbf{F}^* \cdot \mathbf{H}$ to give a term $E \propto c\mathbf{G}\mathbf{F}^* \cdot \mathbf{H}$, (2) beam H scattering off the scalar grating $\mathbf{F}^* \cdot \mathbf{G}$ to give a term $\mathbf{E} \propto b\mathbf{H}\mathbf{F}^* \cdot \mathbf{G}$, (3) beam G scattering off the tensor grating $\mathbf{F}^*\mathbf{H}$, and (4) beam H scattering off the tensor grating $\mathbf{F}^*\mathbf{G}$, the last two giving a term $\mathbf{E} \propto a\mathbf{F}^*\mathbf{H} \cdot \mathbf{G}$. Consider grating (1) of amplitude $\propto \mathbf{F}^* \cdot \mathbf{H}$ and of wave vector $\sim 2n\omega/c$. The grating must not move by an appreciable fraction of the grating period $\pi c/n\omega$ during the longest characteristic time t_c associated with the pulse shape and the physical mechanism(s) responsible for the grating (mainly molecular reorientation in CS_2, for which $t_c \sim 1$ psec). This is achieved if the frequencies of the F and H beams are the same to within $\sim t_c^{-1}$ (or if they are correlated in a special way).

The grating also must not move by an appreciable fraction of its period during the time it takes the reading beam G to propagate over the length L of the interaction region. This is achieved if the frequencies of the F and H beams are the same to within $\sim c/L$. In either case, the frequency ν of the reading beam G can be quite different (hundreds of wave numbers) from the frequency of F and H without spoiling the phase matching for the finite lengths L of practical interest. However, the backscattered-image shrinkage factor (ω/ν) may become a problem. All these considerations arise in the usual scalar-wave phase-conjugation experiments, whether with photographic or transient grating media, and apply to the other three gratings mentioned above.

Aside from the obvious application to restoring a beam reflected back through a birefringent distorting medium, vector-wave replication may be used in imaging microscopic inclusions in such a medium. Inclusions that have a complex (nonreal) optical dielectric tensor do not sustain time-reversed propagation, and so they may be imaged by a lens at the observation plane (S of Fig. 1) free of the distortion caused by the surrounding inhomogeneous medium, which has a real (though anisotropic) dielectric tensor.

In conclusion, we have demonstrated, as was expected from theory, the generation by a form of four-wave mixing of a time-reversed replica of a monochromatic image-bearing optical wave of arbitrary nonuniform polarization.

The authors acknowledge the support of the U.S. Air Force Office of Scientific Research under grant no. 78-3479 and the National Science Foundation under grant ENG78-04774.

* Present address, Guidance and Control Systems Division, Litton Industries, 5500 Canoga Ave., Woodland Hills, California 91364.

References

1. See references in A. Yariv, IEEE J. Quantum Electron. **QE-15**, 524 (1979).
2. R. W. Hellwarth, J. Opt. Soc. Am. **67**, 1 (1977).
3. H. Kogelnik, Bell Syst. Tech. J. **44**, 2451 (1965).
4. B. I. Stepanov, E. V. Ivakin, and A. S. Rubanov, Sov. Phys. Dokl. **16**, 46 (1971).
5. B. Ya. Zel'dovich and V. V. Shkunov, Sov. J. Quantum Electron. **9**, 379 (1979).
6. R. W. Hellwarth, "Third-order optical susceptibilities of liquids and solids," in *Progress in Quantum Electronics*, J. Sanders and S. Stenholm, eds. (Pergamon, New York, 1977), Vol. 5, part 1.

Appendix VIII 54

Photorefractive effects and light-induced charge migration in barium titanate

Jack Feinberg, D. Heiman, A. R. Tanguay, Jr., and R. W. Hellwarth
Electronics Sciences Laboratory, University of Southern California, Los Angeles, California 90007

(Received 17 September 1979; accepted for publication 1 November 1979)

We propose a new theoretical model for the light-induced migration of charges which mediates the "photorefractive effect" (light-induced refractive index change) in barium titanate and other crystals. We also present experimental results of various effects of this light-induced charge migration in a single-domain crystal of barium titanate, specifically, (1) energy transfer between two intersecting optical beams, (2) optical four-wave mixing and optical-beam phase conjugation, (3) erasure of spatial patterns of photorefractive index variations, and (4) photoconductivity. The theoretical model predicts the observed dependences of these effects on (1) beam intensities, directions, and polarizations, (2) crystal orientation, and (3) on an externally applied dc electric field. Time dependences of transients as well as steady-state magnitudes are predicted. In this model, identical charges migrate by hopping between adjacent sites, with a hopping rate proportional to the total light intensity at the starting site. The net hopping rate varies with the local electric potential that is calculated self-consistently from the charge migration pattern. In barium titanate the charges are positive with a density of $(1.9 \pm 0.2) \times 10^{16}$ cm^{-3} at 514 nm. The origin of the charges and sites is at present unknown. The hopping rate constant determined from optical beam interactions is used to predict the observed photoconductivity of 1.3×10^{-10} cm Ω^{-1} W^{-1} at 514 nm.

PACS numbers: 42.65. – k, 78.20.Jq, 72.40. + w, 42.30.Va

I. INTRODUCTION

When light is transmitted through certain noncentrosymmetric crystals, it causes a change in the refractive index which persists for hours or longer in the dark and can be erased by flooding the crystal uniformly with light. This "photorefractive" effect arises from a light-induced migration and separation of charge in the crystal which gives rise to internal static electric fields. These fields produce refractive-index changes via the linear electro optic (Pockels) effect.

We propose a new theoretical model for the migration of charges mediating the photorefractive effect in barium titanate. We also present detailed experimental studies of charge pattern erasure, and of two-wave and four-wave mixing of optical beams (in the milliwatt range) in barium titanate. Using our theoretical model we are able to predict the observed dependence of wave mixing on the intensities and polarization of the waves, and on the wave directions relative to each other and to the crystal optical axis. Both the transient and steady-state cases are discussed.

It should be pointed out that the electric fields caused by light-induced charge migration are easily observable in ferroelectrics due to their large electro optic coefficients, but such electric fields may also be produced in materials that have inversion symmetry and consequently lack a linear electro optic effect. Although the fields would not produce any first-order index changes (Pockels effect) in such materials, the fields could produce second-order index changes (Kerr effect) or energy level shifts (Stark effect).

All of our experiments were performed on a single-domain $2.2 \times 2.8 \times 4.2$-mm crystal of barium titanate ($BaTiO_3$).[1] Between 5 and 133 °C, barium titanate is a ferroelectric with tetragonal symmetry C_{4v}. Our sample was slightly wedged with faces cut approximately parallel to the (001), (010), and (100) planes. The crystal has a pale yellow color and gives 10^{-3} extinction between crossed polarizers.

In our "four-wave mixing" experiments, two beams of light of the same frequency, called "writing" beams, intersect in the crystal and create a periodic modulation of its refractive index. This "index grating" is monitored by diffraction of a third "reading" beam incident on the grating (at an angle that satisfies the Bragg condition) to produce a fourth "output" beam. If the two writing beams and the reading beam all have the same frequency (and polarizations if the sample is birefringent), then the Bragg condition is satisfied by a reading beam which propagates counter to either of the writing beams. This geometry is identical to that commonly used in phase conjugation experiments,[2] and our output beam is observed to be the phase conjugate of one of the writing beams. However, in contrast to phase conjugation by ordinary nonlinear refraction, the fraction of the reading beam that is diffracted in the steady state depends only on the relative intensity of the writing beams and is independent of their absolute intensity. A certain optical energy (rather than power) must be deposited in the crystal in order to "write" a grating with a given diffraction efficiency. The optical absorption of our sample was too small to measure ($< 5\%$), but we estimate that several microjoules per image element are required to write a grating of high efficiency.

If the writing beams are turned off, the grating will persist overnight in a darkened room, but reading the grating erases it with a decay rate which increases with the intensity of the reading beam. The grating can also be erased by flooding the crystal with light incident from an arbitrary direction. Wavelengths from 477 to ~900 nm were used to erase, with the longer wavelengths erasing at a considerably slower

 0021-8979/80/031297-08$01.10

rate with the same incident intensity. A red "erasing" beam will erase a grating previously formed by green writing beams, and vice versa. Erasing the crystal will completely restore it to its original state; we have used the same sample for over a year with no sign of damage or discoloration. When making the grating, the rise time of the diffraction efficiency will decrease if the total writing intensity is increased. For example, the exponential time constant varies from a few seconds to a few milliseconds as the total writing intensity is varied from 10^{-3} to 1 W/cm^2. Both the writing and the erasing rates increase dramatically when the crossing angle between the writing beams is increased at small angles.

The diffraction efficiency R depends on the orientation of the crystal with respect to the writing beams as follows. R is largest when the c axis of the crystal is aligned normal to the planes of the intensity grating, and least when the c axis is parallel to these planes. R increases as the square of the interaction length of the beams, and we have measured values of R as high as 35% at 515 nm with an interaction length (crystal length) of 4 mm.

One of the more interesting and easily observed effects is that the writing beams emerge from the crystal with a different relative intensity than when they entered it[3,4]; energy is clearly transferred from one beam to the other. The direction of energy transfer is determined by the orientation of the c axis relative to the writing beams. No energy transfer is observed if the sample is slightly vibrated or when the beams do not intersect in the sample. The magnitude of energy transfer can be easily made to approach 100% for equal input intensities: one writing beam emerges from the crystal almost extinguished, while the other writing beam emerges with twice its original intensity.

A dc electric field externally applied along the c axis of the crystal enhances both the diffraction efficiency and the magnitude of the energy-transfer effect. These effects will be discussed in detail in the following sections.

In Sec. II our model is developed, and is compared to our experimental results in Sec. III. Section IV applies our model to the experimental results of others, and discusses the differences between our model and previous models.

II. THEORY

We describe here a model for charge migration in photorefractive crystals which, with two parameters, predicts the energy exchanges among two or four optical beams. This exchange, in both transient and steady-state regimes, is shown to depend on the intensities, polarizations, and angles of the beams, and on an applied static electic field for a given orientation of the crystal. Given the charge-migration patterns from our model, one can derive the quasistatic electric fields inside the crystal, and from this the refractive index changes caused by the electro optic effect.

According to our model, there are a certain number of charges which can occupy a larger number of sites in any of a large number of permutations. In darkness, each charge stays fixed at a site, but when a charge is exposed to an optical intensity I, it tends to "hop" to an adjacent site with a probability per second that is proportional to I. Let W_n be the probability that a migrant charge occupies the nth site which is at position x_n. If the optical intensity at this site is I_n, then the model may be expressed mathematically by

$$\frac{dW_n}{dt} = -\sum_m D_{nm} [W_n I_n \exp(\beta\phi_{nm}) - W_m I_m \exp(\beta\phi_{mn})], \quad (1)$$

where the sum is over neighboring sites m.

The rate constant $D_{nm} \exp(\beta\phi_{nm})$ measures the tendency toward light-induced hopping from site m to site n. We have written it in terms of the parameters $D_{nm} = D_{mn}$ and of the static potential difference ϕ_{nm} between the sites. Here β equals $q/(k_B T)$, where q is the charge, k_B is Boltzmann's constant, and T is the lattice temperature. This form makes explicit in Eq. (1) that the relative site occupation probability in steady state under weak uniform illumination will obey statistial mechanics, i.e., that $W_m/W_n = \exp(\beta\phi_{nm})$. Specifically, ϕ_{nm} is equal to $\phi_n - \phi_m$ where $\phi_n = \phi(x_n)$, and $\phi(x)$ is the quasistatic potential existing in the crystal due to internal charge migration, externally applied fields and intrinsic chemical potentials. Whenever light is present, the gradient of ϕ will cause a net drift by hopping of charges in time, away from a stationary background of neutralizing charge (which we assume does not hop). In our model this drift is governed by Eq. (1), for hopping in all directions.

In barium titanate, the omission from the hopping rate of any dependence on the probability of occupation of the final site is consistent with the experimental results. That is, in our experiments the site occupation probabilities W_n appear to be much less than unity, implying that most sites are unoccupied. It is straightforward to account for final-site occupation by appending factors $1-W_m$ to the rate to hop to site m in Eq. (1), should it prove appropriate.

To analyze our present experimental results we will need to consider only the case where I_n varies from the interference of two "writing" optical beams of the same temporal frequency whose complex electric field amplitudes at position x are $\hat{e}_1 E_1 \exp(i\mathbf{k}_1 \cdot \mathbf{x})$ and $\hat{e}_2 E_2 \exp(i\mathbf{k}_2 \cdot \mathbf{x})$. See Fig. 1. The complex polarization vectors $\hat{e}_1$ and $\hat{e}_2$ are normalized by $\hat{e}_1^* \cdot \hat{e}_1 = 1$, etc. Therefore, we may write

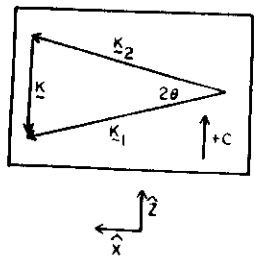

FIG. 1. Two writing beams with wave vectors $\mathbf{k}_1$ and $\mathbf{k}_2$ intersect at an angle 2θ in the crystal to produce an intensity grating with wavevector $\mathbf{k} = \mathbf{k}_1 - \mathbf{k}_2$. The direction of the positive c axis is shown.

$$I_n = G_0 + \mathrm{Re}G\exp(i\mathbf{k}\cdot\mathbf{x}_n)\,, \tag{2}$$

where $\mathbf{k} = \mathbf{k}_1 - \mathbf{k}_2$, $G \equiv 2E_1E_2^*\hat{e}_1\hat{e}_2^*$, and $G_0 \equiv \Sigma_i |E_i|^2$ (the sum extends over the two writing beams plus any other beams that are present). An important parameter is the complex modulation index m defined as

$$m \equiv G/G_0\,. \tag{3}$$

Note that $0 < |m| < 1$.

If $|m| \ll 1$, it is appropriate to try approximate solutions for W_n and ϕ_n of the form

$$W_n = W_0 + \mathrm{Re}W\exp(i\mathbf{k}\cdot\mathbf{x}_n) \tag{4}$$

and

$$\phi_n = \phi_{0n} + \mathrm{Re}\phi\exp(i\mathbf{k}\cdot\mathbf{x}_n)\,, \tag{5}$$

where ϕ_{0n} is the potential at $\mathbf{x}_n$ due to any charges external to the crystal, applied fields, or chemical potentials. Note that, according to Poisson's equation, the potential- and charge-distribution amplitudes ϕ and W must be related by

$$\phi = W\rho q/\epsilon\epsilon_0 k^2\,, \tag{6}$$

where ρ is the average density (number per unit volume) of sites, ϵ_0 is the permittivity of free space, and the screening dielectric constant is, in general,

$$\epsilon = \hat{k}\cdot\boldsymbol{\epsilon}\cdot\hat{k}\,, \tag{7}$$

where $\boldsymbol{\epsilon}$ is the static dielectric tensor and $\hat{k} \equiv \mathbf{k}/k$.

In the process of substituting Eqs. (2)–(6) into Eq. (1) to solve for the amplitude $W(t)$ of the charge-density wave, we will make some simplifying assumptions that are appropriate for our experiments in barium titanate. First, the direction of any uniform electric field ($-\mathrm{grad}\phi_0$) and $\mathbf{k}$ are assumed to be parallel (or antiparallel) to the optical c axis in a uniaxial crystal. In this case it will not significantly alter the result to assume that the sites are equally (rather than randomly) spaced by the (rms) distance l in the z direction. Further we take $kl \ll 1$, as is suggested by our data. In this case the form of the result is unaltered by assuming that the hopping rate D_{mn} is zero except between nearest-neighbor sites when it has the value D. Typically, $l \sim 10^{-6}$ cm, and β corresponds to room temperature ($\sim 1/40$ eV), so that if the internal electric fields are below 50 kV/cm, $|\beta\phi_{mn}$ is much less than unity in Eq. (1). The field-induced electro optic effects we observe suggest that in our experiments internal fields rarely approach this value, and so it is justifiable to keep only the terms in Eq. (1) that are of the lowest (first) order in ϕ_{mn}.

With the foregoing approximations, substitution of Eqs. (2)–(6) in Eq. (1) gives [by equating coefficients of $\exp(i\mathbf{k}\cdot\mathbf{x}_n)$]

$$\frac{dw}{dt} = -\Gamma\left[(w+m)(\alpha^2 + i\alpha f) + w\right]. \tag{8}$$

Here

$$\Gamma \equiv DG_0k_0^2l^2 \tag{9}$$

is a characteristic hopping rate,

$$w \equiv W/W_0 \tag{10a}$$

is the normalized charge wave amplitude,

$$\alpha \equiv k/k_0 \tag{10b}$$

is the grating wave vector normalized by k_0, and

$$f \equiv -(\phi_{0n} - \phi_{0n-1})/(lf_0) \tag{10c}$$

is the uniform electric field strength normalized by a characteristic field f_0. The characteristic wavevector k_0 is defined by

$$k_0^2 \equiv \rho W_0 q^2/\epsilon\epsilon_0 k_B T\,, \tag{11}$$

a key parameter which, once determined by curve fitting to experiment, fixes the average density ρW_0 of migrating charges. (In our barium titanate sample k_0 was found to be $\sim 0.3k_1$ which ipplies a charge density $\sim 10^{16}$ cm^{-3}.) The characteristic field f_0 in Eq. (10c) is

$$f_0 \equiv k_0k_BT/q\,. \tag{12}$$

The characteristic field is seen to be of order ~ 2300 V/cm in our case.

Equation (8) is a differential equation of a familiar form. Even when both the intensity $I(t)$ and the applied electric field $f(t)$ vary with time, the solution to Eq. (8) may be written in terms of simple integrals. We will use solutions of Eq. (8) in special cases to analyze our experiments below. In these experiments, the charge distribution [see Eq. (4)] is detected by scattering from it an optical wave which experiences a spatial modulation of optical susceptibility of the form $\mathrm{Re}\mathbf{X}\exp(i\mathbf{k}\cdot\mathbf{x})$ due to the electro optic effect. The modulated optical susceptibility is written by convention in terms of the third-rank electro optic tensor $\mathbf{R}$ and the amplitude ϕ of the static potential distribution defined in Eq. (5) as

$$\mathbf{X} = i\epsilon_0\boldsymbol{\epsilon}_\omega(\mathbf{R}\cdot\mathbf{k})\cdot\boldsymbol{\epsilon}_\omega\phi\,. \tag{13}$$

The optical dielectric function $\boldsymbol{\epsilon}_\omega$ is diagonal for Cartesian coordinates coinciding with the principal axes. In a uniaxial crystal its zz component equals n_e^2, and its xx and yy components equal n_o^2 (n_o and n_e are the ordinary and extraordinary refractive indices). In barium titanate (which has tetragonal symmetry $4mm$) the nonzero components of the electro optic tensor are[5] $R_{zzz} \equiv r_{33} = 23$, $R_{xzz} = R_{yyz} \equiv r_{13} = 8$, and $R_{yzy} = R_{xzx} \equiv r_{42} = 820$ (in units of 10^{-12} m/V). Here the r_{ij} are the conventional contracted forms of the electro optic tensor. Also, $n_o = 2.488$ and $n_e = 2.424$ (at 515 nm),[6] and the dc dielectric constants at room temperature are 106 and 4300 measured parallel and perpendicular to the c axis.

In our experiments, $\mathbf{k}$ was always along the c axis, and our experiments were not sensitive to motion of charges except along the c direction. However, if $\mathbf{k}$ and $\mathrm{grad}\phi_0$ were not parallel to the c axis, then Eq. (8) for w [from which follow ϕ by Eq. (6) and $\mathbf{X}$ by Eq. (13)] is generalized as follows. The right-hand side of Eq. (8) becomes the sum over j of three terms ($j = x, y, z$), each of the same form as in Eq. (8), but in each of which the symbols are altered in definition as follows: D becomes D_j ($j = x, y, z$); k_0 becomes a function of the direction of $\mathbf{k}$ through its dependence on $\boldsymbol{\epsilon}$ in Eq. (7); l^2 becomes l_j^2 ($j = x, y, z$) in case the sites are not spaced isotropically; $\alpha_j = k_j/k_0$ ($j = x, y, z$); and f becomes $f_j \equiv -\hat{x}_j\cdot\mathrm{grad}\phi_0/f_0$ (which are the normalized space components of the externally applied electric field). We will not pursue this case, nor the further generalizations of Eq. (8) to any of the following cases: $kl > 1$; D_{mn} existing beyond the nearest-neighbor pairs; or randomly placed or multiple classes of sites. Such generalizations do not seem to be needed to treat barium titanate. We now apply Eq. (13) to the erasure transients and steady-state-two- and four-wave interactions studied in our experiments.

A. Grating erasure time constants

Suppose a charge grating is formed by two writing beams which produce a given grating k, and then are turned off, leaving a given grating amplitude w expressed by Eq. (8). A weak reading beam is turned on so that its Bragg-scattered signal monitors the relative magnitude of the grating without erasing it appreciably. The crystal is simultaneously flooded with a stronger uniform ($m = 0$) illumination (not phase matched) which then causes the grating amplitude w to decay exponentially by Eq. (8). The signal is expected to display an exponential decay, $\propto |w|^2$, with decay rate A_e given by

$$A_e = 2\Gamma(1+\alpha^2)\,. \tag{14}$$

Note that A_e is independent of any applied dc field. The dependence of this rate on α is experimentally verified in Sec. III.

B. Steady-state four-wave mixing

We consider here the special form of four-wave mixing that is also known as transient volume holography.[7] Two optical beams cause charge migration, which in turn produces a steady-state periodic electric field and consequently a modulation of the optical susceptibility [see Eq. (13)]. A third "reading" beam $\mathrm{Re}\hat{e}_3E_3\exp(i\mathbf{k}_3\cdot\mathbf{x} - i\nu t)$ is introduced into the crystal and Bragg scatters off the optical susceptibility variation. In other words, with the susceptibility this beam creates a polarization density in the medium that is equal to $\mathrm{Re}\hat{e}_4E_4\mathbf{X}\cdot\hat{e}_3\exp[i(\mathbf{k}_1 - \mathbf{k}_2 + \mathbf{k}_3)\cdot\mathbf{x} - i\nu t]$. The ratio R of the power radiated by this polarization density (with field polarization $\hat{e}_4$) to the input power of the "reading" beam is (for $R \ll 1$)

$$R = \left|\frac{\nu}{4n_3c}\hat{e}_4^*\cdot\mathbf{X}\cdot\hat{e}_3L\right|^2. \tag{15}$$

where L is the effective interaction length of the beams, n_3 is the refractive index of the reading beam, and c is the velocity of light. This ratio R is called the grating scattering efficiency. If $\hat{e}_4 = \hat{e}_3$, if the third "reading" beam is nearly antiparallel to the two writing beams, and if the latter are unaffected by the scattering, then one can write a more general formula for R, valid for long interaction lengths, in which R can approach unity.[3] Attenuation can be accounted for in Eq. (15) by using complex k vectors in the foregoing analysis.

As an example, consider the optimum scattering configuration in barium titanate where the applied electric field and the grating $\mathbf{k}$ are parallel to the crystalline (z) axis (as above), and the reading beam is an extraordinary ray and the writing beams are ordinary rays. Let $\nu = \omega$, then

$$R = B^2L^2\frac{4I_1I_2}{(I_1+I_2+I_3)^2}\left|\frac{\alpha+if}{1+\alpha^2+i\alpha f}\right|^2, \tag{16}$$

where I_1 and I_2 are the intensities of the writing beams and I_3 is the intensity of the reading beam inside the crystal. Note that when I_3 is much weaker than I_1 and I_2, the above expression for R depends only on the ratio I_1/I_2 and is independent of the total intensity $I_1 + I_2$ of the writing beams. When an optical intensity attenuation of γ cm^{-1} exists, L is approximately $[1 - \exp(-\gamma l)]/\gamma$ for nearly collinear beams interacting over the crystal length l. The coefficient B is very nearly, in this example,

$$B \simeq \omega n_e^3 r_{33} f_0(\hat{e}_3\cdot\hat{\mathcal{E}})^2/4c\,, \tag{17}$$

which has a value ~ 2.4 cm^{-1} for barium titanate at 515 nm. There is also a term in B (much smaller in barium titanate) proportional to r_{13} when $\hat{e}_3$ has a component along x or y. If all four rays were of ordinary polarization, B would be modified by replacing $n_e^3r_{33}(\hat{e}_3\cdot\hat{\mathcal{E}})^2$ by $n_o^2r_{13}$ which (at small writing angles) is predicted to be 3 times smaller, from previous measurements of the r_{ij} coefficients, just as we find in Sec. III by measuring relative R values.

C. Steady-state two-wave coupling

We have seen how two intersecting optical beams of wave vectors $\mathbf{k}_1$ and $\mathbf{k}_2$ create a quasistationary spatial wave of optical susceptibility variation with wave vector $\mathbf{k} = \mathbf{k}_1 - \mathbf{k}_2$ and complex amplitude $\mathbf{X}$ given by Eq. (13). We discussed in Sec. II B how a third beam scatters from this refractive index grating. Clearly, however, this grating can also "scatter" the two beams which produce it. The main effect of this scattering is, as we show now, to transfer energy from one beam to the other, the direction of energy flow being determined by the direction of the c axis. Since we have been able to obtain an analytic solution of Eq. (1) for the charge distribution in the case where one writing beam is much weaker than the other ($|m| \ll 1$), we will assume here that beam 2 is much stronger than beam 1 and hence negligibly affected by the two-wave interaction.[8] The k component of the nonlinear optical polarization density $\mathbf{P}^{\mathrm{NL}}$ has amplitude $|\mathbf{X}\cdot\hat{e}_1E_2$. Since $\mathbf{X}$ is proportional to $G\,(= 2E_1E_2^*)$ via Eq. (3) in Eqs. (8), (6), and (13), this component is linearly related to E_1 (as in the normal linear polarization density) and alters the dispersion relation for $\mathbf{k}_1(\omega)$ to produce a new $\mathbf{k}_1(\omega) + \delta\mathbf{k}_1$. Assuming that both the real and imaginary parts of the (complex) alteration $\delta\mathbf{k}_1$ are much smaller than the unperturbed $\mathbf{k}_1$, one obtains immediately from Maxwell's equations that (for birefringent or optically active media)

$$\mathbf{k}_1\cdot\delta\mathbf{k}_1 = \left(\frac{\omega^2}{4c^2\epsilon_0}\right)\frac{\hat{e}_1^*\cdot\mathbf{X}\cdot\hat{e}_2E_2}{E_1}. \tag{18}$$

The direction of $\delta\mathbf{k}_1$ is usually determined by boundary conditions and is generally not far from parallel to $\mathbf{k}_1$. Using the steady-state solution of Eq. (8) with Eqs. (3), (6), and (13) one obtains the prediction of the hopping model for the altered steady-state complex propagation vector of the weaker wave:

$$\mathbf{k}_1\cdot\delta\mathbf{k}_1 = \frac{i\omega^2f_0}{2c^2}\left(\frac{\alpha+if}{1+\alpha^2+i\alpha f}\right) \times(\hat{e}_1^*\cdot\boldsymbol{\epsilon}_\omega\cdot\{\mathbf{R}\cdot\hat{k}\}\cdot\boldsymbol{\epsilon}_\omega\cdot\hat{e}_2)(\hat{e}_1\cdot\hat{e}_2^*)\,. \tag{19}$$

The most easily observed part of the change in the propagation vector is the imaginary part of $\delta\mathbf{k}_1$ which produces exponential growth or decay of the weaker wave through

$\exp(-2\mathrm{Im}(\delta\mathbf{k}_1\cdot\hat{z}L))$ where L is the interaction length. The wave will experience gain or loss depending on the signs of f_n (which has the same sign as the charge q) and of the appropriate elements of $\mathbf{R}$.

Comparing Eq. (19) with Eq. (17) shows that, when the two intersecting beams are extraordinary rays, the exponential power gain coefficient [i.e., $-2\,\mathrm{Im}(\delta\mathbf{k}_1\cdot\hat{z})$] has a magnitude (when $k = k_0$ and $f = 0$) of $2B$, where B is the coefficient of Eq. (17) that governed the four-wave mixing efficiency. In barium titanate $2B$ is predicted to be $\sim 5\ \mathrm{cm}^{-1}$ at 515 nm, independent of the intensity of the strong beam, as was easily verified. The detailed dependences of gain on beam angles, polarization, and applied fields that is predicted by Eq. (19) have been verified experimentally as described in Sec. III.

D. Moving crystal

If the crystal is moving with a uniform velocity $\mathbf{v}$, then one can see that Eq. (8) for the amplitude w of the charge grating is altered by adding a term $i\mathbf{k}\cdot\mathbf{v}w$ to the left-hand side. The equation is still immediately integrable. It is seen that small velocities ($\gtrsim \Gamma/k \sim 10^{-4}\ \mathrm{cm\ sec}^{-1}$) quench grating formation, as was observed experimentally. For $\alpha f \gg 1$, a resonance in R is predicted when $w\cdot k = -\Gamma\alpha f$.

E. Photoconductivity

If a uniform potential gradient (in excess of any chemical potential) exists in the uniformly illuminated crystal, and Ohmic contacts allow a one-dimensional current flow, one can calculate from Eq. (1) the photoresistivity ρ_I. One finds that ρ_I is inversely proportional to the long-wavelength ($\alpha \to 0$) decay rate Γ of w. This decay rate is given under special conditions in Eq. (9), or more generally, as explained after Eq. (13). Since this decay rate is a (photoinduced) dielectric relaxation rate, it is not surprising that the result is the familiar formula

$$\rho_I \epsilon \epsilon_0 = \Gamma^{-1}, \tag{20}$$

where ϵ is as in Eq. (7) with $\hat{k}$ taken to be the direction of the potential gradient. At 1 W/cm^2, Γ was observed to be ~ 5 sec^{-1}, (see Fig. 7) and Eq. (20) predicts $\rho_I \sim 5\times 10^{9}\ \Omega$ cm (for $\epsilon \approx 10^2$), compared to the measured resistivity of $\rho_I = 8\times 10^{9}\ \Omega$ cm with the above illumination.

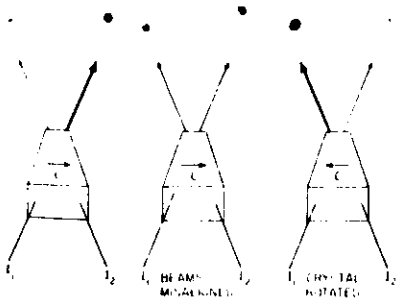

FIG. 2. Steady-state energy coupling between two beams in a poled single crystal of barium titanate. The direction of the positive c axis is indicated. In (a) two beams with equal incident intensities (250 mW/cm^2) emerge with different intensities. In (b) the beams are misaligned so as to not intersect in the crystal, and emerge with their intensities unchanged. In (c) the crystal is either repoled or simply rotated 180° to reverse the direction of the positive c axis. The direction of energy coupling also reverses. The spots were produced by exposing a strip of photographic paper to the beams after they had passed through the crystal. No dc field was applied (except prior to the experiment in order to pole the crystal).

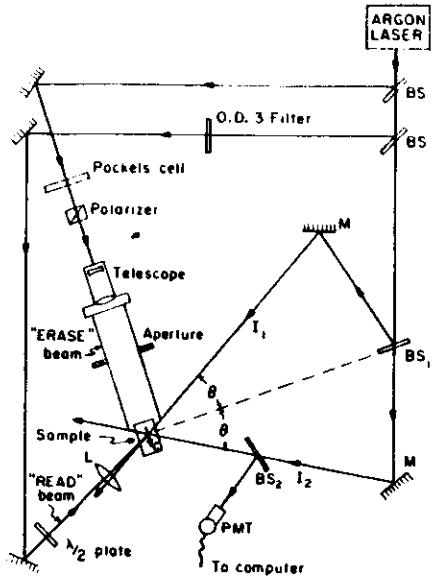

FIG. 3. Experimental setup showing writing beams with intensities I_1 and I_2, reading beam, and erasing beam. For steady-state energy-coupling experiments, the intensity of writing beam 1 (after the sample) was monitored as writing beam 2 was blocked and unblocked. For four-wave mixing experiments, reading beam scatters off the grating produced by the writing beams and is deflected by beam splitter BS_2 into a photomultiplier (PMT). For erase-rate experiments, the writing beams are both blocked and an erasing beam is suddenly turned on. The decay of the grating is monitored with the PMT and analyzed by computer. The intensity of the erasing beam is controlled by a Pockels cell followed by a linear polarizer.

III. EXPERIMENTAL RESULTS

A. Steady-state energy coupling

The predictions of Eq. (19) were experimentally verified by energy-coupling experiments, in which two beams of equal intensity are crossed in the crystal and one is observed to emerge with more intensity and the other with less. (See Fig. 2.) The predicted dependence of the magnitude of the energy coupling effect on the grating wave vector k (through $\alpha = k/k_0$) was checked by measuring the steady-state coupling as a function of the crossing angle 2θ of the two writing beams, since $k = 2n_0\omega c^{-1}\sin\theta$, where n_0 is the index of the refraction appropriate for the direction and polarization of the writing beams. A multimode argon ion laser[9] supplied two writing beams polarized perpendicular to the plane of incidence. The optical path difference of the writing beams from beam splitter 1 (see Fig. 3) to the sample was kept within 0.5 cm, well within the approximate 5-cm coherence length of the multimode laser. The beams were unfocused and about 2 mm in diameter at the sample. The interaction length of the two beams was determined by the 2.2 mm thickness of the sample and was independent of crossing angle for the range of angles used.

The exit intensity I_1 of beam 1 was measured with beam 2 blocked (no grating). Beam 2 was then unblocked, and the altered intensity $I_1 + \Delta I_1$, was observed to be either greater or smaller depending on the orientation of the c axis of the crystal relative to the writing beams. (See Figs. 2 and 4.) The fractional intensity change $\Delta I_1/I$ was measured with ordinary waves for a range of grating wave vectors (beam crossing angles). The prediction of Eq. (19) for the steady-state fractional gain for $\Delta I_1 \ll I_1$ is

$$\frac{\Delta I_1}{I_1} = -2\ \mathrm{Im}(\delta\mathbf{k}\cdot\hat{x}L) = -\frac{\omega}{c}L f_n n_0^3 r_{13}\frac{\alpha + if}{1+\alpha^2+i\alpha f}. \tag{21}$$

Here n_0 is the ordinary index of refraction, $\alpha = k/k_0$, $f = E_{\text{applied}}/f_0$, and $f_0 = k_0 k_B T/q$. A plot of this function and the experimentally measured values are shown in Fig. 5. The only unknown parameter is the wave vector k_0, which was found to give the best least-squares fit to the measured data when $k_0 = 0.31(2)n_0\omega/c$ for $\lambda = 515$ nm.

Energy-coupling effeciencies measured with both writing beams at 633 and at 458 nm peaked at $k_0 = 0.31(2)n_0\omega/c$ at each wavelength. This implies that $k_0\lambda$ is constant and, from Eq. (11), that the density of filled trap sites ρW_0 increases approximately as the square of the frequency of the writing beams over the limited frequency range explored.

Physically, the peak efficiency of energy coupling was

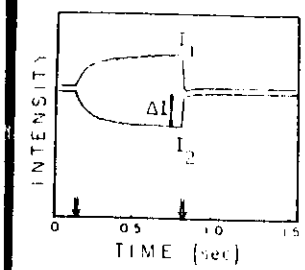

FIG. 4. Intensity of writing beams as a function of time. One beam is monitored, while the other beam is turned on at the time indicated by the first arrow and turned off at the second arrow. Each beam initially had an intensity of 600 mW/cm^2 before entering the crystal. The rise time of the grating is seen to be about 1/10 sec. For beams with equal incident intensity ($m = 1$), the magnitude of the energy coupled ΔI into or out of the other beam is seen to be equal and opposite (here about 20%). The plots for the two beams are slightly displaced for clarity.

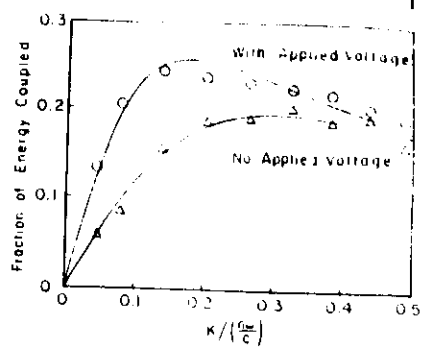

FIG. 5. Fraction of steady-state energy coupled $\Delta I/I$ between two beams in undoped barium titanate as a function of grating wave vector k. The triangles (Δ) are the experimental data with no externally applied dc electric field, and the solid line is the least-squares fit to Eq. (21) with the characteristic wave vector given by $k_0 = 0.31(2)n_0\omega/c$. The open circles ($\circ$) are the experimental data with a voltage of 1000 V applied across the crystal ($d = 2.8$ mm between electrodes) parallel to the c axis. Solid line is the theoretical fit to Eq. (21) using the same value of k_0 and the applied dc electric field inside the crystal as the adjustable parameter.

always found to occur at the same outside crossing half-angle (21°) of the writing beams for all three wavelengths tried. This suspicious coincidence was confirmed by determining k_0 through other experiments, as follows.

B. Erase rate

A uniform beam of light ($m = 0$) incident on the sample at an arbitrary angle will erase any grating that may have been previously stored in the sample, causing the diffraction efficiency to decay at a rate $A_+ = 2\Gamma(1+\alpha^2)$ where $\Gamma = DG_0 k \frac{1}{2}I^2$ and G_0 is proportional to the intensity of the erasing beam [see Eq. (14)].

To verify the dependence on k (through α) of this rate, the angle between the writing beams was fixed while a weak

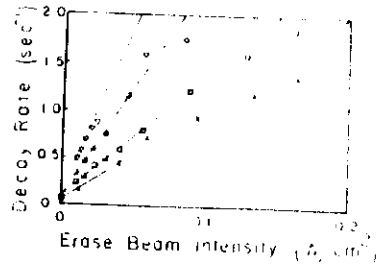

FIG. 6. Decay rate A_+ as a function of erasing beam intensity at various grating wave vectors (crossing angles). The grating k in units of $n_0\omega/c$ is (●) $k = 0.05$, (□) $k = 0.22$, (▲) $k = 0.37$, (▽) $k = 0.52$. The decay rate is linear in the erasing beam intensity for small rates, but begins to saturate for rates greater than 1 sec^{-1}.

extraordinary reading beam ($I_{read} < 10^{-3} I_{write}$), incident on the sample at the Bragg angle, monitored the grating. Leaving the reading beam on, both writing beams were turned off and the erasing beam turned on. Decay curves were accumulated for different erasing beam intensities I_e and stored in an on-line computer (Hewlett Packard 9825A with 6940B multiprogrammer). The decay rate of each curve was determined and the slope of a plot A_e versus I_e found. The experiment was then repeated for different crossing angles of the writing beams, thereby changing k (see Fig. 6). A plot of the slopes as a function of k^2 gave a good straight-line fit (see Fig. 7) and yielded a value for k_0:

$$k_0 = 0.32(2) n_o \omega / c$$

at $\lambda = 515$ nm, in excellent agreement with the k_0 determined by energy coupling experiments. From Eq. (11) this values of k_0 gives a density of filled trap sites of $\rho W_2 = 1.9(2) \times 10^{16}$ cm^{-3}. The origin of these sites is unknown and may be due to traps at impurity or defect sites.

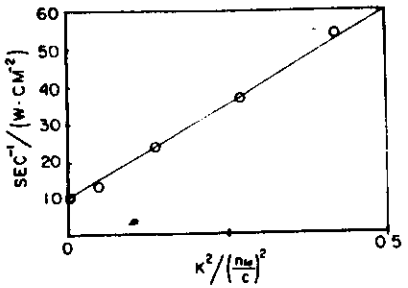

FIG. 7. Plot of the slopes of Fig. 6 (i.e., the decay rate normalized by the erasing beam intensity) as a function of k^2. The circles are the experimentally measured data and the straight line is the best least-squares fit. The ratio of the intercept to the slope of the above graph yields a value of $k_0 = 0.32(2) n_o \omega / c$. The intercept gives a values $2\Gamma/G_0 = 10$ sec^{-1} W^{-1} cm^2 used to calculate the photoconductivity in Eq. (20).

C. Sign of charge carriers

There are many ways to determine the sign of the charge carriers in photorefractive materials.[10,11] The sign of the charge carriers in barium titanate was experimentally determined to be positive by energy-coupling experiments, as follows. From Eqs. (18), (13), and (5), the direction of energy coupling will depend only on the sign of the electro-optic coefficient, the orientation of the crystal relative to the writing beams, and on the sign of the charge carriers.

In order to avoid any confusion in determining the sign of the charge carriers, a method was used which is independent of the definition of the positive direction of the c axis.

The crystal was first poled by painting silver electrodes on the c-axis faces, slowly heating it to about 5 °C below the Curie temperature ($T_c = 133$ °C), and then applying a dc poling field of 3.5 kV/cm along the c axis. The crystal was then slowly cooled to room temperature with the poling field still applied to produce a single-domain crystal. For convenience, we define the positive c-axis direction as pointing toward the electrode that had been connected to the negative terminal of the applied dc voltage. (The final determination of the sign of the charge carriers is independent of this choice.)

Next the sign of the electro optic coefficient was determined to be positive relative to the positive c axis by placing the crystal between crossed polarizers with the c axis oriented at 45° to the direction of polarization. A Babinet-Soleil compensator, also placed between the polarizers, was adjusted to null out the birefringence of the crystal at 515 nm. A dc field was applied in the same direction as the previous poling field, and the compensator was adjusted to give a new null that corresponded to a decrease in the difference of the extraordinary and ordinary indices when the applied field was increased. From (13),

$$n_e(E) = n_e - \tfrac{1}{2} n_e^3 r_{33} E ,$$

$$n_o(E) = n_o - \tfrac{1}{2} n_o^3 r_{31} E ,$$

where $n_e(E)$ is the extraordinary index with applied field E, n_e is the extraordinary index with no applied field, etc. Since $|n_e^3 r_{33}| > |n_o^3 r_{31}|$, a decrease in $n_e(E) - n_o(E)$ with increasing E implies that $r_{33} > 0$.

The poled crystal was then placed at the intersection of two optical beams, and the beam that entered the crystal at an acute angle to the positive c axis was always observed to emerge with the weaker intensity (see Fig. 2). From Eq. (19) [and Eq. (13) with $r_{33} > 0$], this implies that f_0 and hence q is positive.

In similar experiments on $LiNbO_3$, the direction of energy coupling was opposite to that observed here.[11] Assuming that the pyroelectric determination of the positive direction of the c axis used in that work[12] agrees with the definition used here, the signs of the charge carriers must be opposite in the two materials. However this point should be checked.

D. Phase and absolute magnitude of index grating

The magnitude of the steady-state energy coupling between two beams depends on the component of the index grating that is 90° out of phase with the intensity distribution of the two beams (i.e., on the imaginary part of δk_1). However, the diffraction efficiency R with which the grating scatters a third reading beam depends on the magnitude of the grating and not on its phase with respect to the writing beams. Therefore, by separately measuring the fraction F of two-beam energy coupling and the diffraction efficiency described in Sec. II B, real and imaginary parts of δk in Eq. (19) can be determined. From Eq. (19) with no applied electric field ($f = 0$), the real part of δk should be zero, and

$$F \simeq 2R^{1/2}$$

when all beams have the same polarizations, $m = 1$, and $R \ll 1$. The above relation was experimentally verified within 10% error over a range of crossing angles and confirmed that the index grating with wave vector k is 90° ± 10° out of phase with the incident intensity distribution.

Equation (19) for the fraction of energy coupling reaches a peak at $k = k_0$ and predicts 18% coupling for a 2.2-mm crystal length using ordinary polarizations.[13] This computed value is 36% less than the peak measured value of 0.28 with $m \simeq 1$ in Fig. 5, which may be due to contributions from higher-order terms in Eq. (8) when m is near unity.

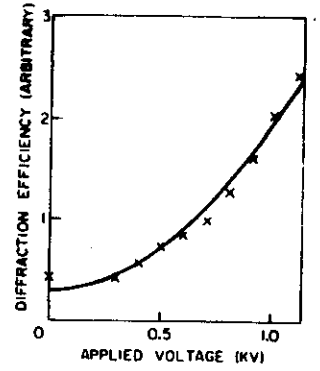

FIG. 8. Four-wave mixing diffraction efficiency R as a function of applied voltage at fixed grating spacing ($k \simeq 0.08\ n\omega/c$). The voltage was applied parallel to the c axis. The crystal was 2.8 mm in width between the c-axis faces. The crosses are the experimental data and the solid line is the theoretical fit to Eq. (16) (if the internal applied field were 40% of the applied voltage divided by the crystal width).

E. Energy coupling and diffraction efficiency with an applied electric field ($f \neq 0$)

To confirm the predictions of our theory in the presence of an applied field, both the diffraction efficiency R and the amount of energy coupled between the two writing beams were measured with and without +1000 V applied across the crystal parallel to the $+c$ direction, and as a function of the crossing angle of the writing beams.

From Eq. (8) the photoinduced electric field with periodicity k is

$$E(x) = \mathrm{Re}\left(i \frac{k_B T}{q} k_0 m \frac{\alpha + if}{1 + \alpha^2 + i\alpha f} \exp(ikx) \right). \tag{22}$$

The diffraction efficiency R is proportional to $|E|^2$ [see Eq. (16)] and has the form

$$R \propto \frac{\alpha^2 + f^2}{(1+\alpha^2)^2 + \alpha^2 f^2}. \tag{23}$$

The dependence of R on applied voltage is shown at a fixed crossing angle in Fig. 8. This cugve represents a vertical slice through the curves shown in Fig. 9 and shows that R is approximately quadratic in f for $k \ll k_0$ (i.e., $\alpha \ll 1$). The fit to the measured data is excellent.

If there were an intrinsic field in the $BaTiO_3$ crystal, as suggested by Chen,[13] then the slope of the graph would be nonzero when the *applied* field was zero. The above data and the observed fact that $R \to 0$ as $\alpha \to 0$ puts an upper limit on such a field of $E_{intrinsic} < 300$ V/cm. However, some assymetry was observed in R for electric fields applied parallel and antiparallel to the c axis and indicates that some intrinsic field may be present in our sample.

The results of energy coupling experiments are shown in Fig. 5. There is a noticeable shift in the peak of the curve toward smaller crossing angles as the applied electric field is increased, and an increase in the magnitude of energy coupled, especially at small crossing angles. The best fit to the data gave a value of the applied field which was 75% of the actual field applied. This discrepancy is possibly due to the poor contact made by the silver paint electrodes or by boundary layers.[14]

IV. DISCUSSION

We here discuss the main differences between our theory and previous theories and experiments on barium titanate and similar photorefractive materials. A semipermanent light-induced change was first observed in lithium niobate and in other ferroelectrics by Ashkin.[15] It soon became apparent that this photorefractive effect or "optical damage" was caused by a redistribution of charges in the material creating an electric field, which then altered the index of refraction through the electro optic effect.[13] It was first postulated that a large intrinsic electric field was necessary to enable the charges to drift in the material,[13] but it was subsequently demonstrated that diffusion alone could account for the observed effects.[16] High-quality holographic storage was subsequently demonstrated in these materials using two optical beams of one wavelength to create a volume hologram, and a beam of a different wavelength to read it.[17] Many theories have been proposed to describe various aspects of volume holograms in photorefractive materials.[18-23]

An important goal of these theories is to predict, from a given incident intensity distribution $I(x)$, the resulting refractive index modulation $n(x)$. The approach followed in previous papers was to first calcualte the number of charge

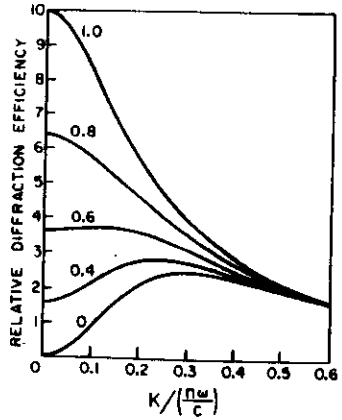

FIG. 9. Theoretical plots from Eq. (23) of the four-wave mixing diffraction efficiency R as a function of grating wave vector k for various applied electric fields. The numbers on each plot are the values of f (the applied dc electric field in units of $f_0 = k_0 k_B T / q$).

centers excited to the conduction band, and then to compute their motion from the forces of drift and diffusion. In all of these theories, the number of charge carriers excited into the conduction band was always taken to be proportional to $I(x)$. This assumption ignores the depletion of charge carriers available to be excited in the high-intensity regions of the sample and is not valid except when writing with short optical pulses. Our theory shows that the density of filled sites is significantly altered by charge migration as steady state is approached, even for very small modulation index m, and cannot be assumed constant. (For $\alpha = 1$, and $m = 1$, the modulation of the filled site density approaches unity.) Consequently, in our theory, we include hopping rates that are proportional to the product of $I(x)$ *and* the probability that the site at x is filled.

In addition most of the previous theories on charge transport limit themselves to the initial stage of grating formation and avoid the effects of the photoinduced field itself in the equation of motion for the charges.[24] However, it is just this field created by charge hopping that counters the force of diffusion and enables the system to reach equilibrium. This is described explicitly in Eq. (1) and results in the steady state as well transient solutions that are evident from Eq. (8) and is an important characteristic of our theory.

A key parameter in our theory is the wave vector k_0 [see Eq. (11)]. The value of k_0 will vary with material and from sample to sample according to the density of filled trap sites available for hopping when excited by light of a given frequency. Alphonse *et al.*[23] have noted a diffraction efficiency in lithium niobate which, as a function of grating wave vector k, has a distinct turning point similar to our Fig. 3 and which they note is "a striking experimental departure from (their) theory." Applying our theory, the peak of their plot yields a value of $k_0 = 0.36(7)n\omega/c$ at 488 nm and a filled trap density of 7×10^{15} cm^{-3} at the optical wavelength employed. This is quite close to the value reported here for our sample of undoped barium titanate. Data reported by Townsend and LaMacchia[19] on barium titanate also show $R \sim k^2$ for small k and a roll off at about $k_0 = 0.2n\omega/c$ at 488 nm which implies a filled trap density of 7×10^{15} cm^{-3}. Two data points of R versus k reported by Peltier and Micheron in a sample of bismuth silicon oxide[25] imply a filled trap density somewhat greater than 2×10^{16} cm^{-3}. If the trap sites are due to impurities or defect sites, it is not clear why the filled trap densities should be similar within a factor of 2 in two different samples of barium titanate and in a sample of iron-doped lithium niobate. Further experiments may perhaps provide some physical insight as to why the concentration of filled carriers is so similar in different materials, and why the density of traps appears to vary as the square of the optical frequency of the writing light.

In summary, we have presented a new charge-transport model to describe the formation of volume-index gratings in photorefractive materials. Predictions of the model for the diffraction efficiency of the grating and for the fraction of the energy coupled between the two writing beams, both in the transient and steady state, are well confirmed by experiment. A closed-form solution is presented for small values of the optical modulation m (and which fits the data well for $m \simeq 1$) and predicts the maximum in scattering efficiency R versus grating wave vector k observed by us and by others. This model also predicts the observed charge-pattern erasure rate as a function of k and the observed dependence of diffraction efficiency on the intensities and polarizations of the optical beams. The model also predicts the observed photoconductivity and predicts effects of sample velocity.

ACKNOWLEDGMENTS

This work was supported by the U.S. Air Force Office of Scientific Research under Grant No. 78-3479 and by the National Science Foundation under Grant No. ENG78-04774. One of us (A.R.T.) acknowledges support from the Joint Services Electronics Program and the National Science Foundation under Grant No. ENG78-05617.

[1]Sanders Associates, 95 Canal Street, Nashua, N.H. 03060.
[2]R.W. Hellwarth, J. Opt. Soc. Am. 67, 1 (1977).
[3]H. Kogelnik, Bell Syst. Tech. J. 48, 2909 (1969).
[4]D.L. Staebler and J.J. Amodei, J. Appl. Phys. 43, 1042 (1972).
[5]A. Yariv, *Quantum Electronics, Second Edition* (Wiley, New York, 1975).
[6]S.H. Wemple, M. Didomenico, Jr., and I. Camlibel, J. Phys. Chem. Solids 29, 1797 (1968).
[7]A. Yariv, Opt. Commun. 28, 23 (1978).
[8]For a solution of the coupled wave problem with pump depletion, see D.W. Vahey [J. Appl. Phys. 46, 3510 (1975)].
[9]Lexel Corporation, Model 95-4.
[10]F.S. Chen, J. Appl. Phys. 40, 3389 (1969).
[11]D.L. Staebler and J.J. Amodei, J. Appl. Phys. 43, 1042 (1972).
[12]G.D. Boyd, R.C. Miller, K. Nassau, W.L. Bond, and A. Savage, Appl. Phys. Lett. 5, 234 (1964).
[13]Pump depletion is minimized by using a short interaction length and ordinary instead of extraordinary polarizations for the writing beams. Also see Ref. 8.
[14]P.E. Bloomfield, I. Lefkowitz, and A.D. Aronoff, Phys. Rev. B 4, 974 (1971).
[15]A. Ashkin, G.D. Boyd, J.M. Dziedzic, R.G. Smith, A.A. Ballman, J.J. Levinstein, and K. Nassau, Appl. Phys. Lett. 9, 72 (1966).
[16]J.J. Amodei, Appl. Phys. Lett. 18, 22 (1971).
[17]F.S. Chen, J.T. LaMacchia, and D.B. Fraser, Appl. Phys. Lett. 13, 223 (1968).
[18]W.D. Johnston, Jr., J. Appl. Phys. 41, 3279 (1970).
[19]R.L. Townsend and J.T. LaMacchia, J. Appl. Phys. 41, 5188 (1971).
[20]J.J. Amodei, RCA Rev. 32, 185 (1971).
[21]L. Young, W.K.Y. Wong, M.L.W. Thewalt, and W.D. Cornish, Appl. Phys. Lett. 24, 264 (1974).
[22]Dae M. Kim, Rajiv R. Shah, T.A. Rabson, and F.K. Tittel, Appl. Phys. Lett. 28, 338 (1976).
[23]G.A. Alphonse, R.C. Alig, D.L. Staebler, and W. Phillips, RCA Rev. Rev. 36, 213 (1975).
[24]However, see Refs. 21–23.
[25]M. Peltier and F. Micheron, J. Appl. Phys. 48, 3683 (1977).

ERRATA

Erratum: Photorefractive effects and light-induced charge migration in barium titanate [J. Appl. Phys. 51, 1297 (1980)]

Jack Feinberg, D. Heiman, A. R. Tanguay, Jr., and R. W. Hellwarth
Electronics Sciences Laboratory, University of Southern California, Los Angeles, California 90007

PACS numbers: 42.65. − k, 78.20.Jq, 72.40. + w, 42.30.Va, 99.10. + g

After the period in line 15 of p. 1298 insert the phrase "For all ordinary beams,... ." In place of the period ending this paragraph insert "but with all extraordinary rays. This is not the maximum for this case; here the maximum occurs for intermediate angles."

The optical susceptibility tensor amplitude $\mathbf{X}$ introduced before Eq. (13) is defined by $\mathbf{P} = \mathbf{X}\cdot\mathbf{E}$ in either the rationalized MKSA or the esu systems. ($\mathbf{P}$ and $\mathbf{E}$ are the complex polarization-density and electric-field amplitudes.) With this convention, one takes ϵ_0 to be equal to 8.85×10^{12} F/m in the MKSA system and equal to $1/4\pi$ in the esu system. In accordance with this convention, the $\mathbf{X}$ in Eq. (15) should be replaced by $\mathbf{X}$.

Insert the following sentence after the period in the 26th line following Eq. (13): "The last term in Eq. (8), $-\Gamma w$, is multiplied by k_j^2/k^2."

Replace the second sentence before Eq. (17) with "When an optical intensity attenuation of γ cm^{-1} exists, the foregoing analysis can be carried through unchanged, with appropriate wave vectors $\mathbf{k}_1$, $\mathbf{k}_2$,..., etc., which are complex instead of real. The spatial integration required to calculate the radiated wave can still be performed analytically if $I_2 << I_1$, I_1 where these symbols now denote incident (unattenuated) values. When $I_1 \simeq I_2$, for example, $L = d\exp(-\frac{1}{2}\gamma d)$ for a crystal length d. In our case, however, $\gamma d << 1$, so that $L \simeq d$."

In Eq. (13) a dot is to be inserted immediately after the first ϵ_n to indicate the tensor dot product. In the line following Eq. (2), a dot is to be inserted between $\hat{\delta}_1$ and $\hat{\delta}_2^*$ to indicate a vector dot product.

Appendix IX

Phase-conjugating mirror with continuous-wave gain

Jack Feinberg and R. W. Hellwarth

Departments of Physics and Electrical Engineering, University of Southern California, Los Angeles, California 90007

Received August 19, 1980

We demonstrate a phase-conjugating mirror that has a continuous-wave power reflectivity much greater than unity (gain ~100). This mirror uses nonresonant degenerate four-wave mixing in a single crystal of barium titanate ($BaTiO_3$). With our mirror we have (1) observed cw self-oscillation in an optical resonator formed by this mirror and a normal mirror, (2) demonstrated a cw oscillator that, in spite of phase-distorting material placed inside the resonator, will always emit a TEM_{00} mode, and (3) demonstrated an optical image amplifier. This mirror will work at any visible wavelength and with weak (milliwatt or weaker) pump beams.

Phase-conjugating mirrors were demonstrated previously with reflectivities that are greater than unity, and self-oscillation observed, but only for a few nanoseconds.[1] The largest reflectivity reported to date for a continuous-wave (cw) phase-conjugating mirror is only 17%.[2] In those experiments, either resonant degenerate four-wave mixing was necessary, which permitted operation only over a small frequency range (~1 GHz), or beams of megawatt power were needed. In this Letter, we report the first known demonstration of a cw phase-conjugating mirror with reflectivity greater than unity. We employ degenerate four-wave mixing of milliwatt beams, mediated by the photorefractive effect in a single crystal of barium titanate of 2.2-mm × 2.8-mm × 4.2-mm dimensions at room temperature. The effect is nonresonant and operates over a large fraction of the visible spectrum. The main disadvantage of this phase conjugating (pc) mirror is its relatively slow response time, of the order of 1 sec at the nominal milliwatt-power levels of common lasers. (However, this response time shortens inversely with the pump-beam power.)

By using our pc mirror, we have (1) observed cw self-oscillation in an optical resonator formed by this mirror and a normal mirror, (2) demonstrated wavefront correction when a phase-distorting medium is placed inside the self-oscillating resonator (that is, the pc mirror alters the transverse-mode structure of the resonator to compensate automatically for any phase distortions in the cavity), and (3) demonstrated optical image amplification.

To understand the operation of this mirror, consider two optical beams, with wave vectors $\mathbf{k}_1$ and $\mathbf{k}_2$, having nonorthogonal polarizations and the same angular frequency ω. Call these beams the writing beams. Where they intersect in the crystal, they form an intensity-interference pattern with wave vector $\mathbf{k} = \hat{k}k = \mathbf{k}_1 - \mathbf{k}_2$. Electrical charges (of unknown origin) migrate in the crystal from the peaks into the troughs of the intensity-interference pattern and eventually reach a static-charge distribution. These charges create a strong, static, spatially periodic electric field equal to $\hat{k}\,\mathrm{Re}\{E\exp(i\mathbf{k}\cdot\mathbf{x})\}$. This field in turn modulates the index of refraction by the first-order electro-optic (Pockels) effect to create a refractive-index grating in the crystal.[3] A third reading beam, also at ω, having a wave vector $\mathbf{k}_3 = -\mathbf{k}_1$, scatters from this grating to create a fourth signal beam of wave vector $\mathbf{k}_4 = -\mathbf{k}_2$, which is a phase conjugate of the second beam.[4,5] (See Fig. 1.)

Let I_1, I_2, I_3, and I_4 be the incident intensities of the writing reference beam, the writing image beam, the reading beam, and the output intensity of the phase-conjugate signal beam, respectively. Consider the case in which all four beams are confined to the y–z plane, with the z direction taken along the c axis of the crystal. (See Fig. 1.) According to our previous theory[6] of grating formation in $BaTiO_3$, when $I_4 \lesssim 0.5I_3$, the mirror reflectivity, here defined as ratio $R = I_4/I_2$ of the intensities of the phase-conjugate beam to the image beam, is well approximated by

$$R_{\mathrm{ord}} = \left|\frac{\omega L E\eta}{4c}\, n_o{}^3 r_{13}\cos\theta\right|^2 \qquad (1)$$

for a reading beam with ordinary polarization and by

$$R_{\mathrm{ext}} = \left|\frac{\omega L E\eta}{4cn_3}\cos\theta\,(n_e{}^4 r_{33}\sin\alpha_1\sin\alpha_2 + 2n_e{}^2 n_o{}^2 r_{42}\sin^2\theta + n_o{}^4 r_{13}\cos\alpha_1\cos\alpha_2)\right|^2 \qquad (2)$$

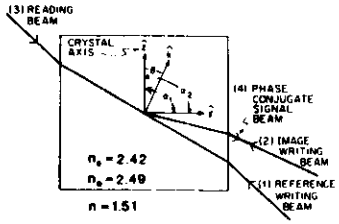

Fig. 1. The reference writing beam (1) and the image writing beam (2) interfere in a crystal of undoped $BaTiO_3$ to make a refractive-index grating with wave vector $\mathbf{k}$. The reading beam (3) Bragg scatters off this grating to produce the phase-conjugate signal beam (4). The crystal is immersed in index-matching oil.

for a reading beam with extraordinary polarization in the crystal. These expressions do not include the effects of two-beam energy coupling[6-8] or the phase mismatch that are due to the change in the index of refraction from each beam alone.[9] Here, c is the speed of light in vacuum, $\eta \equiv (I_3/I_2)^{1/2}$, n_o and n_e are the ordinary and extraordinary indices of refraction in the crystal ($n_o = 2.488$ and $n_e = 2.424$ at 514 nm), and n_3 is the index of refraction for the reading beam. L is the effective interaction length and is approximately $l\exp(-\frac{1}{2}\gamma l)$, where l is the beam length in the crystal and γ is the optical intensity-attenuation coefficient. The r_{ij} are the conventional contracted electro-optic coefficients and in $BaTiO_3$ (in units of 10^{-12} mV) (Ref. 10) are $r_{13} = 8$, $r_{33} = 23$, and $r_{42} = 820$. In Eqs. (1) and (2), θ is the angle between the grating wave vector $\mathbf{k}$ and the direction of the c axis, and α_1 and α_2 are the angles formed by each writing beam with the z axis. From Ref. 6 one sees that the intensity dependence of $E\eta$ is contained in a factor $I_1{}^{1/2}I_3{}^{1/2}/(I_1 + I_2 + I_3)$ so that, for $I_2 \ll I_1$ or $I_2 \ll I_3$, the mirror reflectivity R given by either Eq. (1) or Eq. (2) is independent of the incident intensity I_2 and depends only on the relative intensity I_3/I_1 of the counterpropagating beams. Otherwise, the electric-field amplitude E depends only on the temperature of the crystal lattice, the charge and density of the migrating carriers, the dc dielectric constants of the crystal, and the relative orientation of the crystal and the optical beams.[6] In general, the writing image beam will form an intensity-interference pattern not only with the reference beam but also with the reading beam.[6] For the range of beam angles used below, we estimate that this grating contributes about 10% to the observed reflectivity R.

Inspection of Eq. (2) shows that, for a large range of angles, the reflectivity for extraordinary beams can be larger than unity, owing to the contribution from the unusually large r_{42} coefficient. (Previous experiments with $BaTiO_3$ had $\mathbf{k}$ parallel to the crystal c axis, making $\theta = 0$ and thereby precluding any contribution from the r_{42} term.) For example, with $L \simeq 0.4$ cm ($\gamma l \ll 1$), $I_1 = I_3$, $\theta = 22°$, $\alpha_1 = +8°$, $\alpha_2 = +16°$, and a calculated[11] value of $E = 4.4 \times 10^2$ V/cm, we compute a mirror reflectivity of $R_{\mathrm{ext}} = 3.2$ for extraordinary polarizations at 514.5 nm. By approximating these conditions in an experiment with $I_2 = 0.3$ mW and $I_1 = I_3 = 5$ mW (beam area ~0.25 mm^2), we observed $R_{\mathrm{ext}} \sim 2$. However, in this instance we used ordinary rays for beams 1 and 2 to write the grating and used an extraordinary ray (beam 3) to read the grating [which does not alter Eq. (2) if $\mathbf{k}_1 - \mathbf{k}_2 = \mathbf{k}_4 - \mathbf{k}_3$]. When we used extraordinary rays for all three incident beams, we observed even higher reflectivities ($R_{\mathrm{ext}} \sim 100$) because of the added contribution of energy coupling between beams 1 and 2. (With the above geometry, this coupling is less than 0.02 for ordinary rays but can exceed 50 for extraordinary rays, and the coupling greatly enhances the reflectivity by increasing the intensity of the image writing beam as it propagates through the crystal.)

The optical setup that we used to obtain these large reflectivities is shown in Fig. 1. The optical beams are incident upon the barium titanate at a glancing angle to the surface of the crystal. The crystal is immersed in index-matching oil ($n = 1.51$) in order to increase the angle between the c axis and $\mathbf{k}$. The argon laser produces a TEM_{00} Gaussian mode at 514.5 mm in a single longitudinal mode.

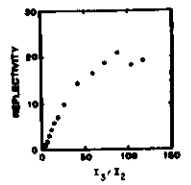

Fig. 2. A plot of the measured mirror reflectivity $R_{\mathrm{ext}} = I_4/I_2$ as a function of the reading-beam intensity I_3. The object-beam intensity was fixed at $I_2 = I_1/4$, and the angles of the incident beams were $\alpha_1 = +6°$, $\alpha_2 = +14°$, and $\theta = 20°$ (see Fig. 1). In this plot, I_3 has been normalized by the fixed intensity I_2.

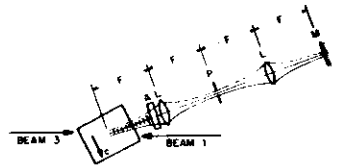

Fig. 3. Optical setup for observing cw self-oscillation. The incident beams 1 and 3 are both linearly polarized in the plane of the figure and are extraordinary rays in the crystal. Self-oscillation is observed to grow between the crystal and a 94% reflectivity plane mirror M. Here L's are lenses with a focal length $F = 100$ mm, and P is a variable pinhole used to control the transverse-mode structure of the oscillation. The phase aberrator A is formed by bubbles of transparent glue on a microscope slide. The angles of the beams are about the same as in Fig. 2.

The following four experiments elucidate the mirror characteristics. In the first experiment, the intensities I_1 and I_2 of the writing beams are fixed, and the scattering efficiency of the grating is measured as the intensity I_3 of the reading beam varies. All the beams are extraordinary rays in the crystal. From Fig. 2, it is seen that the intensity of the reflected beam (or signal beam) can be made to exceed the intensity of either of the writing beams. Since this signal beam is the phase conjugate of one of the writing beams (beam 2 in Fig. 1), the system acts as a phase-conjugate mirror with gain.

In the second experiment, two extraordinary counterpropagating beams (beams 1 and 3) are incident upon the crystal (beam 2 is blocked). A plane mirror is placed within view of the crystal, with the normal to the mirror directed approximately toward the crystal. Two new counterpropagating phase-conjugate beams are observed to grow between the crystal and the mirror with a time constant of the order of 1 sec. If the mirror is tilted, these new beams will fade away, only to reappear on whichever part of the mirror is closest to normal to the crystal. In the process of finding the cavity mode with the least loss in which to oscillate, the crystal finds and directs a beam at the most-reflective surface facing it. Oscillator output fades slowly (~1 sec) if beam 1 is

Phase-conjugating mirror with continuous-wave gain: errata

Jack Feinberg and R. W. Hellwarth

Department of Physics, University of Southern California, Los Angeles, California 90007

Received March 2, 1981

In Fig. 1 of our Letter,[1] the angles α_1 and α_2 should be measured from the z axis instead of from the y axis as shown. Therefore, the 17th and 18th lines on page 520 should read "... direction of the c axis, and α_1 and α_2 are the angles formed by each writing beam with the z axis. From..." On the 42nd line of the same page, the values given for α_1 and α_2 should each be increased by 90°, as should the values of α_1 and α_2 given in the caption of Fig. 2. This correction does not alter any of the calculations or conclusions of the Letter.

Reference

1. J. Feinberg and R. W. Hellwarth, "Phase-conjugating mirror with continuous-wave gain," Opt. Lett. 5, 519–521 (1980).

0146-9592/81/050257-01$0.50/0

blocked but extinguishes instantly if beam 3 is blocked, since beam 1 is helping to write the grating but beam 3 is reading it.

In the third experiment, two identical lenses (L) and an aberrator (A) are placed in the cavity formed by the phase-conjugating mirror (i.e., the crystal) and the mirror M, as in Fig. 3. Self-oscillation is allowed to build up, and its transverse-mode structure is photographed near both the real mirror and the wave-front-reversing mirror. Figure 4 shows these mode patterns, both of which are severely distorted by the aberrator. When a pinhole is placed at the focal length of the lens, in the manner suggested by AuYeung *et al.*,[12] the mode pattern becomes uniform. If the crystal were acting just as an ordinary mirror, the light distribution, returning to the pinhole from this mirror, would be doubly distorted from having passed through the aberrator twice and would spill out and be blocked by the face of the pinhole, causing a large loss in the resonator. In fact, we observed that when the adjustable pinhole is made sufficiently small (800-μm diameter) so as to reject high-order modes, the intracavity power in the resonator decreases at most by about 10% and sometimes increases, indicating that little light is lost on the walls of the pinhole and that the crystal is acting as a high-quality phase conjugator.

In the fourth experiment, an image amplifier with an intensity gain of ~10 is constructed by using two counterpropagating beams and an object beam, all extraordinary rays. When a resolution chart is placed in the object beam, an amplified real image of the resolution chart is observed. (See Fig. 5.)

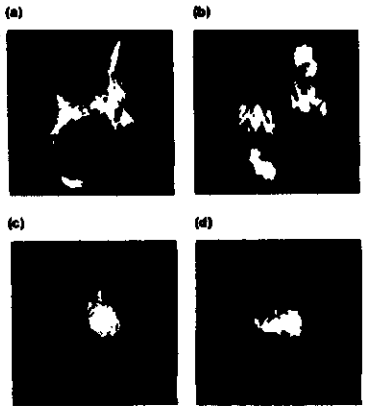

Fig. 4. Photographs of far-field mode patterns of self-oscillation with a severe phase aberrator in the resonator cavity. (See Fig. 3.) With no aperture in the resonator cavity: mode pattern transmitted (a) through the back of the crystal and (b) through the 94% mirror. With a 1-mm-diameter pinhole in the cavity: mode pattern (c) from the back side of the crystal and (d) transmitted through the 94% mirror. These mode patterns were displayed on a white card 2 m from the cavity, photographed with Kodak Plus-X (ASA 125) film, and printed on high-contrast paper.

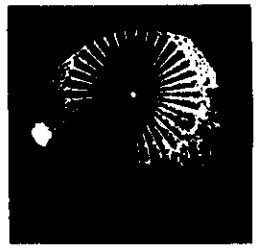

Fig. 5. Photograph of the real image of a resolution test chart (wheel diameter, 1 cm) formed in the object plane. The intensity of the image beam was measured to be ~10 times the intensity of the object beam, demonstrating optical image amplification. The bright spot seen on the left-hand side is from self-oscillation between the crystal and one of the faces of the glass cuvette that holds the crystal. This image was photographed with Kodak Plus-X (ASA 125) film and printed on high-contrast paper. The angles of the beams are about the same as in Figs. 2 and 3.

In conclusion, we have demonstrated a cw phase-conjugating mirror with gain up to 100. We have used this mirror to construct an image amplifier and an optical resonator that self-oscillates. With the aid of a spatial filter, this oscillating resonator will correct phase aberrations inside the resonator cavity and emit a TEM_{00} Gaussian mode.

We would like to thank W. Cooke for helpful discussions. This work was supported by the U.S. Air Force Office of Scientific Research under grant no. 78-3479 and by the National Science Foundation under grant no. ENG 78-04774.

References

1. D. M. Bloom, P. F. Liao, and N. P. Economou, Opt. Lett. 2, 58 (1978); D. M. Pepper, D. Fekete, and A. Yariv, Appl. Phys. Lett. 33, 41 (1978).
2. R. C. Lind, D. C. Steel, J. F. Lam, R. K. Jain, and R. A. McFarlane, J. Opt. Soc. Am. 70, 599 (1980).
3. F. S. Chen, J. Appl. Phys. 40, 3389 (1969).
4. J. P. Huignard, J. P. Herriau, P. Aubourg, and E. Spitz, Opt. Lett. 4, 21 (1979).
5. R. W. Hellwarth, J. Opt. Soc. Am. 67, 1 (1977).
6. J. Feinberg, D. Heiman, A. R. Tanguay, Jr., and R. W. Hellwarth, J. Appl. Phys. 51, 1297 (1980).
7. H. Kogelnik, Bell Syst. Tech. J. 48, 2909 (1969).
8. D. L. Staebler and J. J. Amodei, J. Appl. Phys. 43, 1042 (1972).
9. J. Feinberg, in preparation.
10. A. Yariv, *Quantum Electronics*, 2nd ed. (Wiley, New York, 1975).
11. The light-induced electrostatic field amplitude E is calculated from Ref. 6 by assuming that the charges in $BaTiO_3$ can hop in the x, y, and z directions with equal facility. The present experiment, however, is not sensitive to this assumption. We are pursuing further experiments to search for any anisotropy in the charge-hopping rates.
12. J. AuYeung, D. Fekete, D. M. Pepper, and A. Yariv, IEEE J. Quantum Electron. QE-15, 1180 (1979).

Corrections from Errata published on p. 257 of May '81 issue have been made in this copy.

Appendix X 68

Reprinted from OPTICS LETTERS, Vol. 4 page 124, April 1979

Spatial-diffusion measurements in impurity-doped solids by degenerate four-wave mixing

D. S. Hamilton, D. Heiman, Jack Feinberg, and R. W. Hellwarth

Electronic Sciences Laboratory, University of Southern California, Los Angeles, California 90007

Received November 21, 1978

A method is introduced that measures the spatial-migration rate of electronic excitation in condensed media over distances of the order of 0.1 μm. Two volume holographic gratings of widely differing modulation periods are simultaneously produced, using a phase-conjugate wave geometry of degenerate four-wave mixing. Spatial migration results in a reduced scattering efficiency of one grating and is observed as a polarization rotation of the backward-going output wave. Upper limits are placed on the diffusion constants in pink ruby and Nd^{3+}-doped silicate glass.

In this Letter we extend the analogy between degenerate four-wave mixing and holography to measure the spatial-migration rate of electronic excitation in impurity-doped solids. The production of holographic phase and absorption gratings in an absorbing medium has been well studied.[1-4] In these experiments it is the Bragg scattering of an optical beam from the grating produced by the interference of an image ($\mathbf{E}_i$) and reference beam ($\mathbf{E}_{ref}$) that produces an object beam ($\mathbf{E}_o$). Such a grating can arise from the modulation of the index of refraction that is due to the polarizability difference between optically excited ions and ions in their ground state. A process to produce and monitor two such gratings simultaneously has been discussed by Eichler[5] and, more recently, in a phase-conjugate wave-generation[6] context by several authors.[7,8] The formal analogy between conjugate-wave generation and holography has been discussed by Yariv.[9]

In this dual-grating configuration, one grating is produced by impurity-ion absorption of nearly copropagating beams and has a large grating spacing (~10 μm), while the other, produced by nearly counterpropagating beams, has a much smaller spacing (~0.2 μm). When spatial migration of the excited-state population density is absent or bottlenecked, the lifetime of both gratings is determined solely by the excited-state lifetime and will be independent of grating spacing. The effect of an active spatial-transport process is to make the lifetime of the grating depend on its spacing. Here we show how this dependence can be measured by observing the state of polarization of the scattered object wave rather than by studying the beam transients, as has been done previously.[3-5,8,10]

The experimental geometry is shown in Fig. 1. Three lightly focused (f = 50 cm) equal-pathlength beams from an argon laser operating at 514.5 nm (TEM_{00}) and 500 mW overlap in an absorbing sample. The wavevectors of the two exactly counterpropagating beams are $\mathbf{K}_+$ and $\mathbf{K}_-$ ($= -\mathbf{K}_+$), with associated electric fields $\mathbf{E}_+$ and $\mathbf{E}_-$, respectively. The image beam has wavevector $\mathbf{K}_i$ and electric field $\mathbf{E}_i$, and the phase-conjugate object wave, $\mathbf{K}_o$ ($= -\mathbf{K}_i$) and $\mathbf{E}_o$. The counterpropagating beams $\mathbf{E}_+$ and $\mathbf{E}_-$ are orthogonally polarized, and $\mathbf{E}_i$ is polarized at 45° to each. In general, the output-wave polarization will be at some different angle θ relative to the direction $\mathbf{E}_-$, and we interpret this angle in terms of grating lifetimes, as explained below.

By including the vector nature of the electric fields and extending the discussion of previous authors[3,4,7,8] we find that the electric field of the scattered object wave is proportional to $\tau_q(\mathbf{E}_j \cdot \mathbf{E}_k^*)\mathbf{E}_l$, where τ_q is the lifetime of the grating with wavevector $\mathbf{q} = \mathbf{K}_j - \mathbf{K}_k$. This output wave results from the scattering of $\mathbf{E}_l$ off the grating produced by $\mathbf{E}_j$ and $\mathbf{E}_k$. In our geometry there are two such phase-matched components, and the output wave is

$$\mathbf{E}_o = \frac{i}{2\hbar}\exp(-\beta l/2)\,[1-\exp(-\beta l/2)] \times Q(\Delta\alpha)\,[\tau_{2\hbar}(\mathbf{E}_+ \cdot \mathbf{E}_i^*)\mathbf{E}_- + \tau_{2\hbar}(\mathbf{E}_- \cdot \mathbf{E}_i^*)\mathbf{E}_+], \quad (1)$$

where β is the ground-state absorption coefficient, l is the sample length, and Q is quantum efficiency. The quantity $\Delta\alpha$ is the complex polarizability difference between the excited and ground states of the absorbing ion. For the electric-field orientations indicated in Fig. 1, the output wave will be polarized at an angle

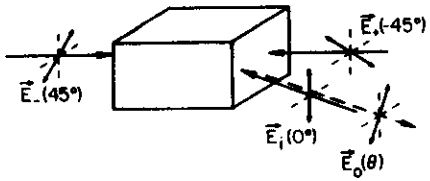

Fig. 1. The four beams have their electric fields along the indicated directions. The crossing angle between $\mathbf{K}_+$ and $\mathbf{K}_i$ is 1° (outside sample), and the polarization angle θ of $\mathbf{E}_o$ is measured from the normal of the scattering plane defined by $\mathbf{K}_+$ and $\mathbf{K}_i$.

0146-9592/79/040124-02$0.50/0

$$\theta = \arctan\left(1 - \frac{\tau_{2\hbar}}{\tau_{\Delta\hbar}}\right). \quad (2)$$

The grating decay rates can be written as $\tau_q^{-1} = \tau_0^{-1} + W(q)$, where τ_0 is the lifetime of the excited state and $W(q)$ represents the additional grating relaxation rate from spatial migration of the excitation among the impurity ions. Assuming an incoherent migration process and a mean step length much less than π/q, the spatial migration is then diffusive in character, and $W(q) = Dq^2$, where D is the diffusion constant.

It is also possible to measure τ_q by observing the temporal decay of $\mathbf{E}_o$ after $\mathbf{E}_+$ and $\mathbf{E}_i$ or $\mathbf{E}_-$ and $\mathbf{E}_i$ are turned off.[3-5,8,10] In situations in which the dynamics are in the nanosecond range, our polarization technique is especially attractive for observation of a spatial-migration process, since picosecond lasers and probe-pulse delay schemes are not required.

In particular, we have produced cw holograms in both Nd^{3+}-doped silicate glass and pink ruby and measured the polarization character of the scattered object wave. In the glass (2 wt% Nd_2O_3), the measured angle θ was less than 2°, indicating little diffusion over $\lambda/4n$ distances.[11] The radiative lifetime of the $^4F_{3/2}$ state of Nd^{3+} is about 0.3 msec, which gives an upper limit on the spatial diffusion constant of $D < 2 \times 10^{-9}$ cm²/sec.

In the ruby, the birefringence of the Al_2O_3 host required careful attention to sample alignment because of phase-matching considerations and the possibility of elliptical field components inside the crystal. With the c axis along the direction of $\mathbf{K}_+$ and $\mathbf{K}_-$, the measured polarization angle θ again was less than 2° in samples containing 0.01 and 0.08 at% Cr^{3+}. This result indicates that the spatial migration of the ^2E excitation in ruby has a diffusion constant less than 1×10^{-10} cm²/sec or is strongly bottlenecked because of trap sites or spatial inhomogenieties.[12] In similar and much higher (~1%) concentration ruby, measurements using a transient grating technique[5] have also shown no spatial migration over distances of the order of 0.1 μm.

The magnitude $|\Delta\alpha|$ of the difference between the complex polarizabilities of the excited and ground states can also be determined from the magnitude of the scattered object wave, as indicated in Eq. (1). At 514.5-nm wavelength, a power-reflection coefficient of 4% in ruby yielded a value of $|\Delta\alpha| \simeq 3 \times 10^{-25}$ cm³, which is in near agreement with the recent measurement of Liao and Bloom.[8] In the Nd^{3+} glass, this reflection coefficient was 0.016%, which gives a similar value of $|\Delta\alpha| \simeq 2 \times 10^{-25}$ cm³. From an oscillator strength calculation,[13] this polarizability difference has been estimated at 8×10^{-25} cm³ for Nd^{3+}-doped glass.

We have discussed the use of wave polarizations in cw holography and phase-conjugate wave generation to measure directly the spatial migration of excitation in impurity-doped glasses and crystals. This technique can also be extended to exciton diffusion problems in organic systems and measurements of spatial dynamics in gases.

This research was supported by the U.S. Air Force Office of Scientific Research under grant AFSOR-78-3479 and by the Department of Energy under University of California, Lawrence Livermore Laboratory subcontract 7509105.

References

1. R. G. Harrison, P. Key, V. I. Little, G. Magyar, and J. Katzenstein, "Bragg reflection of laser light from a phase grating in a Q-switching liquid," Appl. Phys. Lett. 13, 253 (1968).
2. T. A. Shankoff, "Recording holograms in luminescent materials," Appl. Opt. 8, 2282 (1969).
3. H. Eichler, P. Glosbach, and B. Kluzowski, "Investigation of spatial hole-burning in a ruby laser by diffraction of light," Z. Angew. Phys. 22, 378 (1970).
4. K. O. Hill, "Simple transient holograms in ruby," Appl. Opt. 10, 1695 (1971).
5. H. Eichler, "Laser-induced grating phenomena," Opt. Acta 24, 631 (1977).
6. R. W. Hellwarth, "Generation of time-reversed wave fronts by nonlinear refraction," J. Opt. Soc. Am. 67, 1 (1977).
7. R. L. Abrams and R. C. Lind, "Degenerate four-wave mixing in absorbing media," Opt. Lett. 2, 94 (1978).
8. P. F. Liao and D. M. Bloom, "Continuous-wave backward-wave generation by degenerate four-wave mixing in ruby," Opt. Lett. 3, 4 (1978).
9. A. Yariv, "Four-wave nonlinear optical mixing as real time holography," Opt. Commun. 25, 23 (1978).
10. J. R. Salcedo, A. E. Siegman, D. D. Dlott, and M. D. Fayer, "Dynamics of energy transport in molecular crystals: the picosecond transient grating technique," Phys. Rev. Lett. 41, 131 (1978).
11. The accuracy in the measurement of θ is limited to about 2° because of scatter in the data caused by vibration in the optical components.
12. Extrapolating the spectral transfer data of Selzer *et al.* [P. M. Selzer, D. S. Hamilton, and W. M. Yen, Phys. Rev. Lett. 38, 858 (1977)] in 0.08% ruby, we estimate an average ion–ion hop time over a distance d = 30 Å of T_h = 130 μsec and a diffusion constant $D = 8d^2/3\pi T_h = 2 \times 10^{-10}$ cm²/sec. No evidence of a rapid spatial-transport process independent of this slower phonon-assisted mechanism is observed.
13. E. P. Riedel and G. D. Baldwin, "Theory of dynamic optical distortion in isotropic laser materials," J. Appl. Phys. 38, 2720 (1967).

Appendix XI

Theory of phase conjugation by stimulated scattering in a waveguide*

R. W. Hellwarth
Electronic Sciences Laboratory, University of Southern California, University Park, Los Angeles, California 90007
(Received 13 February 1978)

We consider the backward optical wave stimulated by a multimode, monochromatic, incident optical wave in a waveguide filled with a transparent nonlinear medium, when the incident wave is negligibly perturbed by the nonlinear processes. We derive the conditions on guide length, area, mode number, and Stokes shift in order that a given high percentage of the power in the backscattered field be the "phase conjugate" of the incident field, i.e., be proportional to its complex conjugate in the entrance plane of the waveguide.

I. INTRODUCTION

When a strong monochromatic wave (at ν) is incident on a transparent medium it causes waves at lower frequencies ω to experience exponential gain if their frequency offset corresponds to the frequency of some excitation in the medium. If this excitation is an acoustic wave, the effect is called stimulated Brillouin scattering (SBS), otherwise it is called stimulated Raman scattering (SRS). It has long been known that laser sources may produce stimulated gain that is large enough ($\sim 10^{12}$) so that spontaneously scattered light experiences sufficient amplification, in a single pass out of the incident-beam region, to emerge with a power approaching that of the incident beam. More recently, it has been observed that, when the incident beam is multimode (i.e., has a complex wave front), the high intensity backscattered SBS or SRS waves generated in this single-pass process may be nearly the "phase conjugate" to the incident wave.[1-6] That is, in the entrance plane, the complex amplitude $\mathbf{E}_s(\mathbf{r})$ of the stimulated wave is nearly equal to the complex conjugate $\mathbf{E}_i^*(\mathbf{r})$ of the incident wave times a constant. When the incident and scattered frequencies, ν and ω, are nearly equal, phase conjugation makes the scattered wave appear to be nearly a time-reversed replica of the incident wave in a large region of space. Zel'dovich *et al.*[1] suggested that, when $\omega \sim \nu$, this effect should come from the solution of the nonlinear Maxwell equations after they were linearized with respect to the scattered fields. They pointed out that the resulting complicated set of coupled linear equations for the spatial amplitudes would have various solutions which exhibited spatial gain, and that one solution should: (a) have $\mathbf{E}_s \sim \mathbf{E}_i^*$ in some plane, and (b) have significantly ("2 to 3 times") higher gain than the others. As the SBS phase-conjugation experiments had been performed in an optical waveguide, Sidorovich[3] examined the equations appropriate to an optical waveguide, and agreed with these conclusions, however, surmising some "necessary" conditions for this effect for which we will show counter examples here. Zel'dovich and Shkunov pointed out that, when the beams interact in free space (rather than in a waveguide), phase conjugation can occur even when the frequency separation between the beams was large, as in SRS.[4] However, the conditions they find differ from those we will find here. Subsequently, Zel'dovich *et al.*[5] observed SRS from the 656 cm^{-1} Raman line of CS_2 to be largely a phase conjugate to an incident beam comprising about 300 transverse modes. Wang and Giuliano verified the high degree of phase conjugation present in SBS.[6]

In this paper we will analyze the degree of phase conjugation present in waves which are stimulated (from noise) in a waveguide by a strong multimode beam, whose propagation is assumed to be negligibly disturbed by the stimulated processes and negligibly attenuated by linear losses. Phase conjugation by stimulated scattering from an unguided beam (which requires more power and may be spoiled by self-focusing, breakdown, etc.) may be approximated by considering a waveguide whose length equals the diffraction length of the incident beam. We find that, even when a gap exists between the gain of one solution, or wave pattern, and that of the others, the maximum-gain solution is never a perfect phase conjugate to the pump (input) wave pattern. However, a very large fraction (>90%) of this maximum-gain solution is phase conjugate to the pump under conditions which are much less restrictive than those suggested by previous workers.[2,4] First, the waveguide must have a finite number of modes that can be excited and the transverse field patterns of the pump and stimulated modes must be essentially the same. This constitutes very little restriction in practice. More importantly, the product of the waveguide length, the Stokes wavelength shift, and the number of excited waveguide modes divided by their cross-sectional area must be less than a number that is of the order of the square root of the maximum acceptable fraction that is *not* phase conjugate.

Unlike Ref. 3, we find (a) that large differences in the amplitudes of the excited incident modes do *not* spoil phase conjugation; (b) the waveguide does *not* have to be much longer than a diffraction length; (c) the incident beam solid angle does *not* have to exceed the nonlinear index change. The free-space (no guide) theory of Ref. 4 also produces somewhat different conditions that depend on the value of the stimulated gain.

Unlike previous analyses, our conclusions are based on a general perturbation theory for the *non*-phase-conjugate fraction in the wave of maximum gain, valid for any distribution of incident-wave amplitudes and phases. We apply this theory to several models in a rectangular waveguide which have arbitrary distribution of phase and arbitrary distribution among four possible arbitrary amplitudes. What seems truly remarkable is that the many extraneous terms in the original coupled-mode equations fail to spoil the phase-conjugate nature of the guided wave with maximum gain, at least in the quite representative classes of input waves in a rectangular waveguide which we considered. A general proof of the conditions for phase conjugation of all possible inputs into all possible guide shapes is still lacking. However, we feel that our conditions are accurate for cases of interest in the laboratory.

II. FORM OF THE NONLINEAR POLARIZATION

We will consider the interaction in a straight waveguide of a multimode "pump" wave or input wave with stimulated backscattered "Brillouin" waves, i.e., waves generated by interactions with backward acoustic waves. The pump waves will be assumed to be monochromatic at angular frequency ν and to be Fourier analyzable inside the guide in terms of plane waves whose wave vectors lie mainly in a small cone of half-angle θ about the waveguide axis z. We will look for solutions of the nonlinear Maxwell equations which are backward-scattered waves of a single (Brillouin-shifted) frequency ω; solutions at different frequencies superpose. However, stimulated gain will make those solutions predominate which lie in a narrow range about frequency

$$\omega = \nu - \omega_B, \tag{1}$$

where

$$\omega_B \simeq 2n\nu_s\nu/c \tag{2}$$

is the acoustic frequency. Here v_s is the sound velocity, n is the (linear) refractive index, and c is the velocity of light in vacuum.

We will find that the backscattered waves will have wave vectors lying mainly inside a cone whose half-angle is also θ, the angle containing the pump waves. (In fact, the backscattered waves will often be nearly the time-reversed replica, or "phase conjugate," of the pump wave.) Here we will consider only the case

$$\theta < Q^{-1/2},$$

where $Q = \omega_B/\Delta\omega_B$ is the "Q value" of the backward waves and $\Delta\omega_B$ is the linewidth of the resonant response (and of the spontaneous backward Brillouin scattered light). When Eq. (3) holds, it is readily verified that the magnitudes of the sound wave vectors, excited by pump and scattered light waves, lie within the bandwidth $\Delta\omega_B/v_s$ in which the acoustic response is nearly constant—the same as at exact resonance. The independence of Brillouin response to wave vector in this case implies that the amplitude at ω of the nonlinear optical polarization density $\mathbf{P}_\omega^{NL}(\mathbf{r})$ depends only on the optical field at the same position $\mathbf{r}$. That is, we can neglect spatial dispersion when Eq. (3) holds. It is well known that on resonance, the nonlinear Brillouin polarization at $\mathbf{r}$ has the form

$$\mathbf{P}_\omega^{NL} = -iG\,\mathbf{E}_\nu\,\mathbf{E}_\nu^* \cdot \mathbf{E}_\omega \tag{4}$$

where $\mathbf{E}_\nu$ and $\mathbf{E}_\omega$ are the (complex) amplitudes of the pump and backscattered waves. On resonance, G is a real constant which we will relate later to the usual plane-wave Brillouin gain coefficient. [When ω deviates from the resonance condition (1), G becomes complex and of smaller magnitude.] Other nonlinear effects, such as SRS, give a third-order polarization density that is largely imaginary and spatially local as in Eq. (4), and our theory here will apply to these also, after possible minor modification of the tensorial character of Eq. (4).

Although Eq. (3) has been well-satisfied in all experiments to date, we note that it need not be if the waveguide-acceptance angle is larger than $Q^{-1/2}$. In this case phase-conjugation properties can be predicted by considering subsets of excited incident modes, each of which interacts with a different subset of phonon waves, the results of each subset of interactions being treated essentially as we will treat the case obeying Eq. (3).

III. FORMULATION IN A CYLINDRICAL WAVEGUIDE

We will assume that the nonlinear polarization density does not disturb the incident pump waves so that their complex amplitude $\mathbf{E}_\nu(\mathbf{r})$ can be written inside the waveguide as

$$\mathbf{E}_\nu = \sum_m A_m \hat{\boldsymbol{\epsilon}}_m(x,y) e^{ik_m z}. \tag{5}$$

Here the A_m are complex amplitudes for the pump wave to be in various normal modes of the guide, whose transverse mode patterns $\hat{\boldsymbol{\epsilon}}_m(x,y)$ are normalized so that

$$\int dx\,dy\,\hat{\boldsymbol{\epsilon}}_m^* \cdot \hat{\boldsymbol{\epsilon}}_n = \delta_{mn}. \tag{6}$$

We will assume that the transverse refractive index variations or metallic walls, etc., forming the guide are such that the transverse functions $\hat{\boldsymbol{\epsilon}}_m$ do not differ significantly for the various temporal frequencies (pump and Stokes-shifted) that are propagating in the guide. However, the propagation constants k_m, are frequency-dependent and obey

$$k_m^2 + u_m^2 = n^2\nu^2/c^2, \tag{7}$$

where u_m^2 is the (frequency-independent) eigenvalue associated with the function $\hat{\boldsymbol{\epsilon}}_m$. Here, n, the refractive index at

 0030-3941/78/6808-1050$00.50

...axis, is assumed to be real, i.e., linear attenuation ... interaction regions is assumed to be negligible.

We will not need to digress here on the characteristics of waveguide modes; our results will be largely independent of the detailed nature of the waveguide, provided that it propagates a number of modes at ν and ω whose transverse mode patterns $\hat{e}$ are congruent.

IV. NONLINEAR MAXWELL EQUATIONS FOR MODE AMPLITUDES

We now consider Maxwell's equations for the complex amplitude $\mathbb{E}_\omega$ of the waves generated in the guide, at frequency ω, under the influence of the nonlinear polarization density (4). We will try a solution of the nonlinear Maxwell equations of the form

$$\mathbb{E}_\omega = \sum_n B_n\, \hat{e}_n(x,y) e^{-ik_{n\omega}z - \gamma z/2} \tag{8}$$

which is similar to Eq. (5) except that the waves are both traveling and growing in the backwards direction ($-z$). When there is no nonlinear term (4) and $\gamma = 0$, Eq. (8) satisfies Maxwell's equations identically. When the nonlinear term (4) is added as a small perturbation, Maxwell's equations are satisfied in a length L of guide provided that

$$\gamma k\, B_m = 4\pi\omega^2 c^{-2} G \sum_{ijn} \iint dx\, dy\, \hat{e}_m^* \cdot \hat{e}_i\, \hat{e}_j^* \cdot \hat{e}_n \times K_{mijn}\, A_i A_j^*\, B_n, \tag{9}$$

where

$$K_{mijn} = \int_0^L e^{i\Delta k z}\, dz/L \tag{10a}$$

and $\Delta k = k_{m\omega} + k_{i\nu} - k_{j\nu} - k_{n\omega}$. It is useful to note that

$$|K_{mijn}| = x^{-1} \sin x, \tag{10b}$$

where $x = \Delta k L/2$ equals zero when $i = j$ and $m = n$.

In Eq. (9), as in the following formulas, repeated space indices are assumed to be summed unless otherwise stated. We have approximated a factor $k_{m\omega}$ on the left-hand side of (9) by its average k; the small difference is negligible, as will be seen by an obvious extension of the perturbation theory which we will apply to more important terms below.

From Eq. (9) it is seen that the nonlinear Maxwell equations lead to a coupled set of linear equations for the backward-scattered-wave mode amplitudes B_n, when these are too small to affect the incident-wave amplitudes A_m. We have not established the properties of B_n for all possible sets of A_m, but we have solved for B_n for some nontrivial A_m. We have also derived a perturbation expression for the non-phase-conjugated fraction f of that solution $\{B_n\}$ of Eq. (9) having the largest value γ_0 of gain γ. We also calculate γ_0, showing that, when $f \ll 1$, γ_0 is larger enough than the γ for any other solution so that the near-conjugate solution can dominate in practice. The perturbation theory needed to accomplish these tasks takes a form that is familiar to quantum mechanics if we rewrite Eq. (9) in the form of an eigenvalue equation, with eigenvalue Y, in a Hilbert space of dimension N equal to the number of transverse mode patterns that are excitable in the guide. This reexpression of Eq. (9) is

$$\sum_n (H_{mn} + V_{mn} + U_{mn})\, B_n = Y B_m \tag{11}$$

where the "effective unperturbed Hamiltonian" is

$$H_{mn} = \bar{\alpha}\, \delta_{mn} + \bar{\beta}\, a_m^* a_n \tag{12}$$

and the first perturbation Hamiltonian is (no implied summations)

$$V_{mn} = \sum_l (\alpha_{nl} - \bar{\alpha})\, a_l^* a_l\, \delta_{mn} + (\beta_{mn} - \bar{\beta}) a_m^* a_n. \tag{13}$$

Here the a_n are normalized dimensionless pump-beam amplitudes

$$a_n = A_n \left(\sum_m A_m^* A_m\right)^{-1/2} \tag{14}$$

The α_{mn} and β_{mn} matrices are derived from mode-overlap integrals according to

$$\alpha_{mn} = \iint dx\, dy\, |\hat{e}_m^* \cdot \hat{e}_n|^2 \tag{15}$$

and (no implied summation)

$$\beta_{mn} = \iint dx\, dy\, (\hat{e}_m^* \cdot \hat{e}_n)^2 K_{mnmn}. \tag{16}$$

Their averages $\bar{\alpha}$ and $\bar{\beta}$ are defined by

$$\bar{\alpha} = \sum_{mn} \alpha_{mn} |a_m|^2 |a_n|^2. \tag{17}$$

and similarly for $\bar{\beta}$. One sees that the α terms in Eqs. (12) and (13) are from the terms in (9) for which $i = j$ and $m = n$; the β terms are from the terms in (9) for which $i = n$ and $j = m$. Note that H_{mn} and V_{mn} are Hermitian.

The second perturbation Hamiltonian is (no implied summation)

$$U_{mn} = \sum_{ij}{}' a_i a_j^* \iint dx\, dy\, \hat{e}_m^* \cdot \hat{e}_i\, \hat{e}_j^* \cdot \hat{e}_n K_{mijn}, \tag{18}$$

where the prime on the summation signifies the inclusion of only those terms not included in Eqs. (12) and (13). The K_{mijn} in Eq. (18) have $\Delta k \neq 0$ except when degeneracies occur which make either $k_{i\nu} = k_{j\nu}$ and $k_{n\omega} = k_{m\omega}$ simultaneously, or $k_{i\nu} = k_{n\omega}$ and $k_{j\nu} = k_{m\omega}$ simultaneously.[7] In practice, the K_{mijn} in Eq. (18) for which $\Delta k \approx 0$ can be omitted from consideration for the following reasons. First, the component of $\mathbb{E}$, in any degenerate manifold of guide modes can be taken as one of the basis vectors in this manifold. Then, no terms will exist in (18) with $k_{i\nu} = k_{j\nu}$. The second case is possible when $\omega \propto \nu$, $u_\omega^2 = u_\omega^2$ and $u_j^2 = u_n^2$. However, then it is usual that $\hat{e}_n^* \cdot \hat{e}_i = \hat{e}_j^* \cdot \hat{e}_m = 0$. In a guide with high symmetry, the latter may not be the case, but then the x-y overlap integral in (18) seems to be greatly reduced over that in (16) arising from $i = n$ and $j = m$; in fact it reduces to zero for a rectangular waveguide. Thus we will neglect the terms in (18) for which Δk is accidently near zero, considering next the effects of the remaining terms.

If the difference between $\Delta k L$ values for various mode indices is larger than π, expressions (10) show K_{mijn} to oscillate randomly and cause a great deal of cancellation among terms. If the area of the guide is S, and there are N excitable modes, then $a_n^2 \sim N^2/S$, $|K_{mijn}| \ll 1$, and $\Delta k L$ changes by at least π for most changes in (i, j, n, m) when

$$NL > Sk. \tag{19}$$

We expect therefore that U_{mn} can be neglected compared to H_{mn} when $L > L_d/N^{1/2}$, where L_d is a diffraction length ($\sim Sk/N^{1/2}$). This condition is met by free-space interactions and all practical guides. Therefore we proceed to solve Eq. (11) with $U_{mn} = 0$.

Before proceeding it is useful to relate the eigenvalue Y for any N-dimensional vector solution $\{B_n\}$ of Eq. (11) to its gain γ and the commonly defined stimulated gain coefficient g (Np cm/MW) for plane pump and scattered waves. The "free-space" coefficient g is the same as that (γS + total pump power P) in a guide that is excited in a single mode $\hat{e}_n$ having a uniform intensity profile ($\hat{e}_n$ = const), and for which Eqs. (6), (15), and (16) give $\bar{\alpha} = \bar{\beta} = 1/S$. In this case $V_{nm} = U_{nm} = 0$ and $B_m = a_m^*$ is the solution of (11) with eigenvalue

$$Y_{pw} = 2/S. \tag{20}$$

Since $\Sigma_n |A_n|^2$ is proportional to the power P in the guide, a comparison of Eqs. (9) and (11) shows $Y \propto \gamma/P$ in all cases. Therefore the power gain γ for any solution of (11) with eigenvalue Y is related to g by

$$\gamma(\mathrm{cm}^{-1}) = \tfrac{1}{2}\, Y(\mathrm{cm}^{-2})\, g(\mathrm{cm/MW})\, P(\mathrm{MW}), \tag{21}$$

where the most common units used are indicated. We proceed now to find solutions of Eq. (11) and their gains γ for multimode pump beams.

V. FIRST APPROXIMATE SOLUTION FOR ARBITRARY INPUT

The "unperturbed" matrix H_{mn} in (11) is of the particularly simple form of a unit matrix plus a projection operator P_a onto the conjugate a_n^* of that vector whose components a_n are the complex mode-amplitudes of the incident wave in the guide. Therefore, the eigenstates and eigenvalues $G^{(\nu)}$ of H_{mn} are easily seen to be a_n^*, with eigenvalue

$$G^{(0)} = \bar{\alpha} + \bar{\beta} \tag{22}$$

and any set of vectors $b_n^{(\nu)}$ orthogonal to a_n^* and to each other, which complete the space of guide modes. The latter have eigenvalues

$$G^{(\nu)} = \bar{\alpha}. \tag{23}$$

Note that when all guide modes have the same linear (or elliptical) polarization, and when $\omega \to \nu$, so that by Eq. (10) $K_{mnmn} \to 1$, as in practical SBS experiments, then

$$\bar{\alpha} \to \bar{\beta} \tag{24}$$

and

$$G^0 \to 2G^\nu. \tag{25}$$

That is, the conjugate backscattered wave, whose mode amplitudes are a_n^*, would experience twice the gain as any other mode, provided that V_{mn} can be neglected.

We will find that whenever the scattered-wave's energy is mostly in the phase conjugate to the incident wave, its gain is nearly twice that of any other wave. Furthermore this condition occurs whenever the elements K_{mnmn} of (10) are always near unity, as they are for practical configurations producing SBS. To see this we consider first a class of pump waves for which Eq. (11) can be solved exactly, and then ... general perturbation theory to an even wider class of ... waves.

VI. SET OF EXACT SCATTERED SOLUTIONS AND THEIR GAINS

There is an important class of incident-mode patterns in a rectangular waveguide for which the eigenvectors of both H_{mn} and V_{mn} are the same set, provided $K_{mnmn} \sim 1$ (as for SBS) which we assume here. This is the class of waves for which all N excitable modes of one polarization of the guide are excited with equal energy but with arbitrary phases ϕ_n:

$$a_n = N^{-1/2} e^{-i\phi_n}. \tag{26}$$

For simplicity, assume the first M modes in both x and y directions are excited ($N = M^2$) and label the modes by x and y indices, $(n_x, n_y) \leftrightarrow n$, such that

$$n_x, n_y = 0, 1, 2, \ldots, M\text{-}1 \tag{27}$$

in order of increasing numbers of nodes. The integrals in (15) and (16) are then easily approximated (assume the mode functions are sine waves vanishing at the boundary) to obtain

$$\alpha_{nl} = \beta_{nl} = [2 + \delta(n_x, l_x)]\,[2 + \delta(n_y, l_y)]/4S, \tag{28}$$

where the δ function is 1 if its arguments are equal, and zero otherwise. It is easily verified by substitution in Eq. (11) that the $N = M^2$ eigenvectors have components (mode amplitudes)

$$B_n(l_x, l_y) = M^{-1} \exp[i\phi_n + 2\pi i(n_x l_x + n_y l_y)/M], \tag{29}$$

where pairs of the integers

$$l_x, l_y = 0, 1, \ldots, M\text{-}1 \tag{30}$$

are convenient labels for the N vectors. The eigenvector with $l_x = l_y = 0$ is the desired phase-conjugate state ($B_n = a_n^*$), and it has the largest eigenvalue:

$$Y_{00} = \bar{\alpha} + \bar{\beta}. \tag{31}$$

Then there are $2M$-2 eigenvectors having either $l_x = 0$ or $l_y = 0$ (but not both) which all have the eigenvalue

$$Y_{0\nu} = \bar{\alpha} + (1 + 2M)/4SM^2. \tag{32}$$

Finally the $(M\text{-}1)^2$ states for which $l_x \neq 0$ and $l_y \neq 0$ have the eigenvalues

$$Y_{\mu\nu} = \bar{\alpha} + 1/4SM^2. \tag{33}$$

For the sine-wave modes,

$$\bar{\alpha} = \bar{\beta} = (1 + M^{-1} + M^{-2}/4)/S. \tag{34}$$

Therefore the "gap" in gain between Y_{00} of the conjugate wave and $Y_{0\nu}$ the next nearest gain is

$$Y_{00} - Y_{0\nu} = (1 - \tfrac{1}{2} N^{-1/2})/S \tag{35}$$

which, for a large number N of modes, approaches the gap between Eqs. (22) and (23) for $V_{mn} = 0$. Also, for large N, we see from (21) that the gain of the conjugate wave is the same as for a plane-wave pump of intensity P/S in free space.

Studies of pump beams that do not have equal power in all modes have led us to believe that the gap between the highest and next-highest mode gains is quite generally $\bar{\alpha}$ less a term

34

ERRATUM

"Theory of phase conjugation by stimulated scattering in a waveguide" by R.W. Hellwarth, J. Opt. Soc. Am., Vol. 68, pp. 1050-1056, Aug. 1978.

A term given by

$$\bar{w}\, B_m \equiv \alpha_{mm}|a_m|^2 B_m \qquad \text{(E1)}$$

should be subtracted from the LHS of Eqn. (11). We are grateful to V.V. Shkunov (private communication) for pointing out that this term was double counted in passing from Eqn. (9) to Eqn. (11), and therefore must be subtracted again. This term however, makes only negligible corrections to our results, as follows. It causes a fractional correction of order N^{-1} in our calculated stimulated gain coefficients Y (and γ) of Eqns. (11) and (21). Also, an additional contribution of order N^{-2} is added to the fraction f, defined in Eqn. (40), of non-conjugate power in the (nearly) conjugate) backscattered wave of maximum gain. Because the number N of excited guide modes is assumed to be much larger than unity, these corrections are negligible. However, the following changes in text should be made to acknowledge (E1) and to establish its insignificance.

(please turn over)

35

ERRATUM
P. 2 of 2
"Theory of phase conjugation by stimulated....."
by R.W. Hellwarth

Replace the quantity "$\bar{\alpha}$" in Eqn. (12) by "$\bar{\alpha} - \bar{w}$". Replace the quantity "$\bar{\alpha}$" in Eqn. (13) by "$\bar{\alpha}+\alpha_{nn}|a_n|^2-\alpha_{\ell\ell}|a_\ell|^2$". Before the sentence beginning in the line following Eqn. (17), insert "$\bar{w}\equiv\Sigma_n\alpha_{nn}|a_n|^4$." (This method of subtracting the term (E1) from the LHS of Eqn. (12) preserves the important property of Eqn. (38) for the term V_{mn} which will be treated as a small perturbation.)

Omit the factor "2" in Eqn. (20).

Omit the factor "½" in Eqn. (21).

Subtract "$\bar{w}$" from the RHS of Eqns. (22) and (23).

After the "and" following Eqn. (24) insert ", since $\bar{w} \sim \bar{\alpha}/N \ll \bar{\alpha}$,".

Subtract 9/(4SN) from the RHS of Eqns. (31), (32) and (33).

Replace "$\bar{\alpha}$" by "$\bar{\alpha}-\bar{w}$" in the second line before Eqn. (36).

Replace "$\bar{\alpha}$" by "$\bar{\alpha}+\alpha_{\ell\ell}|a_\ell|^2-\alpha_{mm}|a_m|^2$" in the line following Eqn. (41).

Insert before the sentence beginning in the second line above Eqn. (44) the additional sentence: "We also neglect the terms $\alpha_{mm}|a_m|^2-\alpha_{\ell\ell}|a_\ell|^2$ in $\theta_{\ell m}$ of Eqn. (41) since these contribute to terms in r of order N^{-1} smaller than the other contributions."

Replace "N^2" by "N" in the last line on p. 1052.

[illegible] This gap is usually enough in practice [illegible] calculated solution dominates in experiments [illegible] backscattered wave grows from noise. It remains to be seen in Sec. VII how closely this single solution approximates a phase conjugate to the incident wave.

VII. PERTURBATION SOLUTIONS FOR SCATTERING FROM ARBITRARY PUMP WAVES

Having seen from the exact solutions for B_n in the special case of the previous section that the effect of V_{mn} in Eq. (11) was small when the number N of pump-wave modes excited was large, we are encouraged to treat V_{mn} as a small perturbation on H_{mn} in solving the eigenvalue equation (11) (in which we continue to assume $U_{mn} = 0$ for reasons argued previously). Let us denote the exact eigenvector of $H_{mn} + V_{mn}$, having largest eigenvalue Y_0, by B_{0n}. Since we have already shown in (22) that the eigenvector $b_n^{(0)}$ of H_{mn} having highest eigenvalue $G^{(0)} = (\bar{\alpha} + \bar{\beta})$ was a_n^*, let us write the exact solution as

$$B_{0n} = a_n^* + c_n. \tag{36}$$

Then standard perturbation theory gives for the correction c_n (repeated mode indices are to be summed henceforth)

$$c_n = \sum_{\nu \neq 0} b_n^{(\nu)} b_l^{(\nu)*} V_{lm} a_m^* / (G^{(0)} - G^{(\nu)}) \tag{37}$$

to lowest order in the perturbation V_{lm}. Recall that the $b_n^{(\nu)}$ is the eigenvector of H_{mn} with eigenvalue $G^{(\nu)}$. From Eqs. (22) and (23) we recall that the energy denominator $G^{(0)} - G^{(\nu)}$ in Eq. (37) is a constant $\bar{\beta}$. Since, from its definition in Eqs. (13)–(17), V_{mn} has the property

$$a_m V_{mn} a_n^* = 0, \tag{38}$$

the sum in (37) may be extended over all ν (with constant denominator), and closure invoked to obtain the expression

$$c_n = V_{nm} a_m^* / \bar{\beta}, \tag{39}$$

which is simpler for calculation. The most important quantity to calculate for our purposes is the fraction f of power in the highest gain solution B_{0n} that is *not* in the phase-conjugate wave a_n^*. Since $a_n^* a_n = 1$ by (14),

$$f = r/(1-r), \tag{40}$$

where $r = c_n^* c_n$. From Eqs. (39) and (13) we have

$$r = |a_l|^2 \theta_{lm} |a_m|^2 \theta_{mn} |a_n|^2 / \bar{\beta}^2, \tag{41}$$

where $\theta_{lm} = \alpha_{lm} + \beta_{lm} - \bar{\alpha} - \bar{\beta}$. This is the most important result of perturbation theory for assessing the fraction f of stimulated backward scattering that is not phase conjugate to the pump wave. If r is not much less than 1, the process is useless and it is pointless to calculate further corrections to Eq. (39). If $r \ll 1$ then (39) and (40) are accurate enough. It is of minor interest to note that the gain Y_0 of the important wave is somewhat larger than $G^{(0)}$. From nondegenerate perturbation theory for eigenvalues,

$$Y_0 = G^{(0)} + r\bar{\beta} \tag{42}$$

to second order in V_{mn}. [The correction linear in V_{mn} vanishes because of Eq. (38).] That is, the gain is increased by the fraction r of the gain "gap" $\bar{\beta}$.

We next use (41) to calculate r for [illegible] pump beams.

VIII. MODEL CALCULATION OF NONCONJUGATED POWER FRACTION

We calculate here the nonconjugated power ratio r of Eq. (41) for a realistic set of complex pump-beam amplitudes a_n, each member having arbitrary phase and one of four possible magnitudes, in the ideal rectangular waveguide considered in Sec. VI. Expressing the mode label n in terms of the x and y mode-integers l_x and l_y of Eq. (30), we take for the square magnitudes required in Eq. (41)

$$|a_n|^2 = g_x(l_x) g_y(l_y). \tag{43}$$

The real positive functions g_x and g_y are defined to have the value g_+ for a number N_+ of the M values of their integer argument, to have the value g_- (less than g_+) for N_- of these M values, and to have the value zero for the remainder. The particular members of each of these three sets need not be the same for g_x and g_y. This results in four possible values for $|a_n|^2$:

$$g_+ g_+, \quad g_+ g_-, \quad g_+ g_-, \quad \text{or } 0$$

depending on $n \leftrightarrow (l_x, l_y)$. The total number N of excitable modes equals $M^2 (\geq N_+ N_-)$.

Again we assume all modes to have the same linear polarization $\hat{e}_n$ parallel to $\hat{x}$ or $\hat{y}$ so that $\alpha_{nm} = \beta_{nm}$ in θ_{nm} are given by Eq. (28). The required sums in (41) are then easily done to yield

$$r = 4[(u_\pm^2)^2/(u_\pm)^4 - 1], \tag{44}$$

where the average $\langle\ \rangle$ is to be performed over the two-valued function

$$u_\pm = 1 + \tfrac{1}{2} g_\pm / (N_+ g_+ + N_- g_-) \tag{45}$$

with the two-valued, normalized probability

$$w_\pm = g_\pm N_\pm / (N_+ g_+ + N_- g_-). \tag{46}$$

Clearly r in Eq. (44) is a function of three independent parameters, which we choose as N_+, N_-, and g_-/g_+, whose ranges are

$$0 \leq N_+ \leq M, \quad 0 \leq N_- \leq M, \quad 0 \leq g_-/g_+ \leq 1. \tag{47}$$

Let us consider r for various possible parameter sets representing various possible classes of pump beams.

A. N_- (or g_-) $= 0$; $1 < N_+ \leq M$. This is a pump beam with N_+^2 modes excited with equal amplitude and arbitrary phase. In this case Eq. (44) reduces immediately to $r = 0$. To this order in perturbation theory, the phase-conjugate wave with $B_{0n} = a_n^*$ is exact. We saw above that when $N_+ = M$, this solution is exact to all orders in V_{mn}. In any event we expect this case to yield maximum gain for a wave that is indistinguishable in practice from the phase conjugate.

B. $g_- = g_+$. This is obviously equivalent to case A and gives $r = 0$.

C. $N_- = 0$, $N_+ = 1$. This is the single-mode pump, which we saw above had the conjugate wave as an exact solution to Eq. (11); and Eq. (47) gives $r = 0$ as expected.

D. $N_+ = N_- = 1$. This is the worst case in the model (four modes with three amplitudes), giving the largest nonconjugate ratio r for given g_-/g_+. Simple numerical analysis shows that the maximum of r is

$$r_{max} \sim 0.0669 \text{ at } g_- \sim 0.20 g_+. \tag{48}$$

That is, in the worst case, less than 8% of the backscattered energy should be different from the pure phase-conjugate wave.

E. $N_+ = N_- \gg 1$. For many modes excited among three amplitudes this way, $r \propto N_+^{-2}$. Plots of Eq. (44) show that the maximum r is

$$r_{max} \sim 0.1 N_+^{-2} \tag{49}$$

with little change in the range $0.1 < g_-/g_+ < 0.2$ and rapid drop off when this ratio is smaller than 0.05 or larger than 0.5. A more exact treatment is not useful as clearly the nonconjugate fraction $f \sim r$ becomes insignificant when the number of excited modes is large.

F. $N_+ \neq N_-$, $N_+ \gg 1$. Then $r \propto N_+^{-2}$ as in Eq. (49).

In conclusion, we see that for any pump wave that is distributed among guide modes with arbitrary phase and any distribution among four amplitudes obeying (43), there is never more than 8% nonconjugated power in the stimulated wave with maximum gain and generally much less. We are led to conclude (contrary to Ref. 4) that the stimulated backscattering wave with the highest gain has an order-of-magnitude more power in the phase conjugate than in the useless background, for any distribution of pump-mode amplitudes whatever, provided that, as in SBS, $\nu - \omega \ll \omega$ so that $K_{mnmn} \to 1$. We consider next the relaxation of this condition.

IX. PHASE-CONJUGATION IN STIMULATED RAMAN SCATTERING (SRS)

When the scattered frequency ω is significantly different from ν, then K_{mnmn} in Eq. (16) may not be nearly unity, as we have assumed. We will find that phase conjugation disappears as $|K_{mnmn}|$ declines, but this need not happen, even at sizable Stokes shifts, provided that the guide interaction length L is short enough. Before deriving the conditions ω, ν, and L must satisfy, we consider the possibility of stimulated forward scattering (which does not occur in SBS).

If the B_n in Eq. (11) were to represent amplitudes of forward traveling waves (i.e., $k_{n\omega} \to -k_{n\omega}$), then one sees immediately that there is again often one solution having about twice the gain of any other (when $K_{mnmn} \sim 1$), but that solution has $B_n \sim a_n$. That is, this solution is a sort of replica of the incident wave, but not time reversed or phase conjugated. This possibility may be of interest but we shall not consider it further here.

To consider the effect of reduced K_{mnmn} on backward scattering, we consider again the model of Sec. VI in which the first M modes along both the x and y axes of a rectangular guide are excited with arbitrary phases. Inasmuch as this model produced results close to that of the variable-amplitude model when $K_{mnmn} \sim 1$, we expect it to do so here also. We specialize to a square waveguide for which the transverse eigenvalues u_n of Eq. (7) are

$$u_n^2 = \pi^2 (n_x^2 + n_y^2)/S \tag{50}$$

with the mode integers as in Eq. (27). It is sufficiently accurate to expand Δk of Eq. (10) to lowest order in the u_n^2 to obtain for the (m,n) element

$$\Delta k = q\,(m_x^2 - n_x^2 + m_y^2 - n_y^2), \tag{51}$$

where

$$q = \pi \Delta\lambda / 4S \tag{52}$$

and $\Delta\lambda$ is the difference between the wavelengths in the medium at ω and ν:

$$\Delta\lambda = (c/2\pi)\,(1/n_\omega \omega - 1/n_\nu \nu). \tag{53}$$

Here n_ω and n_ν are the refractive indices at ω and ν.

We use these specific forms now to calculate the nonconjugated fraction r, using the perturbation expression (41), and to find the conditions necessary to keep this below some desired maximum value r_0. With Eqs. (50)–(53) in (10) and (16), the β_{mn} matrix we will need in this calculation is given by

$$4S\beta_{mn} = \int_0^L dz |2e^{iqz(m_x^2 - n_x^2)} + \delta(m_x, n_x)|$$
$$\times |2e^{iqz(m_y^2 - n_y^2)} + \delta(m_y, n_y)|/L, \tag{54}$$

which is seen to reduce to the previous form (28) when $q \to 0$. The α_{mn} terms in (41) for r cancel exactly as before, leaving only the β_{mn} terms to be estimated. This we do by calculating the correction Δr that is lowest order in qL, by expanding (54) in powers of q. Higher-order corrections are not interesting as they only tell more precisely what happens after the phase-conjugated fraction has become uninterestingly small. We will also approximate the sums over integers in the resulting expressions by integrals, since the accuracy of this is quite good, especially at large M. This gives directly for the increase Δr in r from its value when $K_{mnmn} \sim 1$:

$$\Delta r = \frac{2}{45} \left(\frac{\pi \Delta\lambda M^2 L}{4S} \right)^2 (1 + O\,|q^2 L^2| + O\,|M^{-1}|), \tag{55}$$

leading to the condition on the interaction length L

$$L \leq 6 r_0^{1/2} S / N \Delta\lambda \tag{56}$$

in order that the nonconjugated fraction be kept less than r_0 for N equally excited modes in a rectangular waveguide of area S. We feel that Eq. (56) can be applied usefully when there are N unequally excited modes of arbitrary phase, provided that the required nonconjugated fraction r_0 is small.

As Δr increases by (55), so does the gap in gain between the nearly-phase-conjugate wave and its nearest competitor decrease. An estimate of this can be made from Eqs. (22) and (23). However, it is not very interesting to calculate this gap when the waves are already degraded.

In the SRS phase-conjugation experiment of Zel'dovich *et al.*,[6] the incident beam was focused into an "infinite" medium of CS_2. This was roughly equivalent to employing a waveguide whose length was a diffraction length $\sim S\lambda^{-1} N^{-1/2}$.[8] We may use Eq. (55) then to estimate the nonconjugate fraction Δr arising from this finite length, obtaining $\Delta r \sim 0.7\%$, in agreement with the qualitative report of excellent conjugation. (See parameter summary above.)

In conclusion, stimulated backward scattering at ω in a waveguide can be an efficient generator of the phase conjugate of an incident wave at ν, irregardless of the distribution of the N mode amplitudes of the incident wave, provided that the frequency ω is not so different from ν for given guide length as to violate Eq. (56). For some incident beams the nonconjugate fraction contained in the backward wave with highest stimulated gain may be of order 10^{-1} but is generally much smaller, decreasing as N^{-1} as the number of modes N increases. Scattering without a waveguide may be approximated by considering a waveguide one diffraction length long. However, when a waveguide will satisfy the above criteria for phase conjugation, it has the advantage of greatly reducing power requirements and the competition from other nonlinear effects, such as self-focusing.

ACKNOWLEDGMENT

The author wishes to thank V. Wang for many helpful discussions.

*This work was supported in part by the Defense Advanced Projects Agency and monitored through the ONR, and in part by the Joint Services Electronics Project, monitored by the AFOSR under Contract No. F44620-76-C-0061.

[1]B. Y. Zel'dovich, V. I. Popovichev, V. V. Ragul'skii, and F. S. Faizullov, "Connection between the wavefronts of the reflected and exciting light in stimulated Mandel'stam-Brillouin scattering," Pisma Zh. Eksp. Teor. Fiz. 15, 160–164 (1972) [JETP Lett. 15, 109–113 (1972)].

[2]O. Y. Nosach, V. I. Popovichev, V. V. Ragul'skii, and F. S. Faizullov, "Cancellation of phase distortions in an amplifying medium with a 'Brillouin mirror,'" Pisma Zh. Eksp. Teor. Fiz. 16, 617–621 (1972) [JETP Lett. 16, 435–438 (1972)].

[3]V. G. Sidorovich, "Theory of the 'Brillouin mirror,'" Zh. Tekh. Fiz. 46, 2169–2174 (1976) [Sov. Phys. Tech. Phys. 21, 1270–1274 (1976)].

[4]B. Ya. Zel'dovich and V. V. Shkunov, "Wavefront reproduction in stimulated Raman scattering," Kvantovaye Elektron. (Moscow) 4, 1090–1098 (1977) [Sov. J. Quantum Electron. 7, 610–615 (1977)].

[5]B. Ya. Zel'dovich, N. A. Mel'nikov, N. F. Pilipetskii, and V. V. Ragul'skii, "Observation of wave-front inversion in stimulated Raman scattering of light," Pisma Zh. Eksp. Fiz. 25, 41–44 (1977) [JETP Lett. 25, 36–38 (1977)].

[6]V. Wang and C. R. Giuliano, "Correction of phase aberrations via stimulated Brillouin scattering," Opt. Lett. 2, 4–6 (1978).

[7]The degeneracies referred to here are those arising from symmetry, such as occur for similar right- and left-circularly polarized modes in a cylindrical waveguide. That Δk cannot approach zero (to within less than L^{-1}) for any other cases is because otherwise $\omega_n^2 + \omega_l^2$ cannot come within S^{-1} of $\omega_m^2 + \omega_j^2$ without, at the same time, there being a drastic reduction in the z-γ integral in (9). This may be appreciated by studying the example of Eq. (50) for ω_2^2. Here, without the aforementioned degeneracies occuring, one sees that $\Delta kL \gtrsim L/Sk$, and L/Sk is never much less than unity when guiding occurs.

[8]A waveguide which imitates well the interaction of focused unguided waves may be imagined as follows. Construct that complete orthonormal set of free-space Gaussian-beam modes whose parameters are such that the smallest number N of modes need be superposed to give a good representation of the (focused) incident beam. Then let the waveguide axis coincide with the z axis of these modes and let it barely encompass the beam waist over the length where the waist size does not change appreciably. This length is generally of order $S\lambda^{-1}N^{-1/2}$. Calculate the backscattered wave using the mode decompositions in Eqs. (5) and (8) as we have prescribed. The field patterns calculated at the entrance to the waveguide should approximate those in the same plane in free space, since guiding is minimal.

PHYSICAL REVIEW A VOLUME 24, NUMBER 6 DECEMBER 1981

Rapid Communications

The Rapid Communications section is intended for the accelerated publication of important new results. Manuscripts submitted to this section are given priority in handling in the editorial office and in production. A Rapid Communication may be no longer than 3½ printed pages and must be accompanied by an abstract. Page proofs are sent to authors, but, because of the rapid publication schedule, publication is not delayed for receipt of corrections unless requested by the author.

New component in degenerate four-wave mixing of optical pulses in sodium vapor

S. N. Jabr, L. K. Lam, and R. W. Hellwarth

Electronics Sciences Laboratory, SSC 303, University of Southern California, Los Angeles, California 90007

(Received 24 March 1981)

We have observed a new component in the signals produced by degenerate four-wave mixing of 5-nsec optical pulses by the D-line resonances of sodium vapor. This component is comparable in intensity to that previously observed from a grating pattern of excited sodium atoms, but arises rather from a grating of coherently aligned (but not optically pumped) ground-state atoms. This component exists when there are no spatial intensity beats between input waves.

This Communication reports the observation of two different components in the coherent signal from degenerate four-wave mixing by the third-order nonlinear polarization in sodium vapor, at optical frequencies ω near the D-line resonances. The first "scalar" component arises because one of the input beams scatters from a grating of excited sodium atoms that is created by spatial intensity beats between two other input beams. This "population grating" has been studied theoretically by Wandzura[1] and in sodium by Bloom *et al.*[2] Here we examine a second "tensor" component which arises from the scattering of one beam from a grating of unexcited atoms in coherent superpositions of ground-state m sublevels. This "coherent grating" is created by spatial beats between two other input beams, even when they are orthogonally polarized and hence create no significant intensity beats. Our observations are made with dye laser pulses ($\sim$5 nsec) much shorter than the decay time ($\sim$16 nsec) of an excited atom. In this transient situation there is negligible optical pumping of ground-state sublevels (i.e., negligible population redistribution), an effect which alters greatly the character of four-wave mixing in the steady state.[3] We find that, in this transient regime, the wave scattering occurs primarily from the coherent grating.

We employ the degenerate four-wave mixing geometry, usual for phase conjugation, described in Ref. 4. One input "probe" beam 3, represented approximately by $\mathrm{Re}\hat{e}_3E_3\exp(i\vec{k}_3\cdot\vec{r}-i\omega t-\frac{1}{2}\alpha z)$, is caused to overlap (at small angle) two counterpropagating pump beams, represented by $\mathrm{Re}\hat{e}_1E_1\times\exp(ik_1z-i\omega t-\frac{1}{2}\alpha z)$ and $\mathrm{Re}\hat{e}_2E_2\exp[-ik_2z-i\omega t-\frac{1}{2}\alpha(L-z)]$, over the length L of the nonlinear medium whose linear absorption coefficient is α. (Polarization-state vectors are normalized so that $\hat{e}_1^*\cdot\hat{e}_1=1$, etc.)

These three input waves create a third-order polarization density at $(\omega,-\vec{k}_3)$ which generates the mixed-wave signal and whose complex vector amplitude $\vec{P}^{(3)}$ in any isotropic medium must have the form[4]

$$\vec{P}^{(3)}\propto(A\hat{e}_2\hat{e}_3^*\cdot\hat{e}_1+B\hat{e}_1\hat{e}_3^*\cdot\hat{e}_2+C\hat{e}_3^*\hat{e}_1\cdot\hat{e}_2)E_1E_2E_3^*\ . \tag{1}$$

The coefficients A, B, and C for sodium vapor have resonances at the D_1 and D_2 line whose nature we study here. It is easy to appreciate how, near resonance, spatial intensity beats between beams 1 and 3 ($\propto\hat{e}_1\cdot\hat{e}_3^*$) create a population grating of excited sodium atoms from which beam 2 scatters. Clearly this process contributes only to A (and not to B or C). Similarly, intensity beats between 2 and 3 create a population grating from which beam 1 scatters, and this process contributes only to B. Beats between 1 and 2 are both temporal (at 2ω) and spatial and create no population grating in sodium. These processes have been discussed previously.[1-3,5,6] Here we point out that, even if $\hat{e}_3$ is orthogonal to $\hat{e}_1$ and $\hat{e}_2$, gratings of coherently aligned ground-state atoms will be formed (at both $\vec{k}_3-\vec{k}_1$ and $\vec{k}_3-\vec{k}_2$) which scatter with efficiencies comparable to population gratings, i.e., create $C\sim B\sim A$. By using different polarization combinations we observe near the D_1

resonance that $A:B:C \cong 1:1:-1$, as we calculate for a pure coherent grating, taking into account washout of the gratings by atomic motion. We calculate that near the D_2 line a pure coherent grating would create $A:B:C \cong 5:5:-2$. Here, relatively greater background noise (from self-focusing and blooming of the reverse pump beam) has only permitted us to verify that $|A+B+C|^2$ is much larger than $|C|^2$.

Our experiments employed a nitrogen-laser pumped dye laser of the Littman[7] type (grazing incidence) which produced 5-nsec pulses of about 2-kW peak power, and of bandwidth $\sim 0.05\ \mathrm{cm}^{-1}$. Most pulses had most of their energy in a TEM_{00} mode. The laser beam was first split to form two superposed counterpropagating beams (pump beams 1 and 2) of equal intensity and focused to 2 mm diam in a heat-pipe-type cell containing sodium vapor (concentrated in the central 2 cm) at an average density $\sim 4\times10^{14}\ \mathrm{cm}^{-3}$ and ~ 5 torr of argon buffer gas. About 4% of the laser beam was also split off and used as the probe (beam 3) which propagated at an angle of about 1% relative to the pump beams. The wave backscattered along the probe (beam 4) was detected by a photodiode whose output was digitized by a Biomation transient digitizer and fed to a computer programmed to operate as a boxcar integrator.

Figure 1 shows the observed energy in the backscattered wave as a function of the laser frequency for the three combinations of linear polarization. (a): $\hat{e}_3 \| \hat{e}_2 \| \hat{e}_1$, (b): $\hat{e}_3 \| \hat{e}_2 \perp \hat{e}_1$, and (c): $\hat{e}_1 \| \hat{e}_2 \perp \hat{e}_3$. Case (a) is that studied by Bloom *et al.*,[1] who obtained a trace similar to Fig. 1(a). Beam self-focusing (and defocusing) accompanies all signals but is much stronger near the D_2 resonance. The other two cases, however, exhibit very different frequency dependences. In case (b) there is no signal to the low-frequency side of the lines presumably due to differential self-focusing and defocusing.[8] The maximum signal obtained in case (b) was about half as strong as in case (a) for the same pump-beam intensity. In case (c) the signal could also be observed only to the high-frequency side of the D_1 line, and reached a maximum of about $\frac{1}{3}$ of the maximum signal in case (a) for roughly the same pump intensity. The maximum power reflection efficiency $|E_4/E_3|^2$ never exceeded 1% with our apparatus. Self-focusing, absorption, and saturation played strong roles, except far from the centers of the lines, where the signal was low. Maximum efficiencies, therefore, have no simple interpretation; only in the wings can we make meaningful predictions.

To complete a determination of the ratio $A:B:C$ we fixed the dye-laser frequency in the blue wing of the D_1 line, near λ_1 of Fig. 1. We fixed $\hat{e}_1 \| \hat{e}_2$, and varied the angle θ of linear polarization of $\hat{e}_3$ with respect to $\hat{e}_1$. We observed the backscattered signal to be at least 90% linearly polarized at an angle minus θ (to within an uncertainty of $\sim 5\%$). This implies

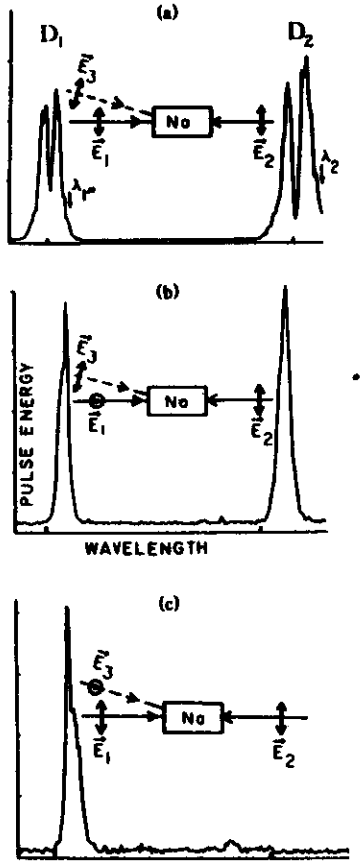

FIG. 1. Backscattered pulse energies as a function of wavelength for three cases of beam polarization as shown. Relative energy scales are described in the text. In the wings, these signals are proportional to (a) $|A+B+C|^2$, (b) $|B|^2$, and (c) $|C|^2$ of the text. The tick marks on the horizontal axes correspond to the D_1 and D_2 line centers. Studies using polarization combinations other than the (a), (b), and (c) cases were carried out at the wing wavelengths marked by λ_1 and λ_2 and determined the ratios $A:B:C$ governing all polarization cases. Intensities near line center are not easily predicted but are shown here for completeness.

$A:B:C \cong 1:1:-1$, as we expect for a coherent grating. Repeating this procedure at λ_2 in the wing of the D_2 line, we found that the backscattered signal was mainly (at least 90%) polarized parallel to $\hat{e}_1$. This shows $|C| \ll |A|$ or $|B|$ at λ_2. Comparison at λ_2 of Figs. 1(a) and 1(b) showed $A - B$ (and of same sign). Together, these results are consistent with a coherent, but not population, grating also at λ_2 for reasons discussed above and further below.

Varying the buffer gas pressure between 1 and 500 torr had little effect on power reflection efficiency in the wings, as we predict for a coherent grating. As expected, the signal in the wings increased roughly proportionally with sodium density until absorption intervened. In the wings the backscattered signal energy varied with the dye-laser-pulse energy U as $U^{3.7\pm0.3}$, consistent with a third-order process. Such a dependence has been previously reported for resonant four-wave mixing in rubidium vapor.[9]

Our theory of the coherent grating treats the atomic vapor in the impact approximation, and neglects hyperfine structure. After each sudden collision, an atom is left with equal probability in the ground sublevels, and then interacts as a free atom with the electromagnetic field until the next collision. We calculate the expected third-order electric dipole moment at time t for an atom of velocity $\vec{v}$ whose last collision was at time $t-T$. The contribution of such atoms to the polarization wave at $(\omega, -\vec{k}_3)$ is averaged over T and $\vec{v}$, and used in Maxwell's equations.

If one assumes a backscattered wave $\mathrm{Re}\hat{e}_4 E_4(z) \times \exp(-i\vec{k}_3\cdot\vec{r} - i\omega t + \frac{1}{2}\alpha z)$ then this nonlinear polarization generates an amplitude E_4 which obeys, in the slowly-varying-envelope approximation,

$$\frac{\partial E_4}{\partial z} = \sum \frac{\pi\omega N \chi_{1234}}{2nc\hbar^3}\left\langle \frac{2\Gamma + i\vec{k}_{13}\cdot\vec{v}}{D_A D_B D_C D_D}\right\rangle E_1 E_2 E_3^* e^{-\alpha z/n} . \tag{2}$$

Here L is the path length in the vapor, N is the atomic density, n is the refractive index at ω, and Γ equals the interatomic collision rate Γ_{coll} plus the spontaneous emission rate γ. The energy denominators are (assuming a single transition dominates)

$$D_A = \Gamma + i\Delta - i\vec{k}_3\cdot\vec{v} , \tag{3a}$$

$$D_B = \Gamma_{\mathrm{coll}} + i(\vec{k}_1 - \vec{k}_3)\cdot\vec{v} + \tau^{-1} , \tag{3b}$$

$$D_C = i(\Delta + \vec{k}_1\cdot\vec{v}) + \Gamma , \tag{3c}$$

$$D_D = -i(\Delta + \vec{k}_3\cdot\vec{v}) + \Gamma , \tag{3d}$$

where $\Delta = \omega_0 - \omega$; ω_0 is the frequency of the dominant (D_1 or D_2) transition. The $\sum'$ indicates that a second term is to be added which differs from that shown by interchanging beam subscripts 1 and 2 everywhere. The effect of finite pulse length τ is accounted for by the τ^{-1} in (3b). The $\langle\ \rangle$ indicates a normalized average over the atomic velocity $\vec{v}$. The estimate given elsewhere of this average[10] is not valid for frequency shifts outside the Doppler width in which we are interested here; behavior in this regime is easily seen directly from (2). The polarization dependence is contained in

$$\chi_{1234} = \hat{e}_4^*\cdot(A\hat{e}_2\hat{e}_3^*\cdot\hat{e}_1 + B\hat{e}_1\hat{e}_3^*\cdot\hat{e}_2 + C\hat{e}_3^*\hat{e}_1\cdot\hat{e}_2) , \tag{4}$$

where for both terms in $\sum$

$$A = B = g_0^{-1}\sum_m |\alpha_m^+|^4 ,$$
$$C = g_0^{-1}\sum_m (|\alpha_m^+|^2|\alpha_m^-|^2 + |\alpha_{m+2}^-|^2|\alpha_m^+|^2) - A , \tag{5}$$

where g_0 is the ground-state degeneracy and

$$\alpha_m^\pm = 2^{-1/2}\langle m \pm 1, J'|M_x \pm iM_y|m,J\rangle \tag{6}$$

are matrix elements between ground $|m,J\rangle$ states and excited $|m\pm1,J'\rangle$ states of components of the electric-dipole-moment operator $\vec{M}$ of an atom. Note that $\alpha_m^- = \alpha_m^{+*}$. For the D_1 line $\alpha_{1/2}^- = \mu(\frac{2}{3})^{1/2}$ and $\alpha_{1/2}^+ = 0$. For the D_2 line $\alpha_{1/2}^- = \mu(\frac{1}{3})^{1/2}$ and $\alpha_{1/2}^+ = \mu$. Here μ is the usual radial dipole matrix element. A useful solution of (2) is immediate if one takes E_1, E_2, and E_3 to be peak amplitudes (in time) having negligible variation with z. The independence of E_4 from the pressure of the buffer gas (i.e., Γ_{coll}) is evident in (2) provided that $\Gamma \gg |\vec{k}_1 - \vec{k}_3|v$ (v = rms velocity) as in our experiments. The $A:B:C$ ratios quoted earlier for a coherent grating follow directly from (5) and (6). The D_2 ratio implies a signal at λ_2 in Fig. 1(a), that is 16 times greater than at λ_2 in Fig. 1(c), consistent with the low signal observed in the latter case.

To understand the apparently minor role of the population grating here we have extended our model so that after a collision an atom has a probability $w(\vec{v},\vec{r})/g_1$ to be in each excited sublevel, and a probability $(1-w)/g_0$ to be in each ground sublevel. The probability w depends on the (assumed unchanging) velocity $\vec{v}$ of the molecule and the position $\vec{r}$ in the intensity grating at the time of the last velocity-changing collision. This probability has terms proportional to $E_1E_3^*$ and $E_2E_3^*$ corresponding to the two possible gratings discussed earlier. The different linear susceptibility of these excited atoms causes scattering of the third beam. After averaging over $\vec{r}$ we find that these additional scattered terms give another contribution to (2) that is the same as in (2) except for the following:

(i) The Γ_{coll} in Eq. (3b) is replaced by the rate at which collisions or photons deexcite the upper level.

(ii) The unpermuted term in $\sum'$ has $B = -C = 0$ and

$$A = \frac{1}{g_0 g_1}\left|\sum_m |\alpha_m^+|^2\right|^2 . \tag{7}$$

(iii) The permuted $(1 \rightarrow 2)$ term in $\sum$ has $A = C = 0$ and B the same as in (7).

(iv) A factor equal to the fraction of all upper levels excited ($\frac{1}{3}$ for the D_1 line and $\frac{2}{3}$ for the D_2 line) should multiply χ_{1234} when Γ_{coll} exceeds the radiative decay rate; i.e., when collisions redistribute excited atoms among all upper levels.

Based on χ_{1234} alone of this revised model, the population grating contribution to the signal is never more than $\frac{1}{6}$ that of the coherent grating, and in most cases is much less, or zero. This accounts in large measure for the apparently small contribution of the population grating.

We identify the two terms in the sum $\sum$, of both model results above, as arising from gratings of wave vectors $\vec{k}_1 - \vec{k}_3$ and $\vec{k}_2 - \vec{k}_3$, respectively; this is because of the velocity dependence of the dominator D_θ of (3b). In the pressure regime of main interest here, $|\vec{k}_1 - \vec{k}_3|v \ll \Gamma \ll |\vec{k}_2 - \vec{k}_3|v$ so that the velocity average in (2) causes the second term in $\sum$ (describing the larger wave-vector grating) to be reduced relative to the first. This effect, referred to as motional washout,[6] is predicted to make $B \ll A$ for the population grating but leave $A = B$ for the coherent grating. That our experiments show $A \cong B$ at λ_1 and $A \sim B$ at λ_2 is further corroboration of the dominance of the coherent grating.

In conclusion, we have observed and explained a strong new component in the resonant degenerate four-wave mixing signal from sodium vapor. This component does not involve exciting any sodium atoms, but rather arises from a grating of coherently aligned, but not optically pumped, ground-state atoms.

This work was supported by the National Science Foundation under Grant No. ENG78-04774 and by the U.S. Air Force Office of Scientific Research under Grant No. 78-3479. One of us (R.W. Hellwarth) would like to thank the Aspen Center for Physics for hospitality during part of this work.

[1] D. M. Bloom, P. F. Liao, and N. P. Economou, Opt. Lett. 2, 58 (1978).
[2] S. M. Wandzura, Opt. Lett. 4, 208 (1979).
[3] P. F. Liao, D. M. Bloom, and N. P. Economou, Appl Phys. Lett. 32, 813 (1978).
[4] G. Martin, L. K. Lam, and R. W. Hellwarth, Opt. Lett. 5, 185 (1980).
[5] L. M. Humphrey, J. P. Gordon, and P. F. Liao, Opt. Lett. 5, 56 (1980).
[6] D. G. Steel *et al.*, Appl. Phys. Lett. 35, 376 (1979).
[7] M. G. Littman and H. J. Metcalf, Appl. Opt. 17, 2224 (1978).
[8] J. E. Bjorkholm and A. Ashkin, Phys. Rev. Lett. 32, 129 (1974).
[9] D. Grischkowsky *et al.*, Appl. Phys. Lett. 33, 805 (1978).
[10] J. Nalen and A. Yariv, J. Opt. Soc. Am. 71, 180 (1981).